CRANFIELD UNIVERSITY

Defence Academy - College of Management and Technology

Department of Engineering & Applied Science

PhD

2011

Piranavan Suntharalingam

Kinetic Energy Recovery and Power Management for Hybrid Electric Vehicles

Supervisor:

Dr John Economou

February 2011

Abstract

The major contribution of the work presented in this thesis is a thorough investigation of the constraints on regenerative braking and kinetic energy recovery enhancement for electric/hybrid electric vehicles during braking. Regenerative braking systems provide an opportunity to recycle the braking energy, which is otherwise dissipated as heat in the brake pads. However, braking energy harnessing is a relatively new concept in the automotive sector which still requires further research and development. Due to the operating constraints of the drivetrain architecture and the varying nature of the braking conditions, it is unlikely that all the stored kinetic energy of the vehicle can be recovered during braking.The research work in this thesis addresses the effect of braking conditions on kinetic energy recovery enhancement of the vehicle. The challenge in kinetic energy recovery enhancement lies in braking conditions, power/torque handling ability of the electric propulsion system, managing the dual braking systems, employed energy conversion techniques, and energy storage capacity. In this work a novel braking strategy is introduced to increase the involvement of the regenerative braking system, so as to increase the kinetic energy recovery while achieving the braking performance requirements.

Initially mathematical modelling and simulation based analysis are presented to demonstrate the effects of braking power variation with respect to braking requirements. A novel braking strategy is proposed to increase the kinetic energy recovery during heavy braking events. The effectiveness of this braking strategy is analyzed using a simulation model developed in matlab- simulink environment. An experimental rig is developed to test various braking scenarios and their effects on kinetic energy recovery. A variety of braking scenarios are tested and results are presented with the analysis. At the end, suggestions are made to further continue this research in the future.

Acknowledgements

I would like to thank to my supervisor Dr. John Economou for providing me the opportunity to carry out this research project. I really appreciate his encouragement and his positive support during the course of my studies. I feel privileged to get the opportunity to work along side him for the last three years.

I would also like to take this opportunity to thank Prof. Kevin Knowles for his kind and valuable advice during thesis meetings and Prof. John Hetherington for his support.

The support provided by the work shop to construct the experimental test bench is unforgettable. Thank you very much guys.

My special and sincere thanks go to Dr. Graham Stabler, without whose support and advice this thesis could not have been completed. I also would like to thank all my friends in the Heaviside lab, who provide company during this research.

Finally I would like to thank my family for their continuous encouragement and support.

Contents

List of Tables

List of Figures

Nomenclature

All units are in SI unless otherwise stated

Alphanumeric

F_f	Front wheel braking force
F_r	Rear wheel braking force
R_f	Front wheel rolling resistance force
R_r	Rear wheel rolling resistance force
m	Mass of the vehicle
F_{res}	Resultant braking force
θ	Road inclination angle in radian
a	Deceleration rate of the vehicle
ν	Coefficient of the rolling resistance
F_a	Density of the air
C_D	Aerodynamic drag coefficient of the vehicle
v	Ground velocity of the vehicle
V_{wind}	Effective wind velocity against the vehicle
$\hat{F}_f$	Maximum applicable front wheel braking force
$\hat{F}_r$	Maximum applicable rear wheel braking force
N_f	Normal forces acting on front axle
N_r	Normal forces acting on rear axle
μ	Terrain adhesive coefficient
L	Longitudinal distance between front and rear axle

l_1	Longitudinal distance between *CG* and front axle
l_2	Longitudinal distance between *CG* and rear axle
h	Hight of the *CG* from ground
P_b	Braking power demand
P_{MG}	Power rating of the motor generator
t	Time
U	Initial velocity of the vehicle
V	Final velocity of the vehicle
ΔE	Kinetic energy drop of the vehicle
E_u	Kinetic energy of the vehicle at velocity U
E_V	Kinetic energy of the vehicle at velocity V
η_R	Regenerative braking efficiency
τ	Mechanical torque of the electric motor
κ_i	Torque constant of the motor
κ_v	Speed constant of the motor
i	Current flow rate of the motor
E_{emf}, V_g	Back electromotive force
ω	Angular speed of the motor
V_c	Bus terminal voltage
τ_{brake}	Braking torque
k_1	Normalized regenerative braking percentage
k_2	Normalized mechanical braking percentage
τ_{mg}	Torque produced by the motor

τ_{hm}	Torque produced by the mechanical braking system
S	Braking distance
E_{uc}	Stored energy in the UC-bank during the recharging process
V_{uc}	Voltage of the UC-bank
r_c	Internal resistance of the UC-bank
C	Capacitance of the UC-bank
k	Time constant of the circuit
P_{uc}	Charging power of the capacitor
D	Duty cycle value
T	Time period
r_g	Internal resistance of the electric motor
A_c	Cross sectional area of the magnetic core in cm^2
W_A	Available core window area for the winding in cm^2
K_u	Mean length per turn in cm
ρ	Resistivity of the winding wire in $\Omega - cm$
P_L	Power loss in the inductor
ζ	Normalized ripple percentage
f_{sw}	Switching frequency of the power converter
Q	Accumulated Charge in the UC-bank
J	Second moment of inertia of flywheel system
N_f	Speed of the flywheel system in rpm

Abbreviations

CG	Center of gravity of the vehicle

ESR_{DC}	DC equivalent series resistance
MLT	Mean length per turn in *cm*
SE	Specific energy
PP	Peak power
CBT	Constant braking torque
CBP	Constant braking power
KE	Kinetic energy
HEV	Hybrid electric vehicle
UC	Ultracapacitor
KVL	Kirchhoff's voltage law
SDC	Standard driving cycle
IEMA	Intelligent energy management agent
PHEV	parallel hybrid electric vehicles
DIE	Driving situation identifier
FTD	Fuzzy torque distributor
DSI	Driving situation identifier
SCC	State-of-charge compensator
IC	Internal combuston
UDDS	Urban dynamometer driving schedule
RKE	Recovered kinetic energy
BR	Braking ratio

Chapter 1

Introduction

Electric propulsion systems have been gaining interest in recent years. Excellent operating efficiency, kinetic energy recovery and emission-less operation are the primary advantages of electric propulsion systems over conventional vehicles. The challenges in kinetic energy recovery enhancement of electric propulsion systems lie in the employed power and energy management strategy, the power limitations of the electric propulsion system as well as the driving behavior of vehicles. Appropriate power management permits the fulfillment of various propulsive requirements. The power handling capability of electric propulsion systems is a primary constraint for regenerative braking performance improvement. To fulfill higher braking requirements, hybrid electric propulsion systems incorporate a mechanical braking system as well as a regenerative braking system. As such, braking power sharing proportion is required to strategies and control to achieve performance requirements as well as kinetic energy recovery during braking. This thesis deals with the braking power management strategy development, implementation and realization to increase the kinetic energy recovery while achieving braking requirements. This chapter describes the motivational factors to conduct this research.

1.1 Motivation

This research is motivated by the increasing interest in electric propulsion systems for transportation applications. Environmental impact, the continuous rise of petroleum prices and depletion of natural resources and emission restrictions in urban areas are driving the development of eco-friendly alternatives to replace conventional propulsion systems. An efficient energy consumption awareness program has become widespread in recent years, encompassing all sectors of the globe. It can be considered as the fundamental requirement to reduce environmental impact, minimize the cost of products and services, and improve economic competitiveness. As illustrated in figure 1.1, close to 30% of global

energy is consumed by the transportation sector. Further to this a 95-96% dependency of petroleum energy is an important matter, which provides a compelling requirement for the development of sustainable energy alternatives. In parallel to that, development of energy efficient systems and energy management concepts provide essential support for efficient energy consumption. Social awareness is also playing an important roll on successful implementation and realization. In essence, sustainable energy with efficient conversion and consumption lead to a healthy and green environment with higher productivity.

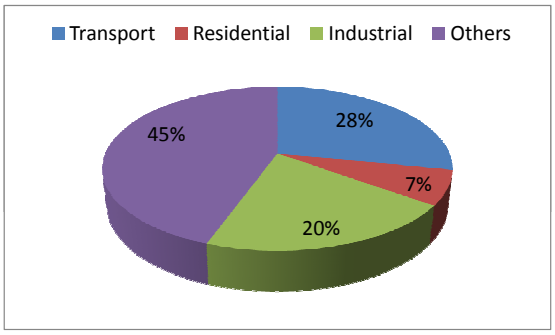

(a) Energy resources consumption in North America (2008)

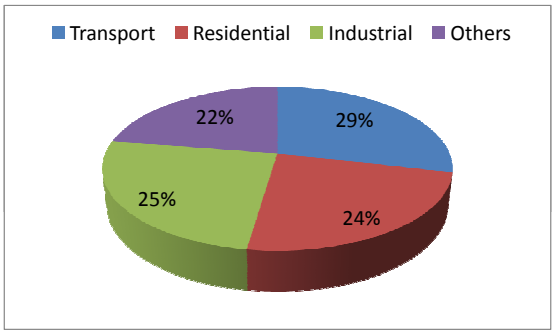

(b) Energy resources consumption in Europe-27 (2006)

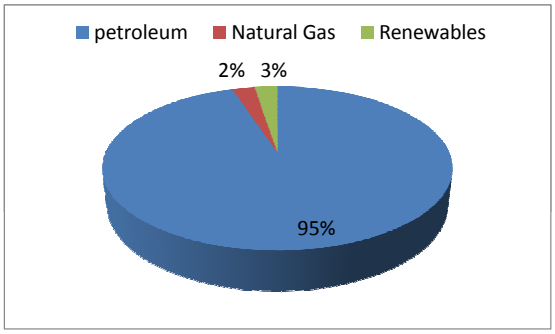

(c) Energy resources consumption for transportation in North America (2008)

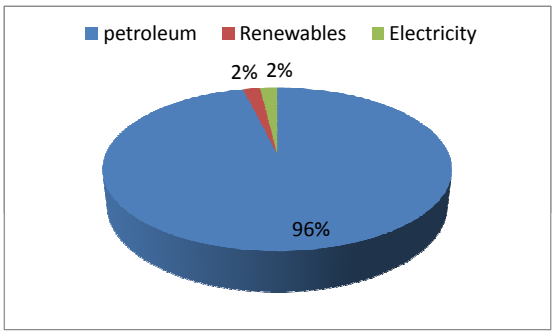

(d) Energy resources consumption for transportation in Europe-27 (2006)

Figure 1.1: Energy resources consumption rates ([4] and [5])

Automobiles can be considered as an integral part of our life. The need for mobility is continuously increasing with population growth. To meet with Kyoto obligations "stabilization of greenhouse gas concentration in the atmosphere at a level that would prevent dangerous anthropogenic interference with the climate system" innovations in technology contribute to the sustainable development concept. Reaching these challenges require many research investigation and development activities.

From the view point of propulsive performance and energy conservation efficiency, electric motors are superior to internal combustion engines (IC engines) in

several aspects. Storage limitations of onboard electrical energy sources are the primary limiting factor, which restricts the driving range of vehicles. Therefore, employment of strategic power and energy management techniques are vital to increase the range and endurance. Kinetic energy recovery during braking is another important characteristic of electric propulsion systems, which is contributing significantly towards the development of an energy efficient propulsion system.

The concept of regenerative braking can be employed not only in electric propulsion systems found in automobiles, but also in the following application domains as well:

- Heavy/light duty industrial robotic applications
- Domestic/industrial lifters
- Loading/unloading cranes
- Electric trains
- Electric boats
- Forklifts
- Heavy/light duty sorting machines
- Various process equipment in manufacturing industry, which undergo frequent acceleration-deceleration cycles.

The realization of recycling the braking energy is accelerating with the global energy crises and the concept of sustainable energy conservation. This fundamental concept requires in depth research investigation and innovation to contribute towards the development of eco-friendly energy solutions. Also this research area provides a unique opportunity for original research contributions.

1.2 Research questions

Based on the literature review, most of the research work has been conducted in the areas related to power management for land based hybrid-electric vehicles. In

the previous work the regenerative energy capturing research has not considered the energy in association to the vehicle size, braking dynamics of the vehicle and drivetrain architecture. This Thesis is focusing in the multi-disciplinary research area of realizable generator sizing with reference to the vehicle physical limitations (mass, volume), and in association with a realizable power electronic design.

Thesis hypothesis is as follows:

Hypothesis:"Land vehicles braking dynamics and braking profile significantly affects the kinetic energy recovery of vehicles. This fact can be effectively employed to enhance vehicles driving range"

Hence the research questions are formulated as follows:

- What are the primary limitations of electric propulsion systems restricting the energy recovery performance?
- What are the braking requirements which often demanded by land vehicles to handle various braking circumstances?
- Does braking requirements have any significant influence on limiting the kinetic energy recovery?
- How the drivetrain architecture affects kinetic energy recovery?
- How the driving terrain would influence the kinetic energy recovery?
- Can the kinetic energy recovery be increased by employing different approaches?

In general, braking objective can be defined as either stop the vehicle or achieve a desired final velocity within the safety braking distance from its initial velocity. Based on this hypothesis, the braking problem of the land vehicle is investigated from the view point of braking distance in this research.

1.3 Research procedure

The research study is carried out in a sequence as depicted in figure 1.2. It begins with the problem investigation in this research domain. Here the primary

constraints of electric/hybrid electric propulsion systems are viewed from the perspective of kinetic energy recovery. Issues related to multiple systems in the hybrid power train architecture are addressed to define the research problem for further investigation.

Following that, theoretical methods are applied to investigate and understand various issues in the kinetic energy recovery process. Mathematical modelling and simulation methods are used for to analyze and verify the research hypothesis. To verify these findings, an experimental test bench is designed. To avoid the exogenous and indigenous vehicle phenomena, a flywheel based vehicle braking system is designed to perform experiments. Subsystems in the electric propulsion system are designed appropriately to fulfil the performance within the boundary conditions.

Using this experimental test bench, theoretical hypothesis are explored. A variety of braking scenarios are tested with different operating modes of the electric propulsion system. Results are compared to verify the research hypothesis and conclusions are drawn at the end. To continue with this research work, guidelines for the future work also highlighted at the end

1.4 Brief outline of contributions

The primary aim of this research is to investigate, formulate, design and develop new knowledge on braking power management strategies to accomplish realistic user/operator braking objectives while increasing the kinetic energy recovery of electric/hybrid electric vehicles. The contributions of this research are listed below:

- Recognition and definition of the kinetic energy recovery requirements and synthesize for hybrid electric unmanned (UGV)/manned ground vehicles (MGV) architectures.
- Determination and synthesis of UGV/MGV operating conditions for kinetic energy recovery. Dynamic force transfer, influence of road adhesion, deceleration requirements, and influence of drivetrain configuration are formulated and analyzed from the view point of the kinetic energy recovery of vehicles.

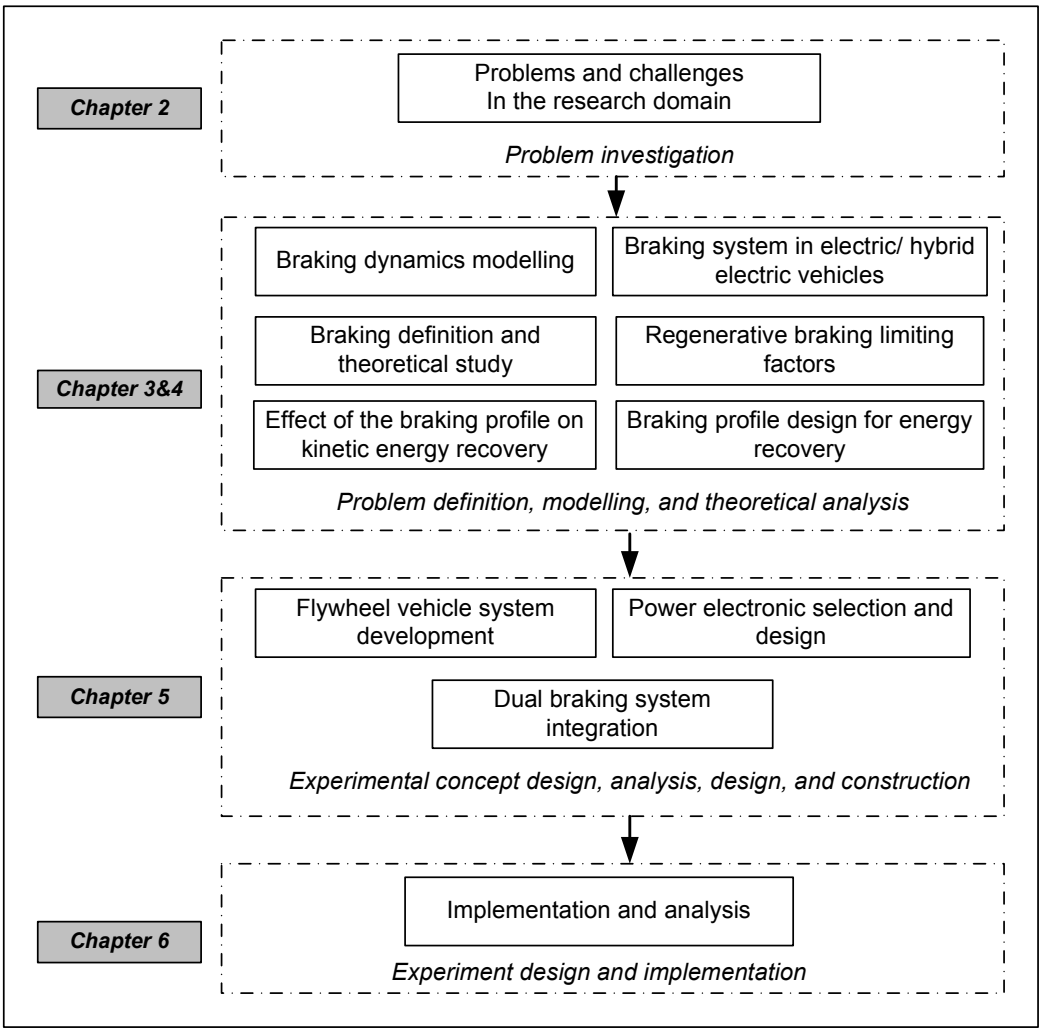

Figure 1.2: Sequence of the research procedure

- Association and organization of the braking behavior of the UGV/MGV operator/user with kinetic energy recovery. Mild, moderate, and heavy braking events and their implications on electric propulsion systems for kinetic energy recovery are analyzed. A novel braking strategy is mathematically formulated, synthesised, analyzed, and simulated in order to verify its effectiveness on kinetic energy recovery.

- Recognition of the potential quantity and frequency of kinetic energy savings and synthesis of the decoupling of exogenous and endogenous vehicle parameters via a representative flywheel kinetic energy storage system.

- Analysis, design, and development of an experimental test bench for val-

idating the kinetic energy recovery. It includes synthesis and integration of mechanical, power electronic converter, power management, and data acquisition systems.

- Recognition of the requirements for reliable and efficient transient energy sources and design and evaluation on energy capturing system.
- Experimental evaluation, validation and comparison of the effect of braking profiles on kinetic energy recovery. A variety of test were conducted to achieve different braking requirements by employing different braking profiles and results were compared to verify their influence on energy recovery efficiency.

1.5 Thesis outline

- Chapter 2 begins with an overview of electric propulsion systems in the context of kinetic energy (KE) recovery. Multiple systems in the electric drivetrain and their direct and indirect influence on drivetrain performance are highlighted. Following that, the trends in research activity in the electric propulsion systems domain is described. Fundamental limitations of electric propulsion systems for KE recovery, methodologies, power management strategies, and the state of the art of electric propulsion system enabling technology are reviewed. Various approaches that have been investigated in the literature to enhance the kinetic energy recovery capability and their issues are highlighted to substantiate this research.
- Chapter 3 presents the braking dynamics of a two axle vehicle. Dynamic force transfer and variation in braking torque distribution with respect to braking conditions are investigated in this chapter. The stability criteria of a vehicle and the braking torque distribution techniques to fulfil the stability criteria as well as regenerative braking performance are discussed. By employing mathematical-simulation models, the braking power requirement of vehicles in different driving conditions are compared with the power handling capability of electric propulsion systems. To illustrate the effect of braking torque distribution on kinetic energy recovery, a simulation study for a front wheel drive vehicle is presented.

- Chapter 4 introduces a novel braking concept to enhance the kinetic energy recovery of the vehicle. In case of a heavy braking events, the electric propulsion system is restricted to its maximum power capacity. As a result of that, a significant amount of energy is simply dissipated in the mechanical braking disks. The possibility of varying the braking power distribution to increase the energy recovery duration in such situations is investigated in this chapter. A mathematical description of this concept as well as a simulation based case study is presented to verify the benefits of this approach.

- Chapter 5 begins with the conceptual design procedure of the experimental platform. Following that, a detailed description of the hardware design, development, and implementation frameworks are presented. Fundamental theories are incorporated for the sizing procedure of components in power converter design and the operating principle of the powertrain system is also described. A data acquisition system is also integrated to capture information about the system during its operation.

- Chapter 6 contains the design procedure of the experiments as well as results and discussion. A vast range of braking scenarios are investigated for different operating modes of the electric propulsion system. A comparison study on the recovered energy quantity under different braking profiles is presented to substantiate the primary benefits of the proposed braking approach presented in chapter 4 during heavy braking conditions.

- Chapter 7 concludes with a summary of the contributions. Following that, the direction of further studies required to continue this research is highlighted in this chapter. Schematics of the experimental rig, power converter, and images of the test bench are provided in the Appendix of this dissertation.

Chapter 2

Literature Review

In this chapter, a broad literature survey on electric propulsion system research is presented. Initially, an overview of the electric propulsion system and its benefits for vehicular applications are presented. This section discusses the primary areas where active research and development activities take place in the electric/hybrid electric vehicles research domain. Subsequently the significant advantages of electric propulsion systems for kinetic energy recovery are illustrated and practical limitations of electric propulsion systems on kinetic energy recovery are described. A discussion is presented at the end of this chapter.

2.1 Overview

Hybrid electric, electric, and fuelcell based vehicles have been gaining interest in recent years. As illustrated in table 2.1, most of the leading automobile companies are keen to develop electric/hybrid electric vehicles. This leads to various opportunities for research contributions in this area, which are yet to be studied for development and implementation [1]. This application oriented research involves multidisciplinary engineering in subjects such as mechanical, electrical, chemical, material and electronics. This results in the investigation of this problem individually and cooperatively as illustrated in figure 2.1. Due to the integrated nature of multiple systems, the real challenge is to integrate in an effective manner so as to develop energy efficient transmission systems.

As illustrated in figure 2.1, there are chains of challenges which need to be resolved. Safety, performance and comfort are basic requirements, they cannot be compromised for any other benefits. Therefore a sector of research work in this domain investigates the issues related to vehicles dynamics and ergonomic aspects.

Study on efficient motor drives is another active research sector. In essence, the primary objective of this study is to improve the motor efficiency while achieving higher power to weight ratio with better speed torque characteristics.

Table 2.1: Leading automobile companies and their HEV brands

Automobile company	Brand of the HEV
Citroen	Xsara Dynactive
Fiat	Multipla
Ford	Escape
GM	Precept
Honda	Insight
Nissan	Tino
Renault	Koleos
Toyota	Coaster, Prius, Post- Prius
Volvo	FL6, B10L

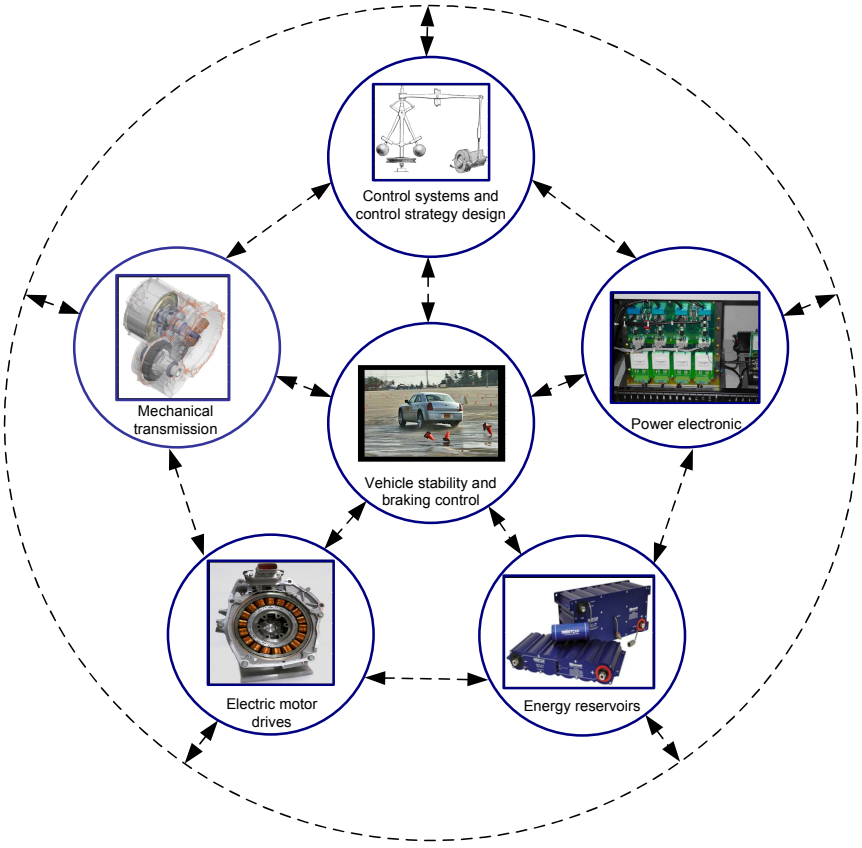

Figure 2.1: Active research areas in the domain of electric propulsion systems research for automobile applications

Electro-mechanical coupling is an intermediate transmission system, which connects the electric motor with the drive axle. Inappropriate transmission system design results in significant efficiency losses. Therefore different types of transmission systems such as continuously variable transmission, wheel hub transmission, and synergy drives are studied for electric propulsion system applications.

Energy density, power density, and nonlinear operational behavior of electric energy reservoirs considerably affect the driving endurance and efficiency of propulsion systems. This is one of the most active research areas in electric propulsion as well as several other domains such as computer power systems and mobile phones. Due to the high energy density of fossil fuels, it is almost impossible to replace them with electric energy reservoirs in electric vehicles. Several studies are investigating other possible methods to develop electric energy storage devices.

The power electronic converter is another device, which connects the electric motor and energy reservoir to control the power flow quantity and direction. The power and energy management task for multiple energy reservoirs is also performed by power converters. It is achieved by appropriately changing the voltage deviation of the output with respect to the input. There are a variety of power converter topologies that have been investigated by many researchers for different drivetrain applications. Increasing efficiency, operating range, and performance are the primary objectives of this research sector.

Involvement of multiple systems with different operational objectives requires a control system. The task of this control system is to monitor all systems and perform supervisory and individual control actions. Various control approaches are studied for hybrid electric vehicle applications. To achieve the optimal performance of the propulsion systems, many studies investigate the problem from a purely mathematical point of view. It illustrates that each and every part of the electric propulsion system is directly or indirectly connected together as depicted in figure 2.1. Due to the sophisticated nature of this system, implementation and realization is an extremely challenging and exciting area of work.

It is intuitive to ask why electric propulsion systems are superior to conventional vehicles? Electric propulsion systems exhibit the following operational behaviors, which are not common in conventional propulsion systems [8]and [9]:

- Regenerative braking
- Emission free operation
- Higher efficiency
- Noise less operation
- Convenient control

The bidirectional operational behavior of electric propulsion systems is an important attribute for regenerative braking applications. The possibility of kinetic energy recovery in electric propulsion systems significantly increases the fuel economy of vehicles. Also this fact not only helps to increase the driving range of vehicles, but also to reduce the emissions and extend the life of the brake disk. The following sections illustrate the ongoing active research work in the area of electric propulsion systems and their findings and realization challenges. This survey is conducted from the view point of regenerative braking and kinetic energy recovery enhancement.

2.2 Regenerative braking

Effective utilization of regenerative braking systems is one of the primary objectives in electric propulsion systems. Recovery of the stored kinetic energy of the vehicle during braking is the fundamental concept behind regenerative braking. Although it is trivial to understand, there are various practical limitations which restrict the kinetic energy recovery in different ways. System limitations and driving behavior are two primary issues, which contribute significantly to determining the energy recovery efficiency [2]. Energy recovery is an attractive approach to increase the driving range with a limited energy reservoir. The kinetic energy recovery of the electric propulsion system increases the driving range by 25 to 30% [10]. According to [10], the "Toyota Prius" hybrid electric vehicle achieves 20% increase in the driving range with the help of kinetic energy recovery and the "Honda Insight " achieves 30% increase in the driving range. However, the relevant driving cycle is not defined in their analysis and it is hard to state these figures without the information of driving conditions.

In general the range and cost appear as the technological and economical limitation for electric and hybrid electric propulsion systems, which stops them from competing in the conventional vehicles market [11] and [1]. Generally, propulsion systems are designed to achieve the acceleration performance requirements of the vehicle [3]. Electric motor, battery system, power converter device, and transmission system are designed in a vehicle to meet the acceleration and maximum speed requirements. Therefore, maximum achievable acceleration and speed can be determined based on system parameters. However, braking power requirements cannot be be predicted based on these parameters. Only the driving behavior determines the braking power requirement. Therefore an emergency braking power requirement may be far beyond the acceleration power requirements, which can be handled by the electric propulsion system. During this circumstances, the stored kinetic energy of a vehicle should be recovered or dissipated within different time frames with respect to braking requirements. Due to this reason, all the braking power cannot be supplied by electric propulsion systems. Although employing a sufficiently large electric propulsion system will ideally recover all the kinetic energy, the additional mass and volume of the vehicle will require extra energy for propulsion [12]. The emerging need of the dual braking system for electric/hybrid electric vehicles are summarized next:

1. Limited electric motor power limits the maximum braking torque
2. As a result of insufficient back-emf, regenerative braking performance is negligible in low speed braking conditions
3. Stored energy in the energy reservoir has a direct influence on regenerative braking performance. Therefore, it cannot be engaged when the energy storage is fully charged.
4. Most of the vehicles are either front or rear wheel drive. However, some braking scenarios require the involvement of front and rear wheel brakes together.
5. Influence of the anti-lock braking system on slippery roads result in reduction of the regenerative braking performance.

Due to these reasons, electric vehicles are incorporated with dual braking systems.

Although this flexibility allows a vast range of braking requirements, dual braking systems need to be appropriately coordinated and managed to maximise the kinetic energy recovery while performing braking tasks. Therefore, the braking power management strategy is playing a vital roll to increase the kinetic energy recovery of an the electric propulsion system. A variety of power management strategies are studied in the literature for this purpose and they are discussed in the following section.

2.2.1 Regenerative braking strategy and power management

A regenerative braking algorithm is proposed by [13] for parallel hybrid electric vehicles. The feed back knowledge of the battery system, vehicle velocity, and motor characteristics are considered to design this algorithm. A similar concept is adopted by [14]. Issues related to the brake pedal feeling are also investigated by using a stroke simulator. To evaluate the performance of this combined braking algorithm, a hardware in-loop simulation is performed by utilizing a hybrid electric vehicle simulator and a matlab-simulink model. Issues related to the power transmission and kinetic energy recovery efficiency are not considered as the primary objective of this study. Rather, achieving the braking objective with human braking feeling is given the priority in this research.

A parametric analysis by [12] illustrates the tradeoff involved in component sizing for kinetic energy recovery systems. Six different drivetrain systems (with the combination of different power electric motor and battery systems) are simulated to achieve Federal Urban Driving Cycle (FUDC) using the advance vehicle simulator (ADVISOR). Due to the effect of kinetic energy recovery, 4 to 19% of the fuel economy is recorded during this simulation study. Here low power motor-battery combination achieved a 4% fuel economy while the higher power motor-battery combination achieved a 19% fuel economy. This study suggests that employing a higher power motor-battery system in a hybrid electric vehicle is desirable to enhance regenerative braking efficiency. However, the tradeoff involved in mass increment with over sizing the motor-battery system also needs to be considered in this study. It should be noted here that FUDC is not representing

all kinds of driving conditions. Therefore a vast number of driving cycles need to be tested in order to verify the effectiveness of the regenerative braking system.

Due to the dynamic force transfer of vehicles during braking, a significant amount of braking torque needs to be shared between front and rear axles [3] and [15]. This ratio will vary with the deceleration rates of the vehicle as well as road conditions. Inappropriate torque sharing may result in loss of stability and steering control. It should be noted here that most vehicles have either a front wheel or rear wheel driving system. For example, let us assume a front wheel drive vehicle is undergoing a braking scenario, where front and rear brakes must be engaged to ensure safe braking. In such situations, a fraction of kinetic energy will be simply dissipated in rear axle brake discs, regardless of the fact that the braking power could be met by the electric braking system alone. Due to this practical limitation, the regenerative braking system's flexibility is further decrease.

A braking torque estimation strategy is proposed by [15] to increase the braking energy recovery during braking. Using the vehicle speed, regenerative braking torque is estimated and has been used as the reference torque to the braking control scheme. Since conventional vehicles are only incorporated with the mechanical braking systems, this problem never exists in conventional vehicles. However, dual braking systems in hybrid electric vehicles require a great degree of control system involvement. Similar to [15], braking dynamic characteristics of hydromechanical and regenerative braking systems are studied by [16]. Feed forward and feed back control approaches are integrated with a coordinated control strategy implementation framework.

A braking torque distribution strategy is proposed by [17] to maximize the kinetic energy recovery of hybrid electric vehicles. A regenerative braking torque optimization strategy is considered as the objective function to design this strategy. The approach is experimented on in a simulation based model.

As illustrated in [3], the primary objective of braking is to quickly reduce the speed of a vehicle while maintains driving direction and stability criteria. However, increasing the kinetic energy recovery is an important objective in hybrid electric vehicles. By considering this, [9] proposed a braking force distribution strategy to achieve the aforementioned goals. The performance characteristics of the electric motor and battery system are used to design the regenerative braking

strategy. General operating principles of this strategy are:

- Identify the required braking strength
- Calculate the braking torque distribution to front and rear wheels
- Calculate the possible regenerative braking torque supply
- Apply the dual braking system to fulfill above three criteria

A simulation was also performed to exemplify the benefits of this study.

A four wheel drive electric vehicle is investigated by [18]. The objective of this study is to understand the effect of braking on vehicle stability. For example, wheel lock, steering control and riding comfort cannot be controlled by the driver by just pressing the brake pedal [3]. Therefore, this study proposes a control method to achieve a stable braking event, which utilizes brake stroke input and estimated vehicle speed, deceleration and dynamic load movement. At the same time it also increases the kinetic energy recovery.

Commonly used strategies such as series braking and parallel braking are discussed in [2]. The analysis shows that the series braking strategy is most suitable for series hybrid, and electric vehicle while the parallel braking strategy is suitable for parallel hybrid, and mild hybrid electric vehicles. The feasibility of employing the electric motor to achieve antilock braking performance without the involvement of a conventional antilock braking system is analyzed in [19]. Indeed most of these works are focusing on achieving better regenerative braking efficiency while ensuring acceptable driving comfort and braking safety.

As described earlier, the involvement of the mechanical transmission system limits the propulsion system efficiency. To avoid this problem, the feasibility of developing in wheel motors for lightweight series hybrid electric vehicles is studied by [20] for urban driving requirements. Based on the standard driving cycles, the author performed a statistical analysis to obtain average deceleration rates. The outcome of this investigation suggested that rear wheel drive systems maintain adequate braking performance in urban driving conditions. A maximum of 0.35 g deceleration rate is recorded in this analysis. Contrary to that,[3] highlights that some deceleration rates can reach 0.8 to 1 g. The driving habits of drivers is also another factor, which results in various deceleration rates. With the increasing

deceleration rates, the braking torque splitting ratio between front and rear axles also varies. Due to this reasons, the involvement of regenerative braking systems will be affected, which results in reduction of the kinetic energy recovery. Therefore the tradeoff between the braking energy recovery and deceleration rates also needs to be taken into consideration in this study.

The contribution of the regenerative braking system on reducing emissions is investigated by [8]. The author claimed that a maximum of 60% of the kinetic energy can be recovered during braking, which contributes to significantly reducing the emissions. However, this efficiency value deviates greatly from [21],[10], and [2] and comparison of them leads to an ambiguous conclusion. A waste energy recovery mechanism for conventional, and hybrid electric vehicles (internal combustion engine based propulsion system) is introduced by [21]. This paper highlights that only 25% of the fuel energy is converted as usable energy for propulsion in conventional vehicles. Also 40% of the fuel energy is simply wasted in the exhaust air. The proposed mechanism recovers a fraction of waste heat energy as electric energy, which is accumulated in a battery system. A DC-DC buck converter is employed to regulate the current and voltage requirements of the charging circuit. This also another attractive way of improving the energy efficiency of IC engine based drivetrain systems. However, the efficiency of this system for this application is not mentioned in this study. Also the issues related to economical viability also need to be considered from the implementation perspective.

Apart from the automobile application, regenerative braking systems for gantry crane applications are investigated by [22]. During the down stroke motion and braking period of the loading-unloading cycles of the crane, energy can be recovered for future use. Under this category, another study is performed by [23], which investigates the regenerative braking control issues for a wheelchair in downhill driving conditions.

Regenerative braking performance is highly dependant upon the employed vehicle power management strategy. For example, utilization of the energy storage device will be determined by the vehicular power management strategy. However, this fact directly affects the regenerative braking receptivity of the energy reservoir (In case of the fully charged condition, extra energy cannot be accepted by the energy storage device). Similar to that, there are many cases in

which both strategies need to be agreed to enhance the vehicles performance. Due to this reason a survey on power and energy management control strategies for electric/hybrid electric vehicles is discussed in the following section.

2.2.2 Power management for hybrid electric vehicles (HEV)

A variety of approaches are studied for power and energy management of hybrid electric vehicles applications. Operating efficiency of each system in a vehicle has an effect on the global efficiency of the drivetrain system. Therefore, each system in the hybrid electric vehicle must be controlled appropriately to achieve their higher performance. It should be noted here that, higher performance of individual systems does not guarantee the global efficiency of the vehicle. This urged the employment of a higher level supervisory controller to feed necessary control inputs to the individual system controllers. This results in the increase of the global efficiency significantly. In fact, power and energy management research is dealing mainly with supervisory control system design.

Optimal control techniques for hybrid electric vehicles are investigated in several research works. Dynamic programming (DP), and quadratic programming are common techniques in this category. Dynamic programming is implemented to maximize the fuel efficiency of HEV's [24, 25]. This approach requires the prior knowledge of the entire driving scenario to perform the control action [25], [24]. The computational burden of the dynamic programming approach has been complained by several researchers [26], [27] and [28]. Due to reasons of impracticality, it is almost impossible to implement it in real systems. However, most of the researchers suggested considering the outcome of this optimization analysis as a benchmark to develop other implementable control methods. [26] performed an off line simulation study of a parallel hybrid electric vehicle (PHEV). Here the author utilized the DP approach to find the optimal control actions for the gear shifting sequences as well as the power splitting ratio between IC engine and electric motors.

Heuristic control techniques such as fuzzy logic, rule based control, and neural networks are another growing area for power management applications in HEV's.

These control techniques are developed based on the human knowledge rather than analytical methods. As a result of this, it is fairly easy to understand and it can be implemented in real systems. Particularly, it is a useful technique to handle highly nonlinear systems with minimum control effort. Due to this reason, it is also described as an intelligent control method. However, the control accuracy will vary depending upon the designer's knowledge of the system. Therefore, it requires a human expert to design the control system for an application.

A number of studies has been conducted on fuzzy logic based power and energy management for hybrid electric vehicle in different contexts. [29] introduced a torque distribution control strategy for a parallel hybrid city bus using a fuzzy logic controller. Here 130 rules were created in the Mamdani based fuzzy model to perform the control action. Two different standard driving cycles are simulated and results are compared with the rule based control strategy to verify the effectiveness of the fuzzy logic control approach. However, this study neglects the power electronics involvement. In reality, power converters play a critical roll on effective energy conversion [30] and their operating efficiency is significant to determine the fuel economy. In addition to that, although the design rules are considering the basic operating characteristics of the drivetrain system, fine details of them also need to be incorporated to increase the accuracy of the model.

Similar to [29], [31] also employed fuzzy logic intelligent energy management agents to enhance effective torque sharing in the drivetrain systems and state of charge management of the battery. The ability to handle nonlinear, multi domain systems with minimum processing time is the potential advantage of the fuzzy logic control approach, which is highly appreciated in several research works. It is emphasized in [31] that, the fuzzy logic approach achieves a higher degree of accuracy compared with the rule based approach. A fuzzy logic based driver advisory system is designed in [32] to provide the essential feed back to the driver, which eventually increases the fuel efficiency while achieving performance requirements.

A fuzzy logic based energy management strategy for a PHEV is presented in [33], [34] and [35]. The efficiency maps of the IC engine, electric motor, transmission and battery are used to design the control system. Based on the power requirement, accelerator pedal position, vehicle speed, and the state-of-charge of the battery, the power sharing between the IC engine and the electric motor is per-

formed. However the authors assumes that, systems in the hybrid electric vehicle follow their efficiency map under all kinds of operating conditions. However, the effects of cold start, frequent start-stop characteristic of the engines, speed-torque characteristic of the electric motor, the effect of temperature on charging efficiency of the battery system, and the requirements of power electronic systems are not considered in this study. In reality, these issues are playing a critical roll to restrict the fuel economy [36].

[37] Proposed an intelligent energy management agent (IEMA) for parallel hybrid electric vehicles (PHEV). Here IEMA distributes the torque between the IC engine and the electric motor. Identifying the driving situations and performing an appropriate control action is the primary task of this IEMA. To achieve this task, IEMA employs a driving information extractor (DIE), driving situation identifier (DSI), fuzzy torque distributor (FTD), and state-of-charge compensator of the battery (SCC). Here the DIE extracts the statistical futures of the driving characteristic, which is used for the future decision making process. Based on DIEs information, DSI identifies the driving characteristic such as road conditions, driving style, and driving trend. SCC maintains the state-of-charge level in the battery to fulfill all kinds of driving requirements. DSI and SCC provides the essential information to FTD to perform an appropriate control action. A vast rage of practical issues related to driving conditions are included in this study. However, incorporating vehicle dynamic and drivetrain limitations will provide more realistic insights, this will lead to the design of higher performance hybrid drivetrain systems.

Another implementable near optimal control method called equivalent consumption minimization strategy is developed by [28]. The primary benefits of this approach are compared with heuristic and optimization control approaches. Here a cost function is developed and the control action is designed to optimize the resources which will lead to minimization of the total cost. Similar to that, [34] suggested a method to optimize the performance of subsystems in the hybrid's drivetrain's. [29] has applied optimal methods, and intelligent methods for multiple energy control systems. A real time control for power distribution and optimization of fuel cells and their associated energy storage (supercapacitor) is studied by [38]. Here an equivalent consumption minimization strategy is utilized for the fuel optimization of the power train.

The importance of component sizing and subsystem scaling of a fuel cell hybrid vehicle is analyzed in [39]. The author addresses the problems associated with hardware, and control system design issues. Here power management system design and component sizing process are performed simultaneously. This combined analysis approach provides an opportunity to design a suitable powertrain and control system. The standard UDDS driving cycle is considered as the benchmark performance requirement in this analysis. However, it is hard to say if most of the drivers will follow the standard driving cycles [40] in reality. Therefore, it is difficult to design a hybrid drivetrain with suitable control system to fulfill all kinds of driving requirements.

As a simulation tool, [41] addressed the potential capability of the QSS- toolbox for hybrid electric vehicular power train design. Various simulations are performed and compared with the real data to demonstrate the reliability of the tool box. The author suggested that it has the capability to simulate various system structures with different parameters to design supervisory control algorithms.

Practical issues such as, driving trend, driving style, and road types play significant rolls in power and energy management problem in hybrid electric vehicles [37]. In a controversial statement, [42] articulates that, it is no matter which control approach is employed for the power and energy management problem, driving cycle determines the energy efficiency and performance characteristic of the vehicle. To support this argument, the authors point out that, a particular control strategy performs entirely differently for different driving requirements.

2.3 Energy storage devices

Energy storage also plays a vital role to limit the kinetic energy recovery and propulsive performance of drivetrain systems. A broad survey on energy storage devices for electric propulsion applications are covered in this section. Basically, this survey discussed commonly used electrical energy storage devices and their operating limitations.

At the beginning of this discussion, it is worth emphasizing the power flow characteristics of electric propulsion systems. Depending upon acceleration rates, deceleration rates, and cruising requirements, power flow of the electric propul-

sion system varies unpredictably [43]. These requirements force the energy reservoir to handle such situations. In addition to that, the electric only driving range is purely dependant upon the storage capacity of the electric energy reservoir. Therefore, an energy storage device should be able to satisfy these two requirements to provide better performance.

An electric battery, ultracapacitor, and flywheel system are commonly used energy storage devices for this application [6]. Although electric batteries hold higher energy density, their lower power density rank them down compared with other alternatives [31]. It can be seen from table 2.2 that, electric batteries hold higher specific energy density compared with the ultracapacitors (UC). In contrast, Ultracapacitors and flywheels show excellent peak power handling capabilities compared to batteries. In the same table it also can be noticed that, Ultracapacitors hold higher specific power density than the electric batteries. Meeting the propulsive power, energy requirements by utilizing only battery or UC will result in oversize of the energy storage. Side effects of this process such as, extra weight and packaging issues take this problem into another dimension. This will again affect systems efficiency, where additional amounts of propulsive power need to be supplied to carry all the extra weight.

Ultracapacitors (UC) share similar properties to batteries and conventional capacitors [6]. The approximate energy density of a UC is close to 20% of the battery's energy density. Also UCs do not require much maintenance compared to batteries. Generic advantages and disadvantages of Ultracapacitors are depicted in table 2.3. Study of this paper suggests that for a short runtime peak power handling application, UC's and flywheels are suitable candidates. As illustrated in figure 2.2, instantaneous charging-recharging capability, maintenance free and noiseless operation, higher power density, and the economically viable nature of ultracapacitors rank as the number one peak power handling energy reservoirs [6].

From the view point of regenerative braking, [8] and [44] suggested that, ultracapacitor banks are a better option for kinetic energy recovery during braking. The author refers to the research work carried out by [45, 46] to explain the primary limitations of batteries for kinetic energy recovery applications. Poor power density of the battery systems is highlighted as the major drawback to employing them as receptive energy reservoirs in this application. Also the author studied

Table 2.2: States of electrical energy storage systems (reproduced from [1] and [2])

Technology	SE(Wh/kg)	PP(W/kg)	Ene eff%	Life cycle	US-Dollar
Lead-Acid	35-50	150-400	>80	500-1000	120-150
Nickel/cadmium	40-60	80-150	75	800	250-350
Nickel/Iron	50-60	80-150	65	1500-2000	200-400
Nickel/Zinc	55-75	170-260	70	300	100-300
Nickel-Metal-Hybrid	70-90	200-300	70	750-1200	200-350
Aluminum/air	200-300	90	<50	-	-
Iron/air	80-120	90	60	500	50
Zinc/air	100-200	30-80	60	600	90-120
Zinc/Bromine	70-85	90-110	65-75	500-2000	200-250
Vanadium redox	20-35	110	75-85	-	400-450
Sodium/Sulfur	150-240	230	85	800	250-450
Sodium/Ni/Cl	90-120	130-160	80	1200	230-345
Li-ion-sulfur	100-130	150-250	80	1000	110
Li-ion	80-130	200-300	>95	1000	200
Li-ion high power	85-95	4000	-	-	-
Li-ion high energy	135-150	600	-	-	-
Ultracapacitors	2.3	2900	-	500,000	-

both flywheel systems and ultracapacitors to obtain the suitable candidate for regenerative braking applications. Due to the short braking duration and peak power handling requirements, [6] suggested that the faster charging-discharging dynamics of the ultracapacitors is preferred to the flywheel systems for the regenerative braking application. The economically viable nature of ultracapacitors is also another advantage, which make them attractive alternatives.

The primary differences between the role of the battery in hybrid electric vehicles are compared with other battery application domains in [43]. The author suggested that, due to the frequent charging and discharging characteristic of the batteries in HEV's, a reengineering work on battery technology should be carried out for this application. A Comparison study on conventional capacitors, supercapacitors ,and lithium- ion batteries was carried out by [47] to evaluate the

Table 2.3: Advantages and disadvantages of the ultracapacitors

Advantages	Disadvantages
Higher charge, discharge cycles	Increasing cost with energy density
Operation in a wide range of temperatures	Low energy density
Higher power density	
Environmental friendly construction	

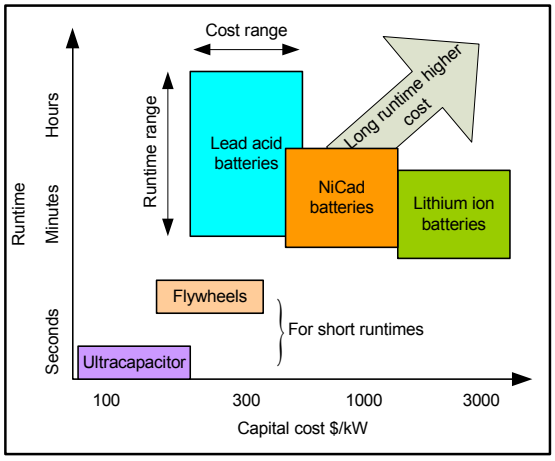

(a) Capital cost Vs run time of energy reservoirs

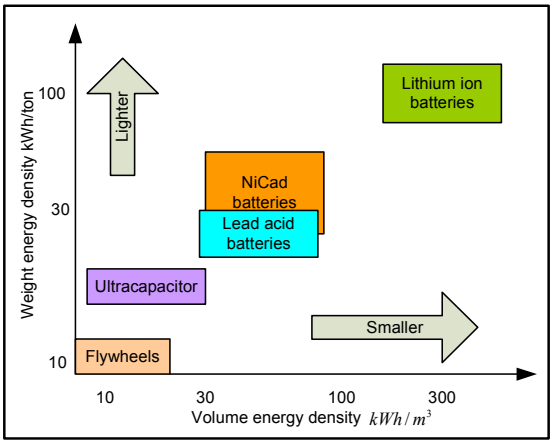

(b) Energy density variation with weight and volume

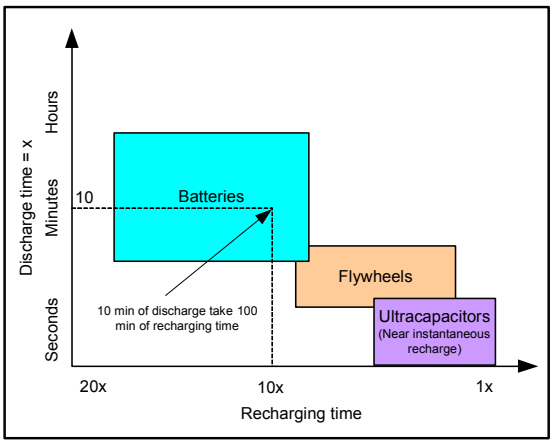

(c) Discharging time Vs recharging time comparison

Figure 2.2: (Reproduced from [6])

suitable candidates for peak power applications. Super capacitors show excellent charging and discharging characteristics and exhibits 20- 200 times greater capacitance than the conventional capacitors.

[48] addressed the feasibility of using ultra batteries as portable energy reservoirs for HEV applications. The ultra battery itself is a hybrid energy storage device, which combines the advantages of led acid batteries and supercapacitors in one unit. Therefore ultra batteries have better power and energy density characteristics. Moreover it has been proven that it shows better performance in handling peak power requirements. As design guidance, [49] introduced the power to energy ratio of the battery as a useful parameter to choose the optimum battery pack for the hybrid power train application.

Developing a hybrid energy storage device by combining a battery system as well as an ultracapacitor is investigated by several researchers [50], [2] and [51]. With the employment of suitable power management systems, peak power handling task are assigned to UC banks while the electric battery provides the average power to the system. Typical power flow characteristics and energy variation of battery and UC banks in a vehicular propulsive application are depicted in figure 2.3. The outcome of this study shows that, hybrid arrangements of electric battery and UC bank contribute significantly to an increase in the drivetrain performance and kinetic energy recovery. It also helps to extend the life cycle of the battery system. Using the Advanced Vehicle Simulator (ADVISOR)package, [52] showed that the hybridisation of battery and UC allowed the battery pack to be downsized to 70%. In summary, primary advantages of this combined arrangement of battery and UC bank can be listed as:

- Involvement of UC bank helps to down size battery system designs
- This hybrid arrangement of UC bank and battery system helps to increase the efficiency of the energy reservoir
- Battery systems are prevented from experiencing thermal stress, which extends the life and increases the storage efficiency of the battery system [43]

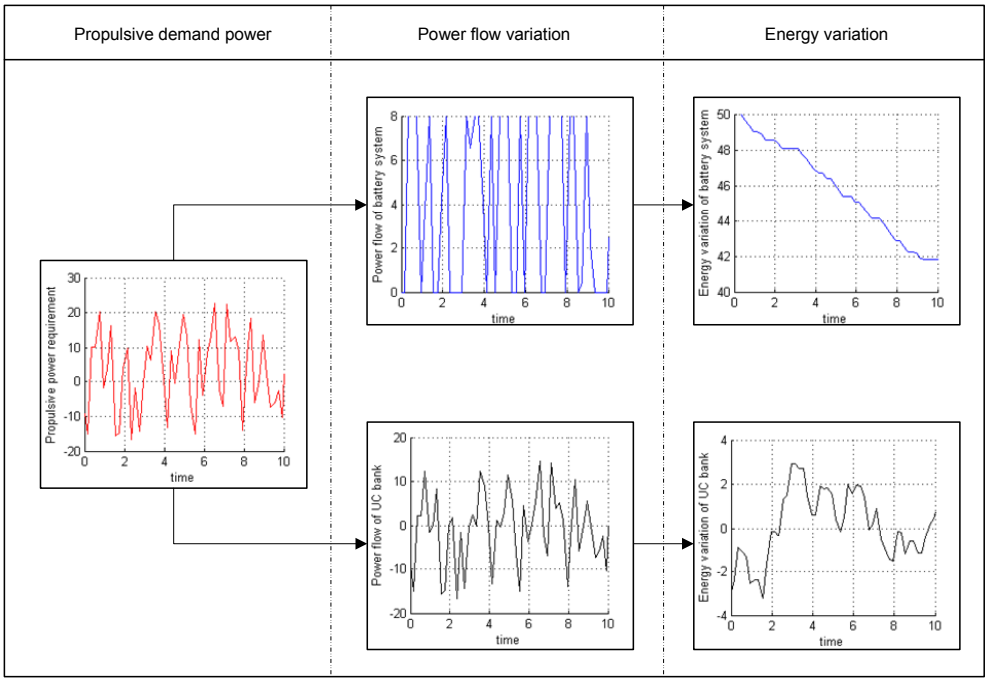

Figure 2.3: Power, energy variation of combined energy storage system in a generic driving cycle

2.4 Power converters for electric propulsion system

The voltage difference between energy storage device and load terminals needs to be controlled to convey the power from one to another. A power electronic device called a power converter functions as an intermediate system to perform this task [53]. There are two types of power converters involved with this process, buck converters and boost converters. Let us assume a case, where power needs to be transformed from the battery to an inverter. In reality, it is not necessary to maintain a positive voltage difference in between battery and electric motor. It can be either positive, zero or negative. Let us consider zero or negative voltage difference. In such situations, input voltage will be increased by the boost converter to meet an appropriate voltage to fulfill the power flow requirement. Similarly, if there is a positive voltage difference, input voltage will be minimized by the buck converter to meet the relevant voltage requirement. Due to these reasons, power converters contribute an important roll in electric propulsion systems.

Increasing the operational efficiency and extending the operating range of the power converters is the primary objective in this research domain. A variety of power converter topologies are investigated in the literature to meet these requirements. Mostly power converters are connected in between the electric energy source and the electric load. In the active power sharing topologies, multiple energy storage devices are also connected with power converters. Figure 2.4 shows a simple block diagram of an electric propulsion system, where battery and UC bank are arranged in a passive configuration.

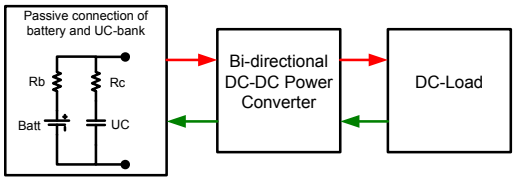

Figure 2.4: Electric propulsion system passive battery configuration

The presence of ultracapacitors regulates the battery current in this topology. This topology also provides the following benefits such as high operating efficiency, small battery pack, easy thermal management, and longer battery life [50]. Lesser terminal voltage variation also reduces the burden of the power converter. [2] provides an analysis for the optimum sizing of ultracapacitor and battery systems for this arrangement.

Power electronic design for hybrid electric propulsion systems is very challenging task for various reasons [54]. Power converters in the propulsion system needs to handle a variety of voltage and current requirements. Larger current operating conditions increase the thermal stress of the power electronic switches and passive components as well as reducing the power converters efficiency. On the other hand, larger voltage operating conditions also increase the voltage stress of the power electronic switches and passive components. Although it is technically possible to designing a power converter to achieve a wide range of voltage and current requirements, increase in weight and volume leads to packaging issues. The analysis in [54] shows the stress exerted on the active and passive components of the converter due to the operating current and voltage variation.

To improve the dynamic response of the fuel-cell and the ultracapacitor based energy storage system, [55] employs a switched mode power converter as illustrated in figure 2.5. The bidirectional buck boost power converter distributes

the power flow of the fuel-cell and the capacitor bank to the drivetrain system. During braking, it controls the charging voltage and current requirements. However this converter topology cannot operate as buck and boost converter in both directions. Due to this reason, kinetic energy recovery of the drivetrain system is limited during regenerative braking conditions. A similar type of fuel cell vehicle is also studied by [56]. Here fuel cell input is connected to the bus terminal via a unidirectional DC-DC converter. Ultracapacitors were connected directly to the DC-bus using relays. Two low pass filters were employed for the power flow control of the DC-DC converter. However, the study in this paper not gives the priority to the kinetic energy recovery of the drivertain system.

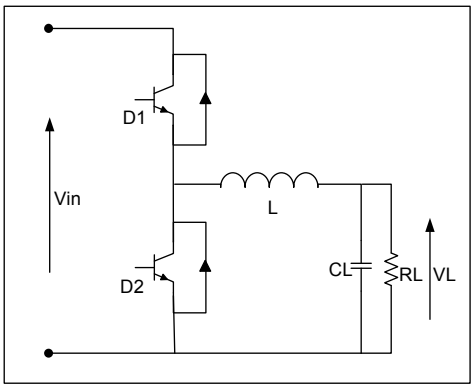

Figure 2.5: Bi directional DC-DC power converter

[57] and [58] studied a hybrid fuel cell power system, which consists of a fuel cell, an inverter, a unidirectional converter, a novel three level bidirectional converter, and a battery as illustrated in figure 2.6.a. A similar converter topology is investigated by [59]. They propose a power management control scheme, which controls the bidirectional converter in different modes of operation such as buck, boost, or shutdown. Similar to [55], these power converter topologies also have the limited access to benefit from the kinetic energy recovery during braking.

The fuel cell is connected to the DC-bus via a unidirectional converter. The battery system is connected to the DC-bus with a bidirectional buck/boost converter as illustrated in figure 2.6.b. Although it allows the power to flow in both direction, it can only function as a boost converter during battery to DC-bus power transmission. Similarly, when the power flow is from DC-bus to battery, it is functioning as buck converter. Due to the back-emf drop of the motor during braking, kinetic energy recovery is limited in this converter topology.

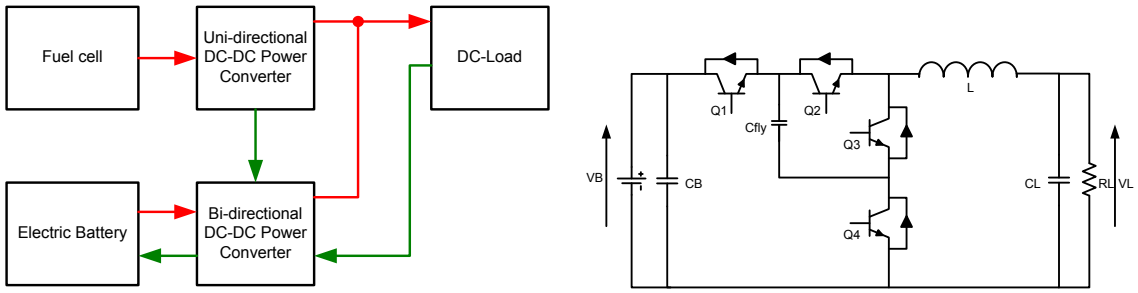

(a) Power train configuration of fuel cell hybrid electric vehicle (Reproduced from **(author?)** *[57])*

(b) Circuit diagram of the bidirectional power converter topology (Reproduced from **(author?)** *[57])*

Figure 2.6: Power converter topologies

Isolated and nonisolated bidirectional DC-DC power converters are investigated in [57] for hybrid drivetrain systems. Depending upon the voltage and current rating of the propulsion system, different convertor topology favors on efficiency enhancement. If the input-output voltage difference is larger, then isolated converters are employed in between the DC-bus and battery system. This prevents the peak current flow from one side to another. Simple structures and control schemes favors the nonisolated converters for use in smaller voltage difference applications.

Passive components sizing is another critical issue in power converter design. In general, inductance sizing of the converter is increasing proportionally with the operating voltage range of the converter [60]. Higher inductance results in a slow dynamic response of the converter. However, the novel arrangement of the three-level bidirectional converter significantly reduces the inductor size and increases the dynamic response [61]. Bidirectional converters employ voltage loop and current loop control approaches. As a design requirement, control circuits should operate the bidirectional converter freely in constant voltage mode and limited current mode.

An energy management strategy is studied by [62] for a hybrid energy storage systems, which consist a supercapacitor and battery. A bidirectional DC-DC converter is employed in between the UC bank and DC-bus. The electric battery is directly connected to the DC-bus. Supercapacitor behavior modeling and energy management strategies are the primary focus of this study. The energy management strategy is designed with a polynomial controller approach and it has been implemented in a real system. Since the battery is connected directly with the DC-bus, the voltage across the DC-bus terminal will remain constant. Therefore,

the current mode control approach is employed to handle various power flow requirements.

2.5 Discussions

In summary, electric propulsion systems and power, energy management concepts have been approached in various ways. A variety of options are suggested for different objectives and there is no consensus in technology development. Moreover, only a few implementation attempts have been made and rest of them are studied in simulation based platforms. Though, there are a few practical implementations, complete detailed descriptions of them can be rarely obtained from the literature.

Another important point is that, standard driving cycles (SDC) are considered as bench marks for performance targets and most of the research works are carried out to satisfy SDC requirements. In reality, driving cycles are highly unpredictable, which varies with the behavior of the driver, driving circumstances, and road conditions [63], [64], [65] and [40]. Correlation between the driving cycle and propulsive efficiency is rarely studied in the literature.

Most importantly, only a few research works investigate the issues related to kinetic energy recovery. It has been recorded that 20 to 30 percentage of the energy can be recovered during braking, however, the primary reasons for this limited energy recovery is not clearly described in the literature. To investigate these issues, an electric propulsion system consisting of dual braking systems (such as regenerative and mechanical braking) sourced by an ultracapacitor bank is chosen as the development frame work. To begin with, a theoretical basis needs to be established. Therefore, braking dynamics of a two axle vehicle are developed in the next chapter in the context of regenerative braking applications.

Chapter 3
Braking Dynamics and Modeling of the Vehicle

3.1 Introduction

The braking dynamics of the vehicle is described in this chapter. In reality, the vehicle is subjected to a variety of braking modes to fulfil a driving cycle. To describe the issues related to different braking requirements, longitudinal braking dynamics of the vehicle are presented, where Newton's second law of motion is used for the derivation. In addition to that, problems associated with braking due to the dynamic force transfer and terrain adhesive coefficient are also presented. Variation of braking power requirements in front and rear wheels during different braking conditions is investigated. Following the description of vehicle braking dynamics, a simulation model is developed in matlab-simulink for the validation of the braking dynamics. Using this model, a simulation study is presented to illustrate the braking force distribution variation in front and rear axles with respect to the deceleration rates and terrain conditions. Following that, the effect of drivetrain topology on kinetic energy recovery enhancement is investigated.

3.2 Forces acting on the vehicle during braking

There are several forces acting on the land vehicle during braking as illustrated in figure 3.1. Mainly these forces can be categorized into four such as, rolling resistance, aerodynamic force, gravitational force and braking force. Detailed illustration of them is described in the following sections.

The total braking force acting on the vehicle, parallel to the road surface, expressed as a composition of forces is,

$$F_{res} = (F_f + F_r + R_f + R_r + F_a + mg.sin\theta) = m.a \tag{3.1}$$

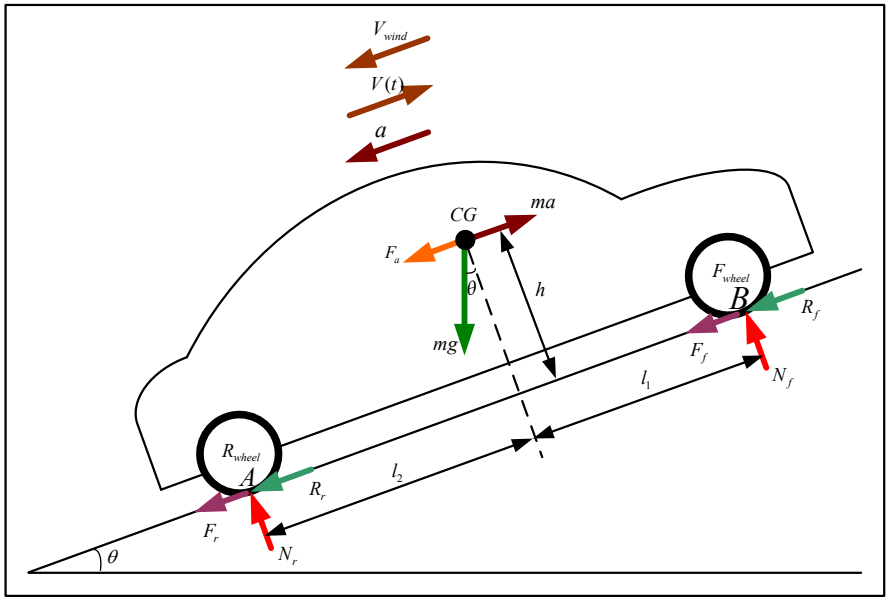

Figure 3.1: Force acting on a two axle vehicle for the braking period

where F_f, F_r are braking forces exerted by the vehicle in front and rear wheels in N, R_f, R_r are the rolling resistance forces in the front and rear wheels in N, F_a is the aerodynamic drag force acting on the vehicle in N, m is the mass of the vehicle in kg, g is the gravitational acceleration in m/s^2, θ is the road inclination angle in radian, $mg.sin\theta$ is the gravitational drag force acting on the vehicle along the longitudinal axis of the road surface in N, a is the deceleration rate of the vehicle in m/s^2.

3.2.1 Rolling resistance (R_f, R_r)

When the wheels are rotating, due to the flexibility of the tire material, there will be an elongation in the tire material with the contact surface. This effect on the tire results in the rolling resistance, which acts acting against the motion of the vehicle. The rolling resistance of the tyre can be expressed as,

$$R_f + R_r = vmg.cos\theta \tag{3.2}$$

where R_f, R_r are the rolling resistance forces acting on front and rear axles, v is the coefficient of the rolling resistance. The rolling resistance coefficient will vary with the surface condition of the terrain and tyre condition. Typical value of v will be within the limit of 0.02 and 0.04 [3].

3.2.2 Aerodynamic force (F_a)

There are two kinds of aerodynamic forces acting on the vehicle:

- Due to the viscosity of the air, there is a surface friction acting on the vehicle body
- Due to the geometrical body shape of the vehicle, there is a downwash of trailing vortices behind the body. This results in an uneven pressure distribution producing the aerodynamical drag force.

These forces are acting against the motion of the vehicle. However, the force component due to the surface friction is several magnitude less than the aerodynamic drag force [66],[30] and [3]. Therefore, only the aerodynamic drag force of the vehicle is considered for the derivation of the vehicle dynamics, where it varies with cross-sectional area, body geometry, vehicle velocity and ground wind velocity. Simplified active aerodynamic drag force can be expressed as,

$$F_a = 0.5\rho A C_D (V + V_{wind})^2 \tag{3.3}$$

where ρ is the density of the air in kg/m^3, C_D is the aerodynamic drag coefficient of the vehicle, V is the ground velocity of the vehicle in m/s, V_{wind} is the effective wind velocity against the vehicle in m/s. The drag coefficient is a geometrical property of the vehicle body design and it varies in a range of 0.3 to 0.52 for passenger cars and 0.5 to 1 for heavy duty vehicles such as container carriers and trucks [3]

3.2.3 Gravitational force ($mg.sin\theta$)

Gravitational force is considered as a static force acting on the vehicle due to the slope of the driving terrain. Uphill braking results in a positive braking force while the down hill braking result in a negative braking force. Gravitational force is proportional to the weight of the vehicle mg in N and $sin\theta$, where θ is the inclination angle of the terrain in radians.

3.2.4 Braking force (F_f, F_r)

By exerting a negative braking torque in the wheels, this braking force is created to reduce the speed of vehicles. Unlike the aerodynamic force, rolling resistance and gravitational force, braking force can be internally controlled by the driver. The braking forces acting on the front, rear wheels are illustrated by F_f and F_r in the figure. Maximum applicable braking force holds a relationship with the terrain adhesive coefficient μ as,

$$\hat{F}_f + \hat{F}_r = \mu mg.cos\theta \tag{3.4}$$

where $\hat{F}_f$ is the maximum applicable front wheel braking force in N, $\hat{F}_r$ is the maximum applicable rear wheel braking force in N. In conventional vehicles, this force is exerted by the hydro mechanical braking system consisting of a disc or hub friction pad which is actuated by a hydraulic calliper[67], where the kinetic energy of the vehicle is dissipated as heat in the brake pad.

A hybrid electric vehicle combines an electrical and hydro mechanical braking system to produce the braking force [68]. Depending upon the drivetrain configuration (such as front wheel drive, rear wheel drive) of the vehicle, driving wheels incorporate both hydro mechanical and electrical braking systems while driven wheels are only integrated with the hydro mechanical braking systems.

3.3 Vehicle braking dynamics

The braking dynamics of the vehicle are derived by applying Newton's second law of motion and taking moment from points A and B in figure 3.1. Applying Newton's law yields the correlation between the longitudinal deceleration rate $\frac{dV}{dt}$, mass m and resultant braking force F_{res} as,

$$F_{res} = m.\frac{dV}{dt} = m.a \tag{3.5}$$

where deceleration rate a is in m/s^2,vehicle's mass m is in kg and vehicle's velocity $V(t)$ is in m/s. By taking moment from point A and B, normal forces acting on

front and rear axles (N_f and N_r) can be obtained as,

$$N_f = \frac{mg.cos\theta l_2 + h(m.a - F_a - mg.sin\theta)}{L} \tag{3.6}$$

$$N_r = \frac{mg.cos\theta l_1 - h(m.a - F_a - mg.sin\theta)}{L} \tag{3.7}$$

where $L = l_1 + l_2$ Maximum applicable braking force in the front axle can be expressed as,

$$\hat{F}_f = \mu\frac{mg.cos\theta l_2 + h(m.a - F_a - mg.sin\theta)}{L} \tag{3.8}$$

It should be noted from 3.8 that the front wheel braking force increases during low speed braking conditions (due to decreasing F_a). Therefore, neglecting the aerodynamic force and calculating the maximum braking force on the front wheels yields,

$$\hat{F}_f = \mu\frac{mg.cos\theta l_2 + h(m.a - mg.sin\theta)}{L} \tag{3.9}$$

From 3.1, replacing $(m.a - mg.sin\theta)$ by $(R_f + R_r + \hat{F}_f + F_r)$ and rearranging 3.9 yields,

$$\frac{\hat{F}_f}{mg} = \frac{\mu cos\theta(l_2 + vh)}{L - \mu h} + (\frac{\mu h}{L - \mu h})\frac{F_r}{mg} \tag{3.10}$$

Similarly, maximum applicable normalized rear wheel braking force can be derived as

$$\frac{\hat{F}_r}{mg} = \frac{\mu cos\theta(l_1 - vh)}{L + \mu h} - (\frac{\mu h}{L + \mu h})\frac{F_f}{mg} \tag{3.11}$$

For the optimum braking condition, both the front and rear wheels should be fully utilized and in this condition normalized front, rear wheels braking forces can be expressed as,

$$\frac{\hat{F}_f}{mg} = \mu cos\theta\frac{l_2 + h(\mu + v)}{L} \tag{3.12}$$

$$\frac{\hat{F}_r}{mg} = \mu cos\theta\frac{l_1 - h(\mu + v)}{L} \tag{3.13}$$

Let us call 3.12 as $C4$ and 3.13 as $C2$. It should be noted here that, under the maximum braking force conditions tyres are about to slide on the road. Therefore, increasing braking force after this point will lead to a wheel lockup and the loss of directional stability of the vehicle. As a result of this, applied braking force must be always less than or equal to the maximum braking conditions. Braking force distribution between the front and rear axles without wheels locking is determined by the above criteria. This design objective is achieved in conventional vehicles by employing hydraulic cylinders with different cross sectional areas or by applying different pressure in front, and rear wheels[67] and [3]. The involvement of the electric braking system in the hybrid electric vehicle creates a great complexity on the control system design for the braking system. Here both hydro mechanical and regenerative braking systems should be coordinated appropriately to achieve the safety braking force criteria while increasing the kinetic energy recovery [69].

The drivetrain architecture (front wheel drive, rear wheel drive and four wheel drive) of the vehicle will determine the location of the regenerative braking system [2]. For example, consider a front wheel drive vehicle, where the regenerative braking system is integrated with the front wheels only. In addition to that, hydro mechanical brakes are also integrated in the front and rear wheels, which supplies the surplus braking force demand. To increase the kinetic energy recovery of front wheel drive vehicles, the use of the electric braking system should be maximized. However, under some terrain conditions, a significant amount of braking force should be given to the rear wheels to achieve an expected deceleration rate while ensuring the stability and steering control of the vehicle (either front or rear wheels should not be locked up). This results in a significant energy dissipation in rear the wheels, which minimizes the kinetic energy recovery of the vehicle. In addition to that, some braking conditions require extra braking force in the front wheels; it cannot be supplied by the electric braking system alone. Therefore the surplus braking force requirement will be supplied by the hydro mechanical braking system; this also leads to a further decrease in kinetic energy recovery. These factors affect critically the regenerative braking of the vehicle in different braking conditions.

3.4 Braking power

The braking power required at an arbitrary time t during the braking event can be expressed as,

$$P_b(t) = (F_f + F_r)V(t) \tag{3.14}$$

where $P_b(t)$ is the braking power demand in W, $V(t)$ is the velocity of the vehicle in m/s at time t. As it has been emphasized earlier, due to the dynamic force transfer of the vehicle there is a force share between the front and rear wheels. This results in a braking power distribution between front and rear wheel's. Therefore the front and rear wheels braking power can be expressed as (where endogenous and exogenous effects of the system were not considered),

$$P_f(t) = F_f V(t) \tag{3.15}$$

$$P_r(t) = F_r V(t) \tag{3.16}$$

Therefore, the percentage of the power lost in a front wheel drive vehicle can be expressed as (provided that all the front wheel braking power can be recovered),

$$\%P_{lost} = \frac{F_r}{F_r + F_f} \times 100\% \tag{3.17}$$

However, due to the power/ torque handling limitations of the electric motor, some braking occasions require the involvement of the mechanical braking system in the front wheels also. Therefore F_f can be further expanded into 3.18,

$$F_f = F_{f-regen} + F_{f-mech} \tag{3.18}$$

Based on this constraints, the regenerative braking power of a front wheel drive vehicle can be expressed as,

$$P_R(t) = (ma - mg.sin\theta - F_r - F_{f-mech} - vmg.cos\theta - F_a)V(t) \tag{3.19}$$

It should be noted from 3.20 that, the regenerative braking power varies with respect to the deceleration rate, the vehicle's velocity and the involvement of the

hydro mechanical braking system in the front, and rear wheels.

For an example, assume a braking scenario, where the vehicle is braking from an initial velocity U to a final velocity V. Therefore the change in kinetic energy of the vehicle can be written as (neglecting the energy accumulated in the rotational mass),

$$\Delta E = E_U - E_V = \frac{1}{2} m(U^2 - V^2) \tag{3.20}$$

where ΔE is the kinetic energy drop of the vehicle in J, E_u and E_V are kinetic energy of the vehicle in J at velocity U and V. Defining the regenerative braking efficiency as the ratio between the electric braking energy over change in kinetic energy of the vehicle yields,

$$\eta_R = \left| \frac{\int_{t_U}^{t_V} P_R(t)dt}{\Delta E} \right| \times 100\% \tag{3.21}$$

where t_U is the time at the start of the braking action when the vehicle longitudinal velocity is equal to U, t_V is the time at the end of the braking action where the vehicle longitudinal velocity is equal to V, η_R is the regenerative braking efficiency of the vehicle. However, it does not mean that this percentage can be accumulated in the energy storage. Operating efficiency of the electric motor, power converter, transmission system, and the energy storage will minimize this percentage further. Figure 3.2 illustrates the braking system in a front wheel drive vehicle and its kinetic energy recovery path. It illustrates the subsystems in the kinetic energy recovery path, where the power dissipation is taking place.

3.5 Simulation model

With the braking dynamic equation described above, a simulation model of a front wheel drive vehicle is constructed in the matlab-simulink environment. This model serves as a platform to simulate braking scenarios in different terrain environments. With this result, issues related to the electric propulsion system sizing can be performed for the energy recovery of hybrid electric vehicles. Correlation between the braking distance and kinetic energy recovery is another

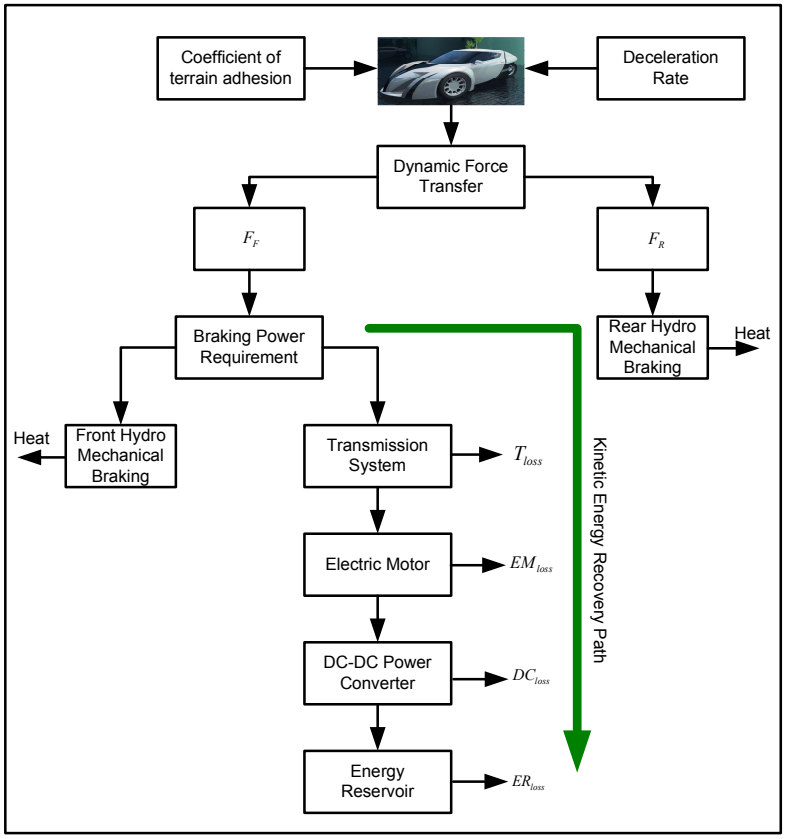

Figure 3.2: Kinetic energy recovery and its limitations

important factor, which is investigated using this model. This model also serves as a platform for experimentation and investigation of the effects on the kinetic energy recovery for some new braking strategies. Figure 3.3 shows the block diagram of the simulation model, where the error of the velocity profile is given as the input variable. Apart from that, information about the vehicle and terrain are also given to the braking system model. Cross sectional area of the vehicle A in m^2, aerodynamic drag coefficient C_d, height of the center of gravity h in m, wheels base l_1, l_2 in m, mass of the vehicle mg in kg and tyre friction coefficient v are the vehicle parameters. The coefficient of adhesion of the terrain μ, inclination angle of the road θ and ground wind vector V_{wind} in m/s are the external factors considered for the simulation.

Based on the input information, this model produces the following output velocity profile, deceleration rates, Front/rear wheels braking forces, front/rear wheels braking power, braking distance, recoverable energy and dissipated energy are obtained as the output variables.

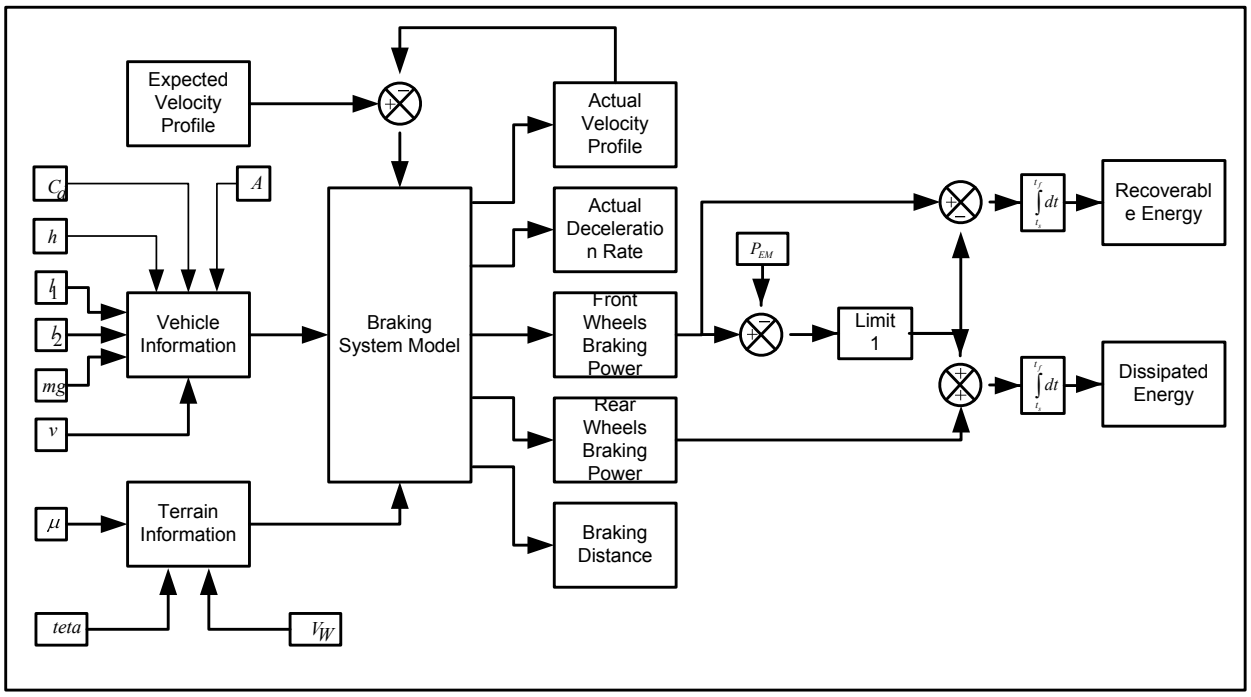

Figure 3.3: Simulation model of the vehicle

To facilitate the understanding of the braking force distribution problem, a simulation study is conducted by varying the terrain adhesive coefficient and deceleration requirement of the vehicle. Information about the simulated vehicle and terrain are listed in table 3.1.

For smaller rolling resistance v, 3.1 can be further simplified as

$$\frac{(F_f + F_r)}{mg} + sin\theta = \frac{a}{g} \tag{3.22}$$

Let us call 3.22 as $C1$.

Figure 3.4 illustrates the maximum front/rear wheels braking force distribution in different coefficients of terrain adhesion. here, 3.5 is depicted by $C3$.

Optimum normalized braking force distribution between front, and rear wheels are depicted by $C3$ (eq: 3.5). Maximum normalized front wheel braking force variation with deceleration rate is depicted by $C2$ and maximum normalized rear wheel braking force variation with deceleration rate is depicted by $C4$. As an example, $S(FW_d)$, and $S(RW_d)$ represent optimum brake sharing ratios for front,

Table 3.1: Information about the simulated vehicle parameters and terrain

Mass of the vehicle (m)	$1500kg$
Rolling resistance of tires (ν)	.02
Aerodynamic drag coefficient (C_D)	.3
Front area coefficient (A)	$2.3m^2$
l_1	$1m$
l_2	$1.7m$
h	$.6m$
Coefficient of terrain adhesion (μ)	0.1 *to* 0.8
Terrain inclination angle (θ)	0^0
Speed variation of the vehicle	30 *to* $0m/s$
Deceleration rate (a)	(0.1 *to* 0.8)g

and rear wheel drive vehicles, where the vehicle is expected to brake with a deceleration rate of $0.4g$ in a terrain adhesion μ of 0.5. In this example, front wheel drive vehicles requires only 10% of the rear wheels braking force while rear wheel drive vehicles require 65% of the front wheel braking force to achieve the expected deceleration rate in the given road condition. This implies that the front wheel drive vehicles can maximize the utilization of the regenerative braking system more than the rear wheel drive vehicles.

Average values of general terrain adhesive coefficient are depicted in table 3.2. It shows that a real time driving cycle can go through variety of terrain conditions, which critically affect the kinetic energy recovery efficiency. If F_b' is the required braking force to achieve a deceleration rate a' in a terrain adhesion μ', then F_b' must be less than or equal to $\mu' mg.cos\theta$. Otherwise, the deceleration rate a' cannot be achieved in this particular terrain. Even if $F_b' \leq \mu' mg.cos\theta$, braking force sharing ratio between the front and rear wheels will vary with respect to the μ' value. This factor is critical to design the drivetrain architecture of the vehicle to enhance kinetic energy recovery. To investigate the braking split ratio for different terrain adhesion μ for front and rear wheel drive vehicles for different deceleration rate a, a simulation study is performed and results are illustrated in figure 3.5.

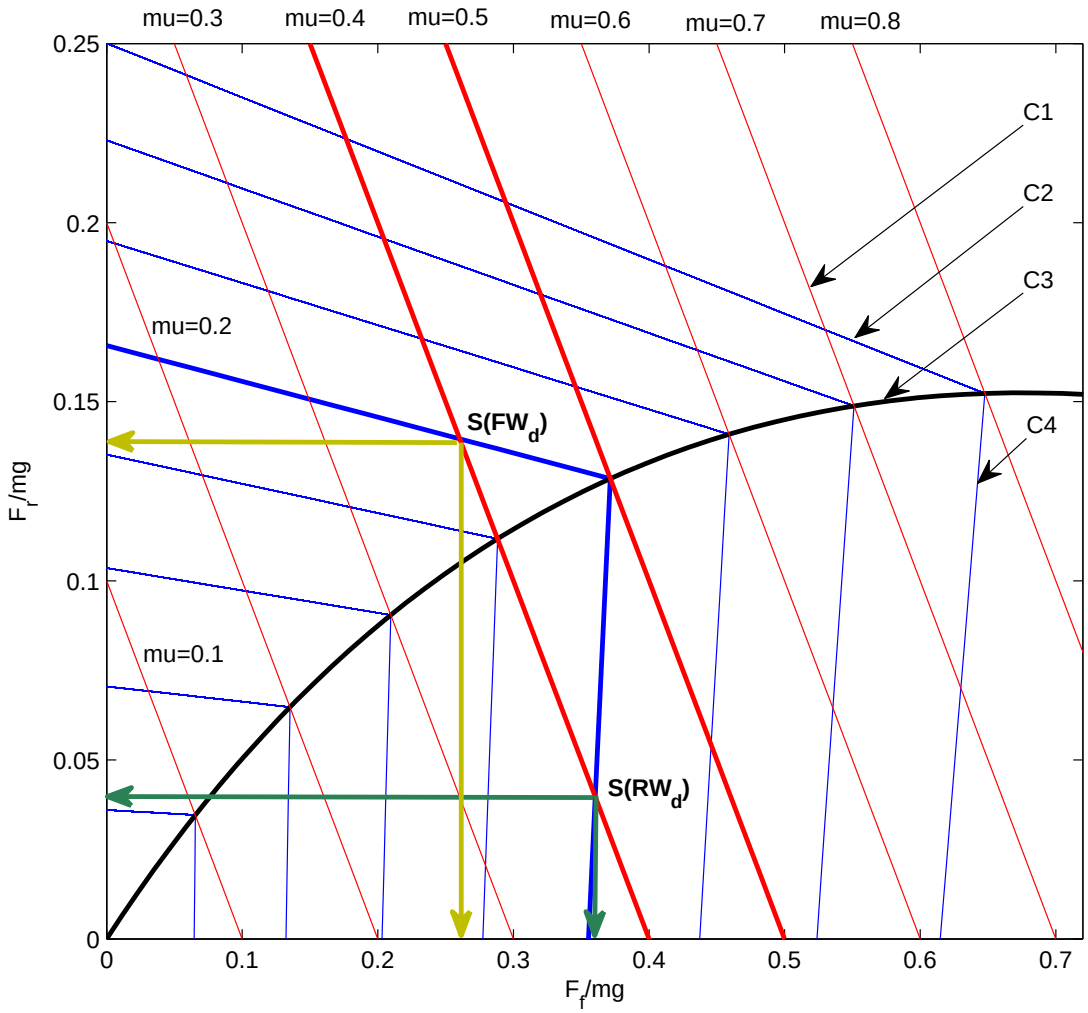

Figure 3.4: Front, rear wheels braking force distribution with respect to different coefficients of terrain adhesion

As we can see from the figure, utilization of front axle brakes in front wheel drive vehicles is significantly higher than the utilization of rear axle brakes in rear wheel drive vehicles. Comparatively, front wheel drive vehicles require lower terrain adhesion than rear wheel drive vehicles to fully utilize their relevant brakes. This shows that, front wheel drive vehicles are more suitable for kinetic energy recovery than rear wheel drive vehicles.

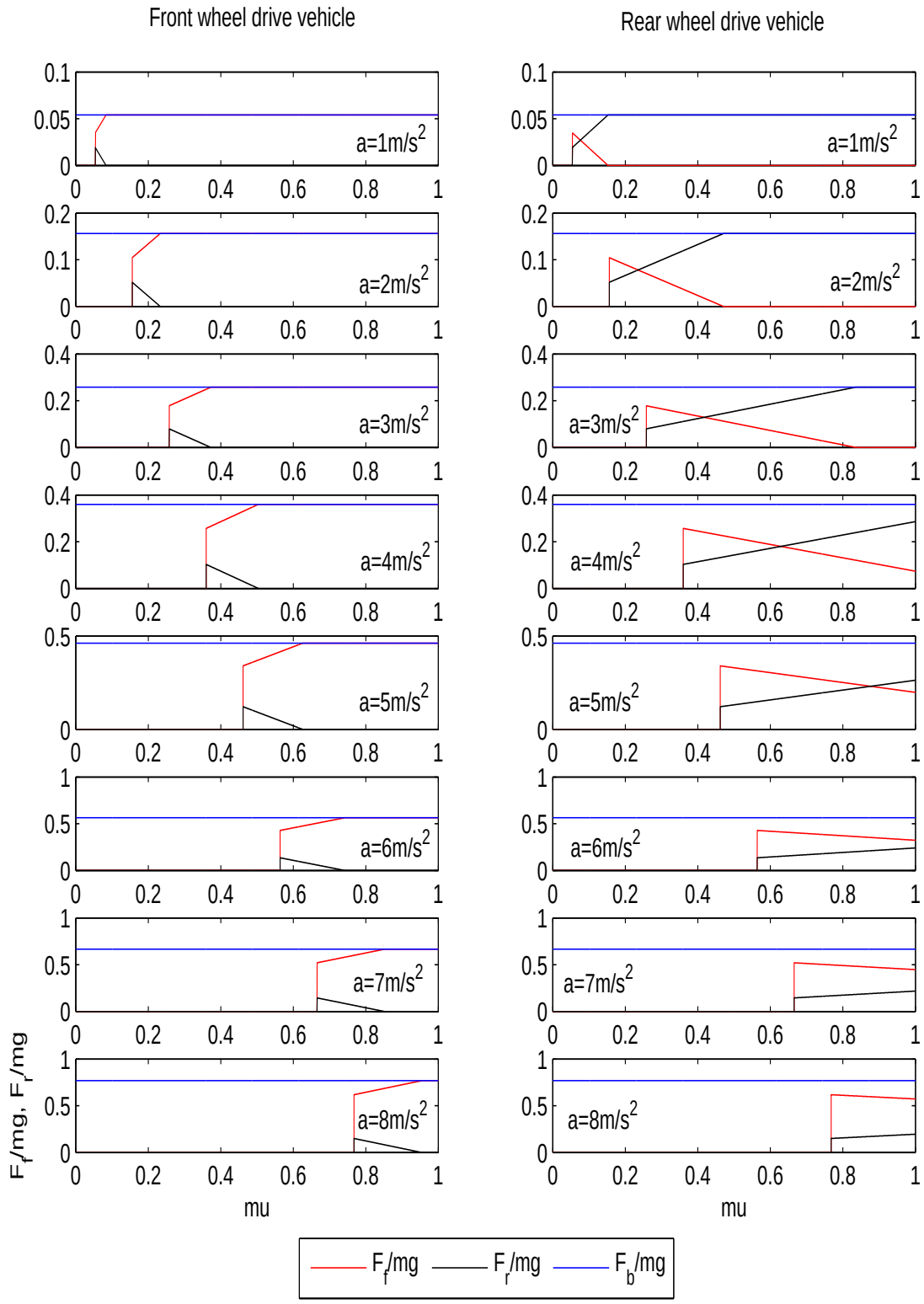

Figure 3.5: Braking force distribution in front, rear wheel drive vehicle in different terrain adhesion and deceleration rates where F_b/mg is the required braking force to achieve the specified deceleration rate at the given terrain adhesive coefficient

Table 3.2: Average values of coefficient of terrain adhesion (taken from [3])

Terrain condition	Peak value μ_p	Sliding value μ_s
Asphalt and concrete (dry)	0.8 - 0.9	0.75
Asphalt (wet)	0.5 - 0.7	0.45- 0.6
Concrete (wet)	0.8	0.7
Gravel	0.6	0.55
Earth road (dry)	0.68	0.65
Earth road (wet)	0.55	0.4-0.5
Snow (hard-packed)	0.2	0.15
ice	0.1	0.07

3.6 Summary

The effect of dynamic force transfer on kinetic energy recovery enhancement of two axle vehicles is investigated in this chapter. It has been shown that, different road adhesion levels limit the achievable maximum deceleration rates and determine the braking torque/power distribution ratios in between the front/rear axles. Although, if the vehicle have a sufficient electric propulsion system to handle the various braking power requirements, it is likely to employ pure regenerative braking during all kind of braking conditions. Here drive train topology is also playing a vital roll on kinetic energy recovery enhancement. The presented simulation based analysis shows that, front wheel drive vehicles hold better kinetic energy recovery potential than rear wheel drive vehicles.

Chapter 4

Braking Profile and Vehicular Brake Power Distribution

4.1 Introduction

Issues associated with the deceleration rates and braking power variation are described in this chapter. Although the effect of deceleration rates on kinetic energy recovery is analyzed in the previous chapter, braking power variation of the vehicle is not considered in detail. This chapter investigates the correlation between the user/operator braking profile and brake power distribution throughout the braking process for manned/unmanned ground vehicles. Here the braking profile is defined as the applied deceleration rate to achieve the required velocity profile with respect to time. The brake power distribution is defined as the variation of the braking power requirement with respect to the time to achieve a desired braking profile. This study investigates:

- How a braking profile will affect the brake power distribution?
- How a braking profile can be utilized to achieve a desired brake power distribution for enhancement of kinetic energy recovery?

It is intuitive to ask, why the brake power distribution of a vehicle is important for kinetic energy recovery? Why is it not possible to design a pure regenerative braking system? What are the other limiting factors for the regenerative energy harvest in electric propulsion systems?

4.2 Deceleration profile and braking power

Fundamentally, the braking power requirement of the vehicle will vary with the following three parameters :

Table 4.1: Vehicle parameters

Mass of the vehicle	$1500kg(Loaded)$
Rolling resistence of the tire (v)	.02
Aerodynamic drag coefficient	.3
Front area coefficient	$2.3m^2$

- Mass of the vehicle
- Velocity of the vehicle
- Deceleration rate of the vehicle

It can be written mathematically as 4.1.

$$P_{braking} = mv\frac{dv}{dt} \tag{4.1}$$

where $P_{braking}$ is the braking power, m is the vehicle mass, v is the vehicle velocity, and $\frac{dv}{dt}$ is the deceleration rate of the vehicle.

Generally, it can be assumed that the vehicle mass remains constant for a given driving mission. However, vehicle velocity and deceleration rates vary with braking requirements which determines the braking power variation. To demonstrate the correlation between the braking power requirement, deceleration rate and the velocity variation, a vehicle with the parameters shown in table 4.1 is simulated in a matlab simulink based kinematic model. As the boundary conditions, the vehicle is expected to brake with four different deceleration rates from a velocity of 30 m/s to 0 m/s . The brake power distributions to fulfill these braking objectives are depicted in figure 4.1.

It can be noticed from 4.1 that, the deceleration rate and velocity of the vehicle are key factors which determine the braking power requirement. Depending upon the deceleration rate and velocity, the variation of the braking power requirement is significant. The effect of the deceleration rate on braking duration is depicted in figure 4.2. It can be noticed from figures 4.1 and 4.2 that, heavy

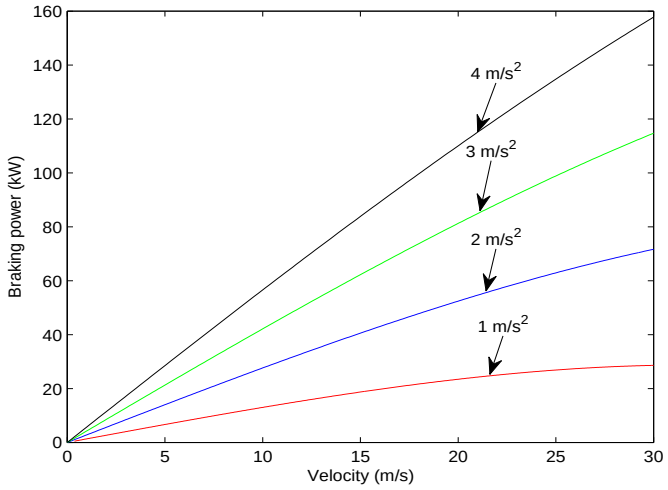

Figure 4.1: Braking power variation of the vehicle with respect to deceleration rate and velocity

deceleration requires more braking power for shorter duration while mild deceleration requires lower braking power for longer duration. The braking system in the hybrid electric vehicle should be able to fulfill a wide range of braking requirements. Since the idea of the regenerative braking system in the hybrid electric vehicle is to enhance the regenerative energy during braking, it is critical to design an appropriate electric propulsion system to handle a variety of braking requirements, while maximizing the regenerative energy harvest. However, as described in the previous chapter, it is not feasible to design a pure regenerative braking system to fulfill all kinds of possible braking scenarios.

At this moment it is worth discussing the issues related to the electric propulsion system sizing for vehicular applications. In theory employing an excessively large electric propulsion system in the vehicle will recapture all the available kinetic energy during braking. However, it is impractical to utilize a large electric propulsion system for the following reasons:

1. It increases the mass of the vehicle, which deteriorates the fuel economy as it must carry the extra mass for all driving conditions [68] and [41].

2. It requires a sufficiently large electric energy reservoir to fulfill all kinds of braking power requirements. Since the weight and volume of the energy

reservoir is proportional to its capacity, it may limit the available user space of the vehicle [70] and [66].

3. The power electronic system also needs to be designed to meet all power requirements and this results in a weight and volume increment [71].

4. Apart from that, economical reasons also significantly constrain implementation.

Due to these negative effects, it is not desirable to integrate a sufficiently large electric propulsion system into hybrid electric vehicles to meet the all possible braking power requirements.

The operational characteristic of the electric propulsion system is an important factor, which determines the regenerative braking performance [72], [73] and [1]. The following section describes the primary limitations of the electric propulsion system for regenerative braking applications. The properties of the electric motor and its operational characteristics are considered to address this problem.

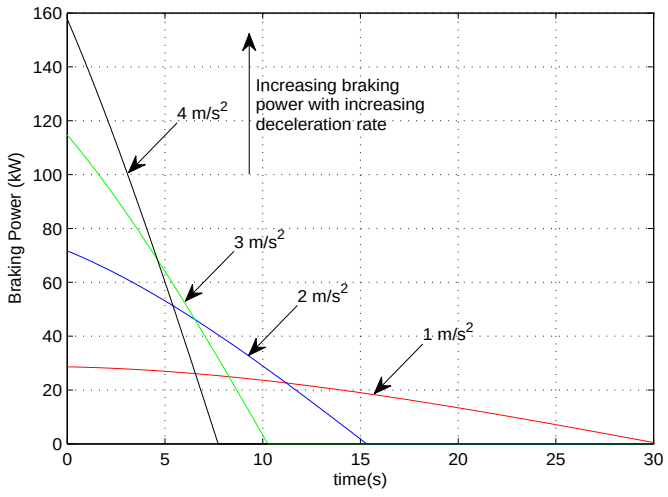

Figure 4.2: Braking power distribution over the time with respect to deceleration rates of the vehicle

4.3 Operational characteristics of the electric propulsion system

The dual mode operational characteristic of the electric motor positively contributes to achieving fuel economy in hybrid electric vehicles by enhancing the regenerative energy [73]. However, the electric propulsion system in the hybrid vehicle is bounded by its power and torque handling capabilities, which affect the regenerative braking performance. This section investigates the correlation between the mechanical and electrical power domains. The purpose of this investigation is to define the limitations of regenerative braking systems from the view point of kinetic energy recovery and braking performance.

A simplified circuit diagram of an independently excited electric propulsion system is depicted in figure 4.3, where it is operating as a generator. Basic operational characteristic of an electric motor can be described as [2], [30] and [73]:

1. Mechanical torque of the electric motor is proportional to the current
2. Angular speed of the motor is proportional to the induced back electromotive force

It also can be written as 4.2 and 4.3.

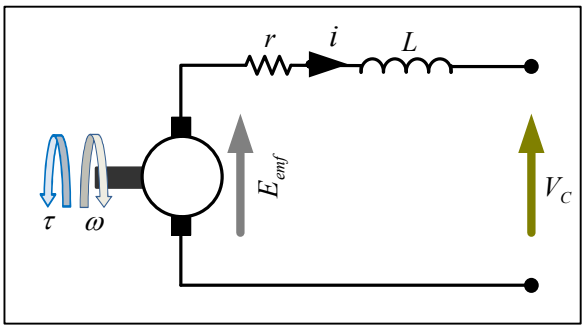

Figure 4.3: Simplified circuit diagram of an independently excited electric propulsion system

$$\tau = \kappa_i . i \tag{4.2}$$

$$E_{emf} = \kappa_v.\omega \tag{4.3}$$

where τ is the mechanical torque in Nm, κ_i is the torque constant of the motor, i is the current flow rate in A, E_{emf} is the back electromotive force, V_c is the bus terminal voltage in V, κ_v is the speed constant of the motor, and ω is the angular speed of the motor in rad/s

When we apply Kirchhoff's voltage law to the circuit, E_{emf} can be obtained as,

$$E_{emf} = V_c + i.r + L.\frac{di}{dt} \tag{4.4}$$

where L is the inductance of the motor in H.

Zero current ripple in the steady state condition yields 4.5

$$E_{emf} = V_c + i.r \tag{4.5}$$

This illustrates that, the maximum torque is limited to the maximum current rating of the motor while E_{emf} is limited to the maximum speed. The graphical representation of the speed, torque and power characteristics of a typical electric motor during regenerative braking is depicted in figure 4.4. Due to the current and power limitations, it has two operational regions; constant torque and constant power. The base speed of the motor separates constant torque ($A-B$) and constant power ($B-D$) operating regions. Since E_{emf} is proportional to the rotational speed of the motor, which is also a determining factor for the current flow in the circuit as shown in 4.5, the motor-generator cannot produce much current at low speed. Therefore torque decreases as depicted by $O-A$, at low speeds. As a result of this the braking torque requirement cannot be supplied by the regenerative braking system in low speed braking conditions.

From the application perspective, a braking system should be able to produce various braking torques regardless of the limitations of the electric motor. This

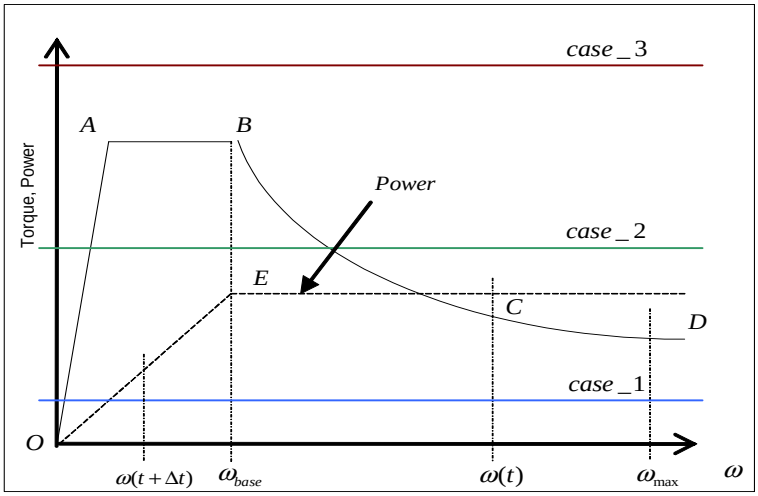

Figure 4.4: Speed, torque, and power variation of the electric motor/ generator

provides a clear explanation that a vehicle cannot rely upon a pure regenerative braking system. Instead as illustrated in the previous chapter, this problem can be solved by incorporating a secondary braking system. However, it requires an appropriate torque/power management strategy to coordinate and control the dual braking system to achieve a range of braking requirements while increasing the kinetic energy recovery. Therefore, the primary tasks of the braking system controller are categorized as:

1. Achieve the expected braking requirement
2. Under any given braking conditions, maximize the utilization of the regenerative braking

To fulfill these two requirements with the limitations of the electric motor, all the possible braking scenarios can be categorized in to three cases as depicted in figure 4.4.

Case 1 A mild braking scenario is shown here, where the required braking torque can be supplied by the regenerative braking system regardless of the velocity variation of the vehicle

Case 2 A moderate braking scenario is shown here, where depending upon the vehicle's initial speed, involvement of the secondary braking system will be determined.

Case 3 A heavy braking event is depicted in case 3, where regardless of the speed variation of the vehicle, the secondary braking system needs to be utilized to achieve the braking demand.

4.4 Hybrid electric vehicles and regenerative braking systems

In reality a driving cycle may go through various braking circumstances. Braking torque varies proportionally with the deceleration requirement of the vehicle. However, as described in the previous section, the regenerative braking system has its own limitations in fulfilling all kinds of braking torque and power requirements. Therefore, this problem can be solved easily by integrating a secondary braking system, which will supply the excess braking torque-power demand.

On the other hand, since the major objective of the regenerative braking system is recapturing the kinetic energy of the vehicle, the regenerative braking system should be given priority under any given braking condition. However, when the braking power demand increases in high speed braking conditions or when the braking torque demand increases in low speed braking conditions, a significant amount of braking effort needs to be produced by the secondary braking system. Limitations of the energy storage capacity is another constraint, which minimizes the regenerative braking performance in fully charged conditions. In such situations the secondary braking system is also employed to achieve the braking objective. Nevertheless it should be noted here that, incorrect coordination of the dual braking system further deteriorates the kinetic energy recovery. Therefore, the braking power management strategies and control system play a vital role to increase the energy recovery of the vehicle. The operating algorithm of the dual braking system in the hybrid electric vehicle is shown in the figure 4.5, where the vehicle braking power requirement will be supplied by the regenerative braking system and the mechanical braking system. The decision making procedure to operate the dual braking system is described by the following inequalities :

1. If the braking power requirement is lower or equal to the power rating of the motor-generator ($P_b \leq P_{MG}$) and if the energy reservoir is not fully charged

($E_{res} < E_{res\ max}$), then the braking power will be given by the regenerative braking system

2. If the braking power requirement is lower or equal to the power rating of the motor-generator ($P_b \leq P_{MG}$) and if the energy reservoir is fully charged ($E_{res} = E_{res\ max}$) then the braking power will be given by the mechanical braking system

3. If the braking power requirement is greater or equal to the power rating of the motor-generator ($P_b > P_{MG}$) and if the energy reservoir is not fully charged ($E_{res} < E_{res\ max}$) then the regenerative braking system will be fully utilized while the excess power ($P_b - P_{MG}$) will be supplied by the mechanical braking system

4. If the braking power requirement is greater or equal to the power rating of the motor-generator ($P_b > P_{MG}$) and if the energy reservoir is fully charged ($E_{res} = E_{res\ max}$) then all the braking power (P_b) will be supplied by the mechanical braking system only

The mathematical equation for sharing the braking torque among the dual braking system is defined in 4.6, where k_1 and k_2 are the weighting factors for the regenerative braking system and the mechanical braking system, τ_{mg} is the torque produced by the motor in Nm, τ_{hm} is the torque produced by the mechanical braking system in Nm. Therefore, a range of braking torque requirements can be achieved by varying these weighting factors. However, in order to fully utilize the regenerative braking system, these weighting factors will be calculated based on the aforementioned inequalities.

$$\tau_{brake} = k_1.\tau_{mg} + k_2.\tau_{hm} \tag{4.6}$$

From 4.6, the braking power requirement to fulfill the braking demand is extracted as 4.7,

$$P_b = (k_1.\tau_{mg} + k_2.\tau_{hm}).\omega \tag{4.7}$$

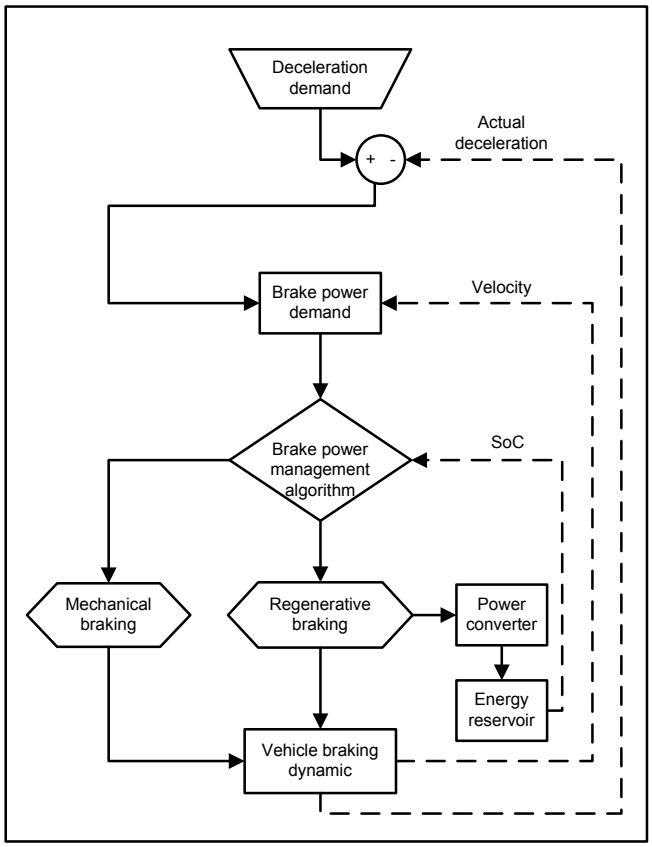

Figure 4.5: The functionality and the working principle of the dual brake system in the hybrid electric vehicle

Where k_1 and k_2 satisfy the inequality $0 \leq k_1, k_2 \leq 1$. Under any braking condition, k_1 will be given the priority to maximize the regenerative braking efficiency.

One can easily notice from 4.6 and 4.7 that, when the vehicle is braking from a high speed with higher deceleration rate, then a significant amount of braking power needs to be supplied by the mechanical braking system which will deteriorate the regenerative braking efficiency. As a result of this, most of the available energy of the vehicle is simply dissipated as heat under heavy braking scenarios (where the heavy braking scenario is defined as the braking condition, where the expected braking power cannot be supplied by the regenerative braking system alone). In contrast, most of the kinetic energy of the vehicle can be recaptured by the regenerative braking system in mild and moderate braking events. It implies that the deceleration rate and vehicle speed critically affects the kinetic energy recovery efficiency of the vehicle.

The primary objective of the braking process is to control the vehicle speed or stop the vehicle within the desired braking distance. Therefore, if it is possible to achieve a desired braking distance while employing different braking power over the time, it is appropriate to choose a brake power distribution that minimizes the utilization of the mechanical braking system and maximizes the utilization of the regenerative braking system . Since the deceleration rate and velocity of the vehicle are the key factors which determine the braking power requirement, any given brake power distribution can be produced through controlling the deceleration rate and velocity of the vehicle over the given braking distance. The influence of the deceleration profile on the brake power distribution of the vehicle and the regenerative braking efficiency is investigated in the next section.

4.5 Deceleration profile and brake power distribution

In reality, an infinite number of deceleration combinations can be produced to reduce the vehicle speed from an initial velocity U to a final velocity V within the braking distance A-B as depicted in figure 4.6. Equation 4.8 illustrates the The correlation between the braking distance S, initial velocity U, final velocity V, and deceleration rate a of the vehicle [67].

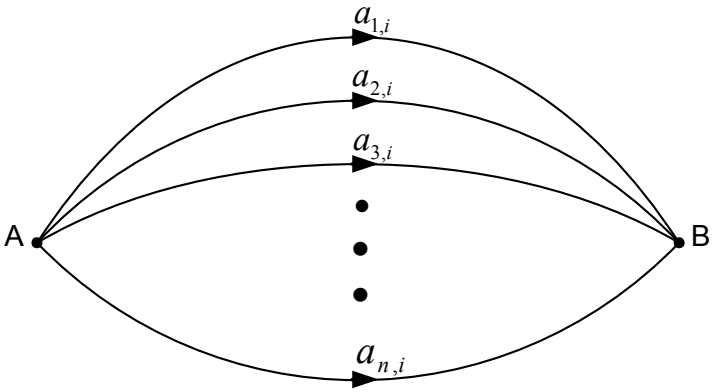

Figure 4.6: Function of deceleration rates

$$S = \frac{U^2 - V^2}{2.a} \tag{4.8}$$

However it should be noted here that, the same braking distance can be achieved through an infinite number of intermediate state combinations. Therefore 4.8 can be further expanded as 4.9, where the braking distance, initial and final velocity are remaining consistent while the deceleration rates are varying with respect to the intermediate velocity of the vehicle.

$$S = \frac{U^2 - v_1^2}{2.a_1} + \frac{v_1^2 - v_2^2}{2.a_2} + ... + \frac{v_{n-1}^2 - v_n^2}{2.a_n}, v_i > v_{i+1} \tag{4.9}$$

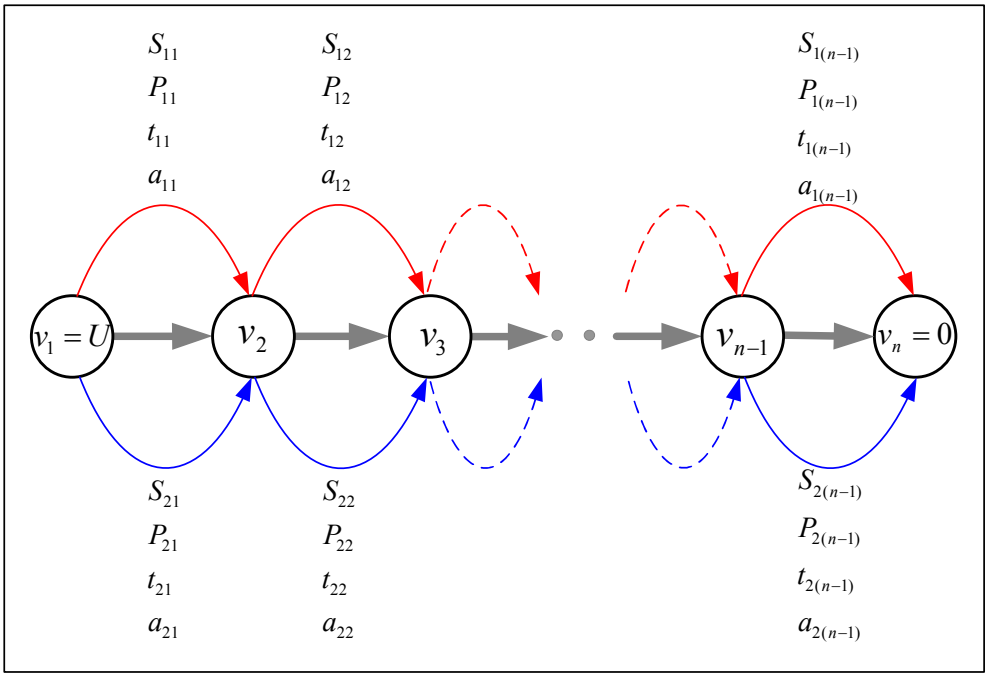

Figure 4.7: State flow for the two different braking scenarios

The graphical representation of the braking process is explained by the state flow diagram for two specific braking scenarios in figure 4.7. By controlling the deceleration rates of the vehicle with respect to the velocity, different brake power distributions can be obtained while ensuring the following conditions:

1. $\sum S_{1i} = \sum S_{2i} = S$
2. $\sum P_{1i}.t_{1i} = \sum P_{2i}.t_{2i} = \Delta E$

here ΔE is the kinetic energy difference of the vehicle in J, where the vehicle is braking form an initial velocity U to a final velocity V.

For an example, let us assume a simple braking scenario, where the vehicle is expected to brake from a velocity v_1 to v_3 within a braking distance S. There will be an intermediate velocity v_2, such that $v_3 < v_2 < v_1$. Based on these constraints, two different braking scenarios have been designed as shown in figure 4.8 to achieve the braking requirements. For simplicity, the intermediate braking distance with respect to the intermediate velocity has been designed as $S_{11} < S_{12}$ and $S_{21} > S_{22}$. Therefore, there are three unknowns (P_{ij}, t_{ij} and a_{ij}) that need to be solved in order to obtain the braking profile and brake power distribution of the vehicle.

let us solve the unknowns for case 1:

$$S_{11} = \frac{v_1^2 - v_2^2}{2a_{11}} \tag{4.10}$$

a_{11} is obtained as $\frac{v_1^2 - v_2^2}{2S_{11}}$ (4.10).

Since a_{11} becomes the known variable, applying the standard equation $V = U + at$ yields.

$$t_{11} = \frac{2(v_1 - v_2)S_{11}}{v_1^2 - v_2^2} \tag{4.11}$$

From 4.10 and 4.11, the average braking power during the time interval t_{11} can be derived as 4.12.

$$P_{11} = m\frac{(v_1 + v_2)}{2}\frac{v_1^2 - v_2^2}{2S_{11}} \tag{4.12}$$

Since $S_{11} < S_{21}$, the following conclusion can be drawn from 4.10, 4.11 and 4.12:

- $a_{11} > a_{21}$
- $t_{11} < t_{21}$

Table 4.2: Deceleration rate, braking power and time duration with respect to the braking distance and velocity of the vehicle

Var	S_{11}	S_{12}	S_{21}	S_{22}
a_{ij}	$a_{11} = \frac{v_1^2 - v_2^2}{2S_{11}}$	$a_{12} = \frac{v_2^2 - v_3^2}{2S_{12}}$	$a_{21} = \frac{v_1^2 - v_2^2}{2S_{21}}$	$a_{22} = \frac{v_2^2 - v_3^2}{2S_{22}}$
t_{ij}	$t_{11} = \frac{2(v_1 - v_2)S_{11}}{v_1^2 - v_2^2}$	$t_{12} = \frac{2(v_2 - v_3)S_{12}}{v_2^2 - v_3^2}$	$t_{21} = \frac{2(v_1 - v_2)S_{21}}{v_1^2 - v_2^2}$	$t_{22} = \frac{2(v_2 - v_3)S_{22}}{v_2^2 - v_3^2}$
P_{ij}	$P_{11} = m\frac{(v_1+v_2)}{2}\frac{v_1^2 - v_2^2}{2S_{11}}$	$P_{12} = m\frac{(v_2+v_3)}{2}\frac{v_2^2 - v_3^2}{2S_{12}}$	$P_{21} = m\frac{(v_1+v_2)}{2}\frac{v_1^2 - v_2^2}{2S_{21}}$	$P_{22} = m\frac{(v_2+v_3)}{2}\frac{v_2^2 - v_3^2}{2S_{22}}$

- $P_{11} > P_{21}$

Similarly all other unknowns are obtained as depicted in the table 4.2. Based on the above comparison, velocity profile, deceleration rate and the brake power distribution of the vehicle with respect to the time are depicted in figure 4.9. The

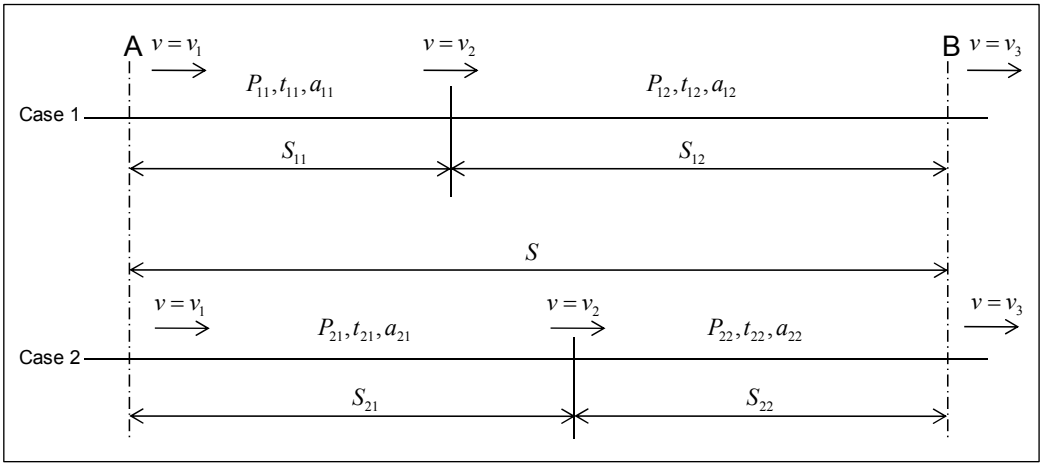

Figure 4.8: Graphical represent of the two different braking profiles

principle to distribute the braking power flow over the braking duration can be further expanded for general braking conditions. The discrete combination of the deceleration rates are derived as the following function, where the deceleration rates are varying with the vehicle velocity.

$$a_{ji} = f(v_i) \tag{4.13}$$

The equation for the braking distance is derived as 4.14, where $v_0 = U$ and $v_n = V$

$$S = \sum \frac{v_{i-1}^2 - v_i^2}{2.a_{1i}} = \sum \frac{v_{i-1}^2 - v_i^2}{2.a_{2i}} = ... = \sum \frac{v_{i-1}^2 - v_i^2}{2.a_{ni}} \tag{4.14}$$

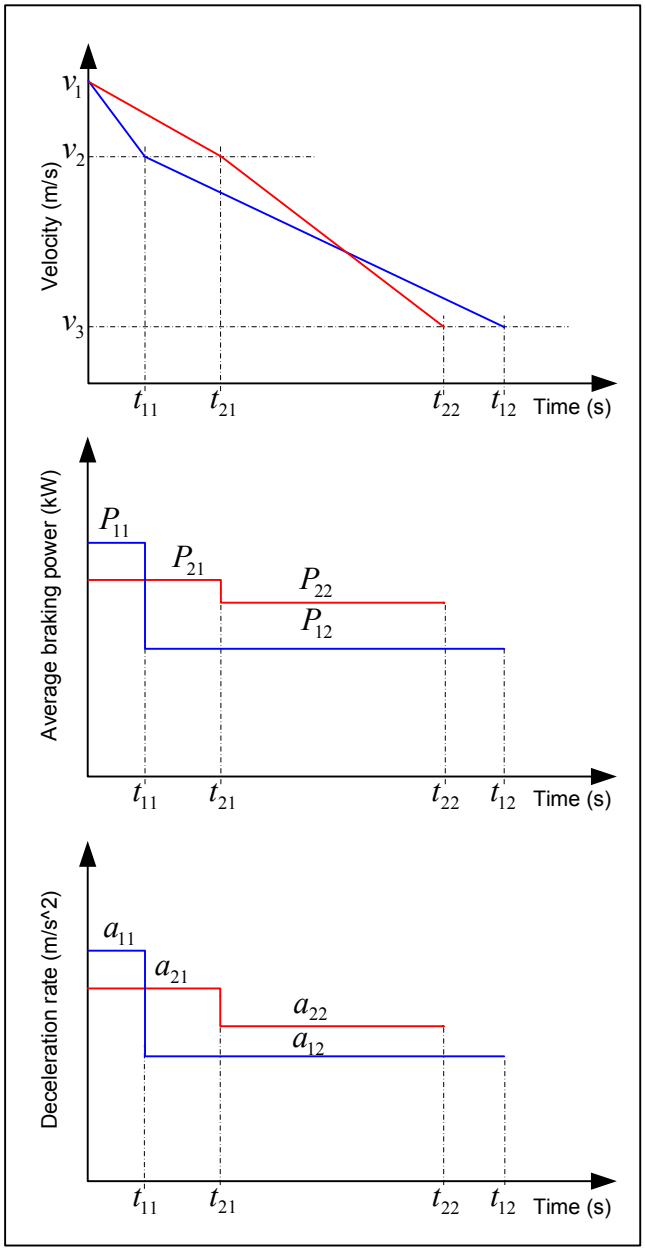

Figure 4.9: Velocity profile, deceleration rate and brake power flow distribution of the vehicle with respect to the time

In order to explain the difference in the braking duration, two different deceleration profiles (Constant and variable deceleration rates) are chosen and compared. The mathematical equations for the braking period for the described braking profiles are shown by equation 4.15 and 4.16.

$$t_1 = \frac{v_0 - v_n}{a} \tag{4.15}$$

$$t_2 = \frac{v_0 - v_1}{a_{11}} + \frac{v_1 - v_2}{a_{12}} + ... + \frac{v_{n-1} - v_n}{a_{1n}} \tag{4.16}$$

However, it can be notice from 4.15 and 4.16 that, it is possible to achieve the expected braking distance and velocity constraints in different time frames, which will vary depending upon the applied deceleration rates with respect to the velocity. As a result of this, the objective is to design the braking profile to increase the kinetic energy recovery duration of the vehicle. For an example, the $V - T$ graph for two different braking profiles to achieve a desired braking distance is depicted in figure 4.10, where both of the braking profiles are achieving a fixed braking distance in different time frame (here $A_1 = A_2$). By employing this technique,

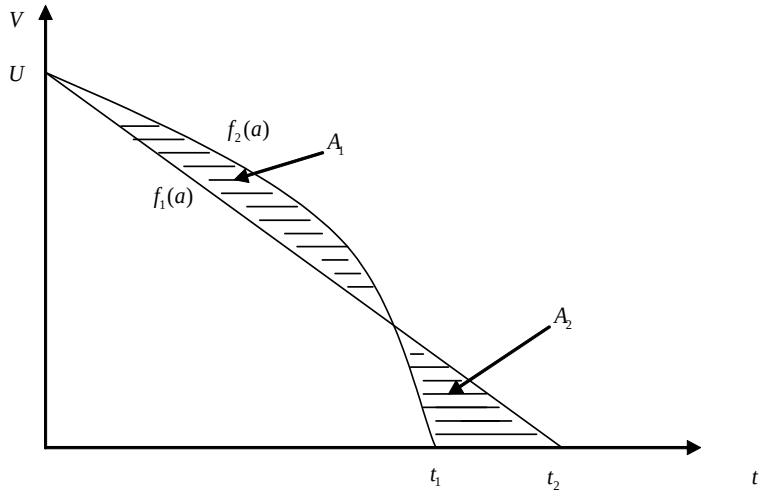

Figure 4.10: Velocity variation with respect to the time in the braking duration

different braking power distribution can be obtained to achieve a fixed braking distance. Depending upon the time duration of the braking, kinetic energy recovery efficiency will vary in heavy braking conditions. Therefore, choosing an appropriate braking profile increase the energy recovery of the vehicle. Figure 4.11 depicts the difference in the brake power distribution for two different braking profiles, where braking profile 1 recover more energy than braking profile 2. A simulation based case study is conducted in the next section which exemplifies this analysis.

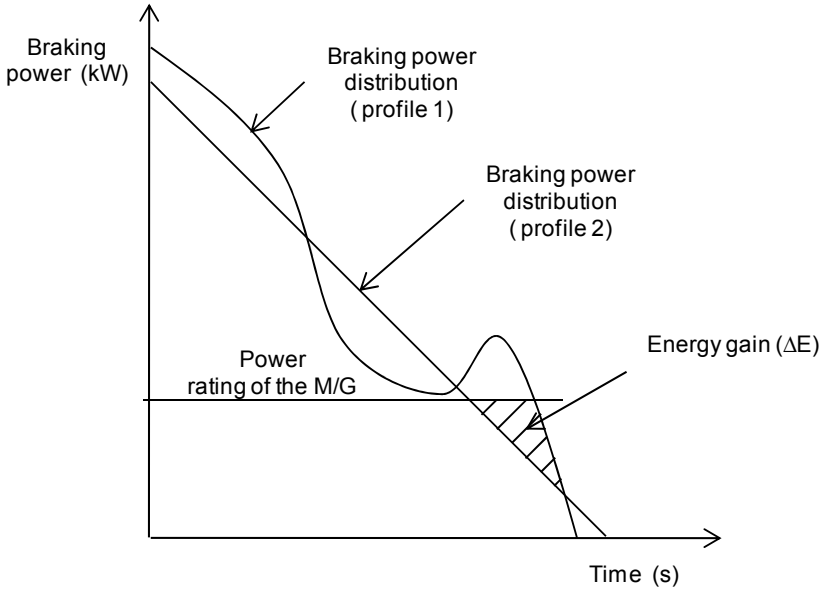

Figure 4.11: Braking power demand variation with respect to the braking profiles

4.6 Case study for the influence of deceleration profile on kinetic energy recovery

The objective of this study is to demonstrate the influence of the braking profile on kinetic energy recovery. As described in the previous section, two different braking profiles are designed to achieve a fixed braking distance. As the boundary conditions for this study, the vehicle was expected to brake from a velocity of 30 ms^{-1} to standstill within a braking distance of 155m. The vehicle parameters which are used for simulation and analysis purposes are listed in table 4.1. Initially, a fixed braking scenario was designed, where the vehicle's deceleration rate was 2.9 ms^{-2}. For variable deceleration rates, another braking scenario is designed with three intermediate deceleration rates as follows:

- From 30 ms^{-1} to 20 ms^{-1} : $\Rightarrow$ 3.4 ms^{-2}
- From 20 ms^{-1} to 10 ms^{-1} : $\Rightarrow$ 2.3 ms^{-2}
- From 10 ms^{-1} to standstill : $\Rightarrow$ 3.4 ms^{-2}

These two braking profiles were simulated using a kinematic model of the vehicle. Similar to Toyota Prius 1 synergy drive, a 30 kW electric motor is considered in

this parallel hybrid drivetrain architecture. Figure 4.12 depicts the speed torque characteristic of this electric motor, which is used in this model [7]. With respect to the above boundary conditions, the velocity profiles of both braking scenarios are plotted in figure 4.13 for comparison. Similarly figure 4.14 depicts the braking

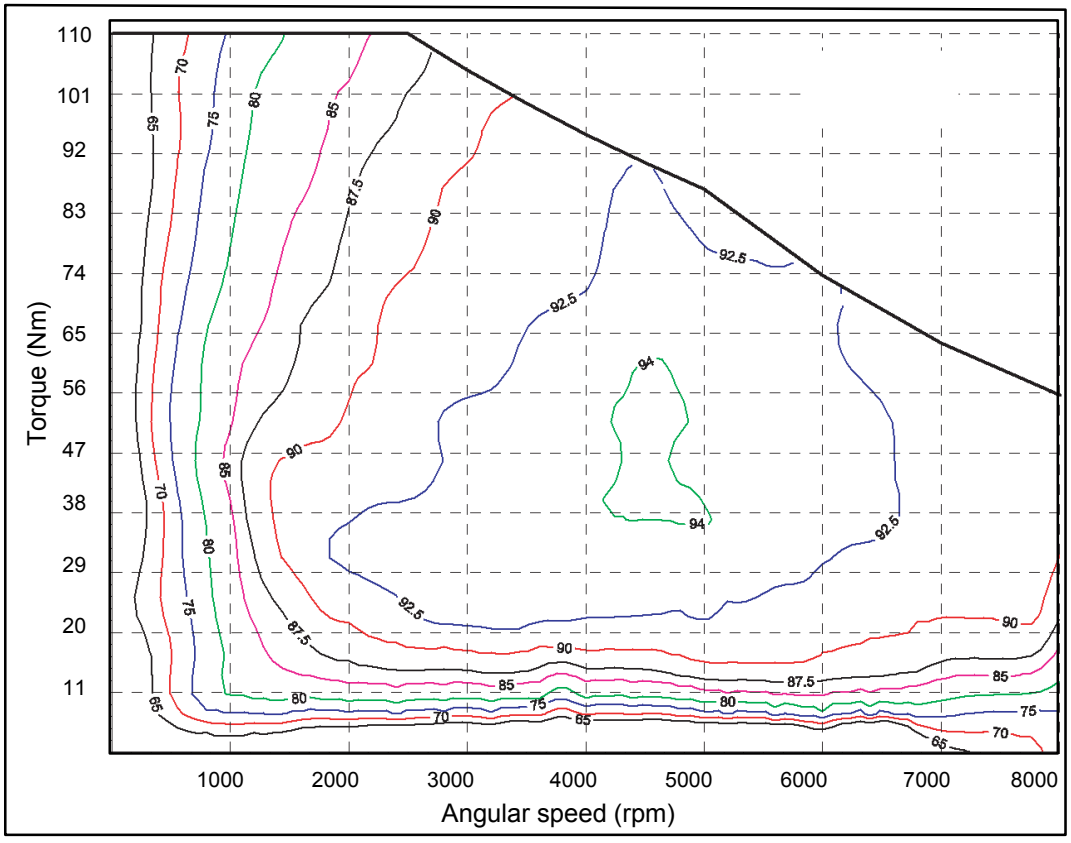

Figure 4.12: Efficiency map and speed torque characteristic of the motor (Modified from [7])

distance of both braking profiles. It shows that, both braking profiles achieve the targeted braking distance of 155 m. As a result of this, these two braking profiles achieve the primary braking objective. Figure 4.15 illustrates the braking power variation with respect to time. Since the electric motor is limited to its power/

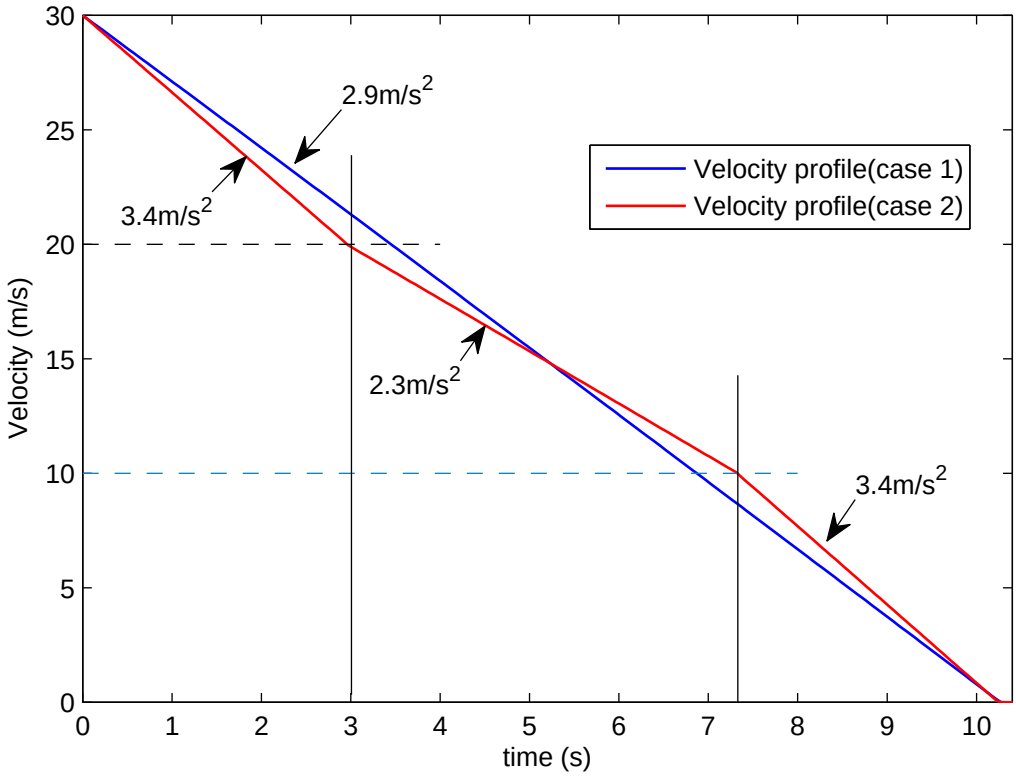

Figure 4.13: Velocity variation with respect to the time

torque handling capability, a significant amount of braking power is dissipated as heat in the secondary braking system. However, it should be noted here that, with respect to the braking profile, the braking power distribution also varies.

$$E(t) = \int_0^t P(t).dt \tag{4.17}$$

In addition to that, the correlation between the power, time and energy is derived in 4.17 which shows that the accumulated energy can be given by integration of regenerative braking power with respect to the time. Therefore, by employing 4.17, one can calculate the regenerative energy for both braking conditions. Regenerative braking energy, mechanical braking energy, and the stored kinetic energy of the vehicle are depicted in figure 4.16. It can be noticed from the figure that, the braking energy distribution varies with respect to the chosen braking profile. Recovered kinetic energy during both braking scenarios are compared in figure 4.17. Further it can be noticed from the figure that the second braking

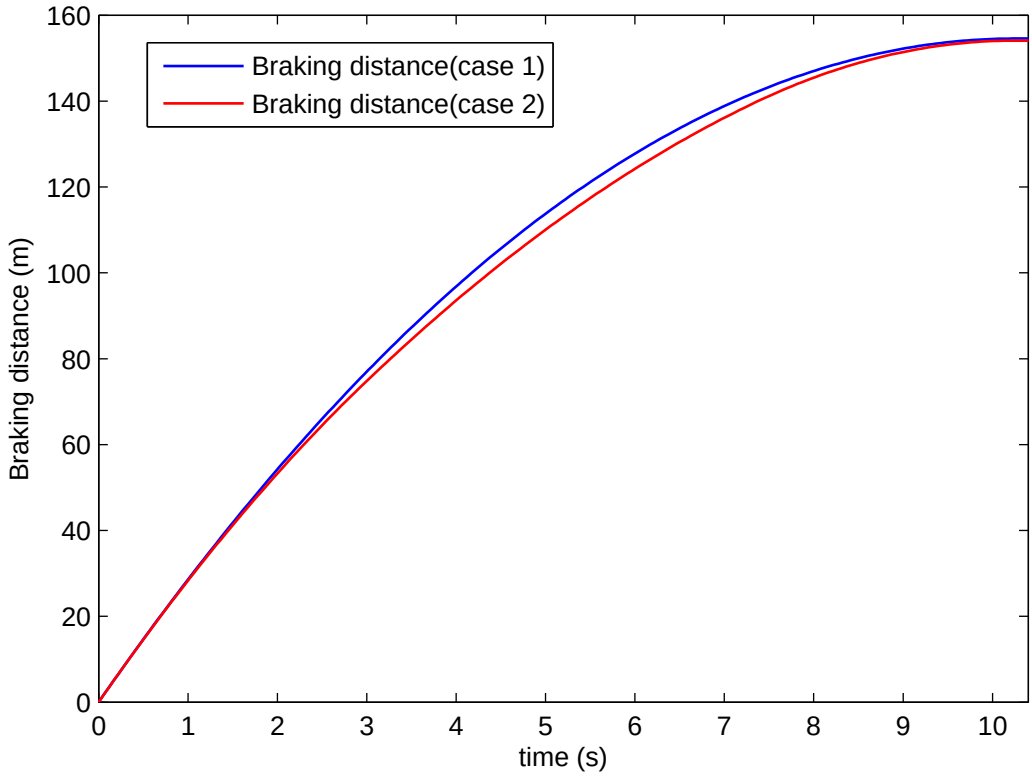

Figure 4.14: Braking distance variation with respect to the time

profile effectively utilizes the regenerative braking system to recapture more regenerative energy than the first braking profile. It results in to increase the kinetic energy recovery by 1.4%, otherwise it is simply dissipated as heat in the first case.

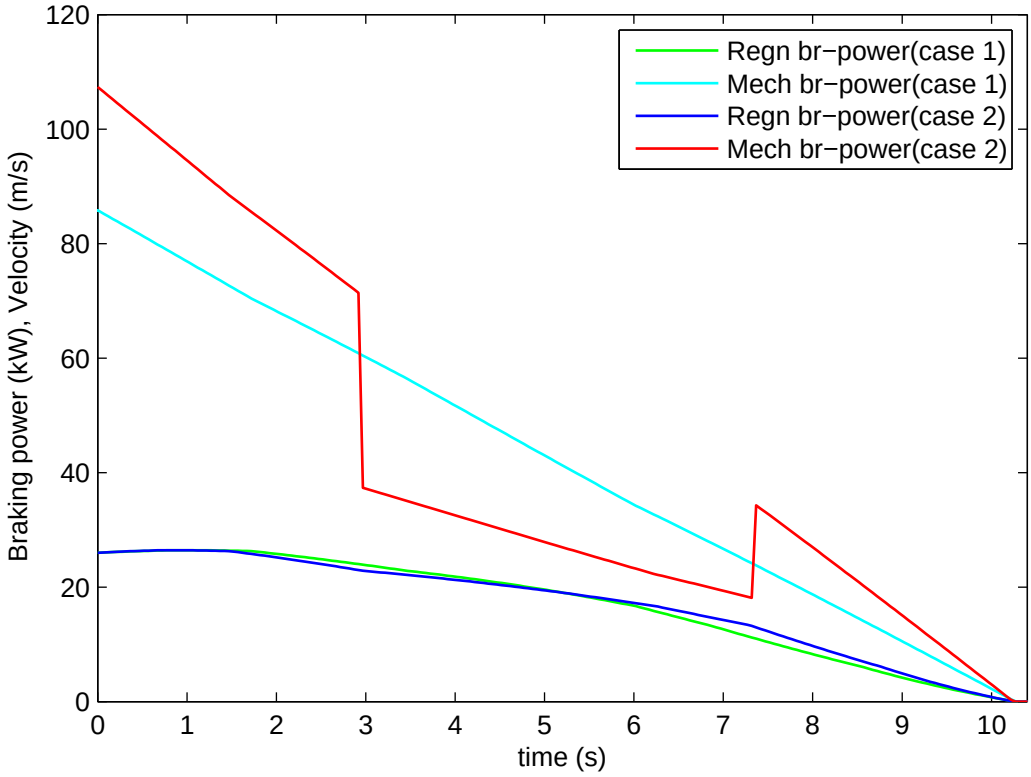

Figure 4.15: Comparison of braking power variation with respect to the time

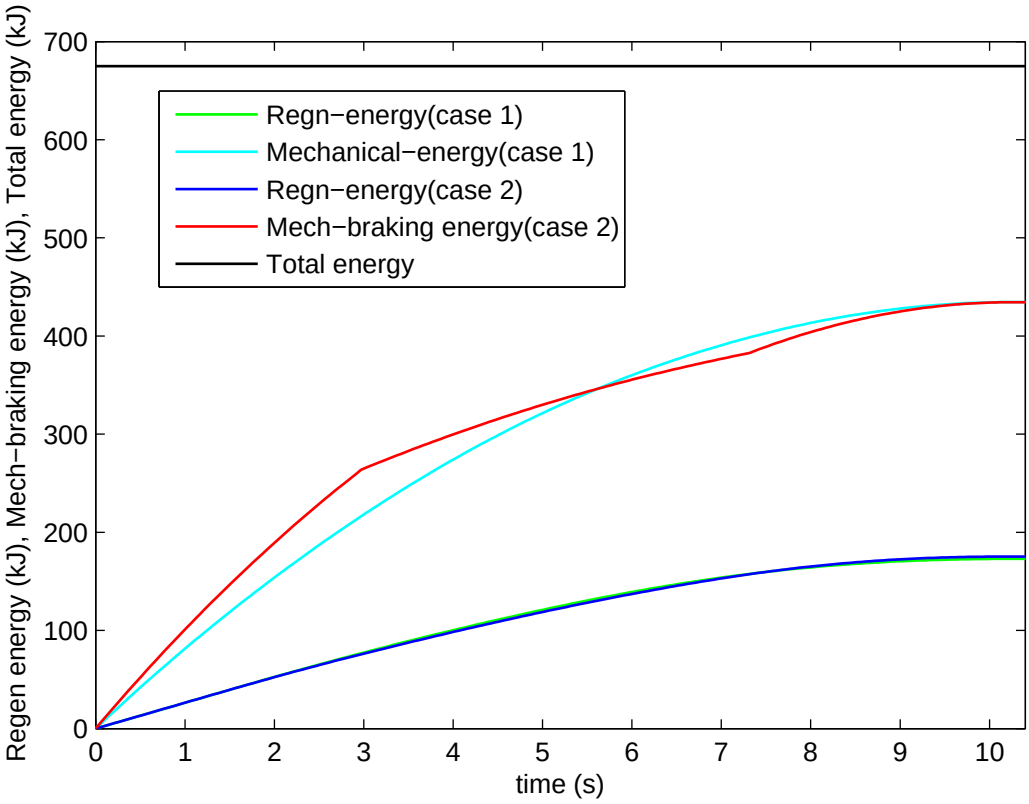

Figure 4.16: Comparison of braking energy variation with respect to the time

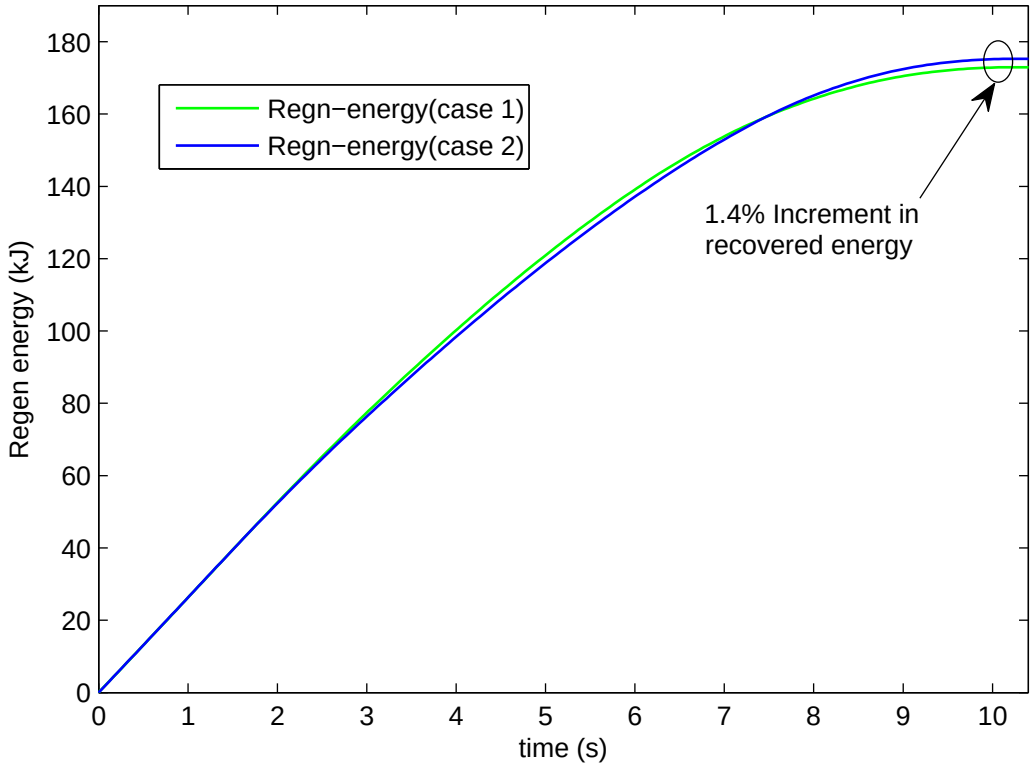

Figure 4.17: Comparison of kinetic energy recovery variation with respect to the time

4.7 Practical issues

Real time driving issues such as driveability and passenger comfort are critical in manned vehicles. Human psychology plays a major roll in real time driving circumstances. Knowing the braking distance at the beginning of braking process is another issue, which is very difficult for the driver to judge before hand. Therefore, adopting the proposed braking profile in real time driving requires significant involvement of learning processes for manned vehicles. Due to the lack of man-machine interaction in autonomous vehicles, it can be implemented in unmanned autonomous vehicles. Since autonomous vehicles navigate based on sensor based information, the expected braking distance can be obtained before the initiation of the braking process. Depending upon the boundary conditions, an appropriate braking profile can be designed to achieve the braking requirement while enhancing the braking energy recovery.

4.8 Summary

The effect of the deceleration profile on regenerative braking energy enhancement in the hybrid electric vehicle is addressed in this work. Due to the power limitations of the electric propulsion system in the hybrid electric vehicle, heavy braking power requirements cannot be achieved by only a pure regenerative braking system. Therefore, incorporating a secondary braking system will enhance the braking performance to achieve higher deceleration demands. However, the involvement of the secondary braking system deteriorates the kinetic energy recovery. In this study different braking profiles are investigated from the view point of increasing the kinetic energy recovery while achieving the braking performance. The reason for this study is to identify the possibility of maximizing the regenerative energy harvest during different braking conditions. It has been determined from the simulation study that, effective use of the braking profile enhances the kinetic energy recovery.

Chapter 5

Experimental Setup and Power Converter Design

5.1 Introduction

Considerable effort has been taken towards the development of the experimental setup to serve as a test platform for regenerative braking system research. The issues related to the energy recovery in regenerative braking systems and the theoretical reasoning for it are explained in the previous chapter, however the experimental validation is important to crosscheck the reality with theory. To perform real time experiments and understand the practical issues in the regenerative braking system, a test platform has been built. This chapter describes the design procedure for the experimental rig and the corresponding subsystems, which are involved with the braking system in hybrid electric vehicles. There are six subsystems integrated together to construct the conceptual design of the dual braking system as shown in figure 5.1. The detailed descriptions of these subsystems and the sizing procedure are presented in the following sections.

5.2 The experimental test bench

The experimental rig consists of a flywheel-that represents the kinetic energy storage of a manned/unmanned vehicle by nature of its moving mass. This flywheel vehicle representation avoids the exogenous and endogenous phenomena of the vehicle such as tyre slip, road conditions, vehicle driving stability issues, engine braking torque, and efficiency of the mechanical transmission system. Isolation of these issues provides a great degree of flexibility to perform kinetic energy recovery experiments.

As the purpose of this experimental setup is to understand the kinetic energy recovery of the vehicle during braking, acceleration and cruising conditions of

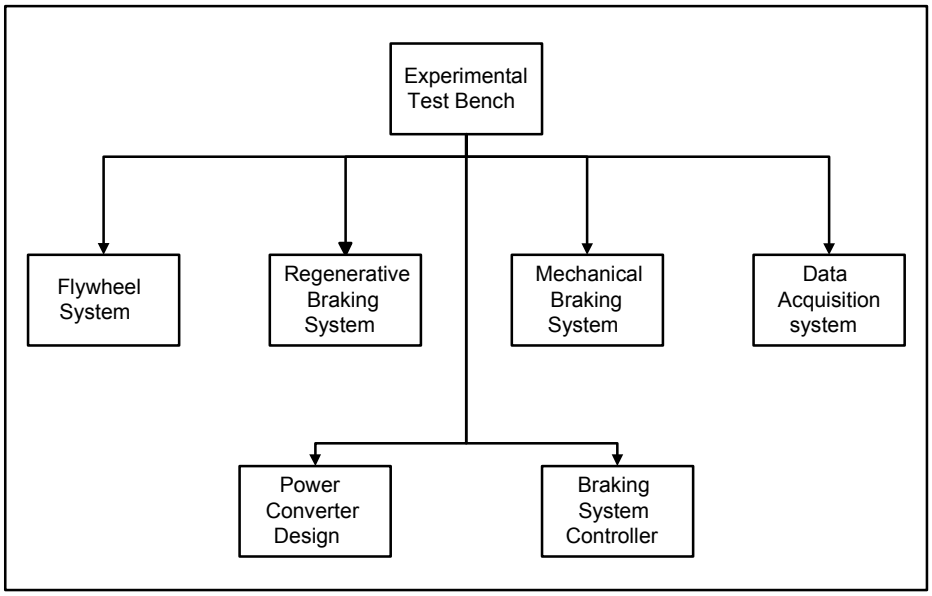

Figure 5.1: Experimental rig and subsystems

the vehicle are not considered in this study. An external DC power supply is used to energize the flywheel system. A disc brake system is also integrated with the flywheel system to act as mechanical brake. Therefore the flywheel system can utilize both the electric and mechanical braking systems for braking, which is similar to the braking system in hybrid electric vehicles. An ultracapacitor bank is used as the energy storage device, where it stores the recovered kinetic energy of the flywheel system. In addition to that, a DC-DC bidirectional buck-boost power converter is also integrated in between the electric motor and the energy storage device, where the converter regulates the regenerative braking torque-power while ensuring the active charging process of the ultracapacitor bank. In summary, the similarities between the conceptual experimental platform and hybrid electric vehicles can be categorized as:

- The flywheel system and hybrid electric vehicles store kinetic energy.
- Both of them incorporate an electrical and a mechanical braking system for the braking purpose.
- Both of them have an electrical energy storage device to store the kinetic energy during braking.

- The flywheel system and hybrid electric vehicles utilize DC-DC power converters to regulate the regenerative braking torque-power.

In addition to that, it is more convenient to perform experiments for braking in a stationary test bench than in real vehicle systems. Therefore these reasons justify the construction of this test bench for experimental purposes.

The involvement of the dual braking system requires a braking strategy to coordinate and distribute an appropriate braking share to enhance the kinetic energy recovery. In addition to that, both systems need to be controlled individually to ensure there operating performance. An embedded micro controller (Parallax Propeller microcontroller) is utilized for the purposes of control of the dual braking system in this experimental rig. As the experiment requires the capture of a variety of information regarding the braking condition for analysis purposes, a data acquisition system is also integrated with this test bench. The detailed specifications of the subsystems are described in the table 5.1 and their sizing procedure and operating principle is briefly explained in the following sections.

Table 5.1: Detail specification of the experimental rig

Flywheel System	
Moment of inertia	0.24 kgm^2
Maximum speed	1200 rpm
Module maximum stored energy	0.5 Wh (1.89 kJ)
Electric motor	
Motor rated power	73W
Motor rated current	3A
Motor rated voltage	24V
Motor rated speed	3500- 3600rpm
Terminal resistance	1.4 ohm
Energy storage (ultracapacitor)	
Module capacity/ maximum voltage	350 F, 2.5 V
Module internal resistance (ESR DC)	3.2m ohm
Module internal resistance (ESR @ 1khz)	1.6m ohm
Module maximum stored energy	0.3 Wh
Quantity and configuration	10 in series
System nominal voltage	25 V
Power electronics interface	
Maximum power	150W
Semiconductor technology	MOSFET
DC voltage band width	5-24 V
Maximum current rating	5-6 A
Switching frequency	20kHz
Thermal dissipation	air cooled

5.3 DC power supply

The propulsive power is supplied by an external DC power supply. The output voltage and current limits of the power supply as depicted in the manufacturers data sheet are 0-30 V and 0-10 A. In addition to that, depending upon the output requirements, the voltage and current limits can be controlled manually. Due to the voltage and current rating of the electric motor, the power supply is limited to a maximum voltage of 24.5 V and a maximum current of 5 A. An electric relay is employed in between the motor and power supply connection. This enables the motor to be connected and disconnected with the power supply. In addition to that the stepper motor in the mechanical braking system is also powered by this power supply.

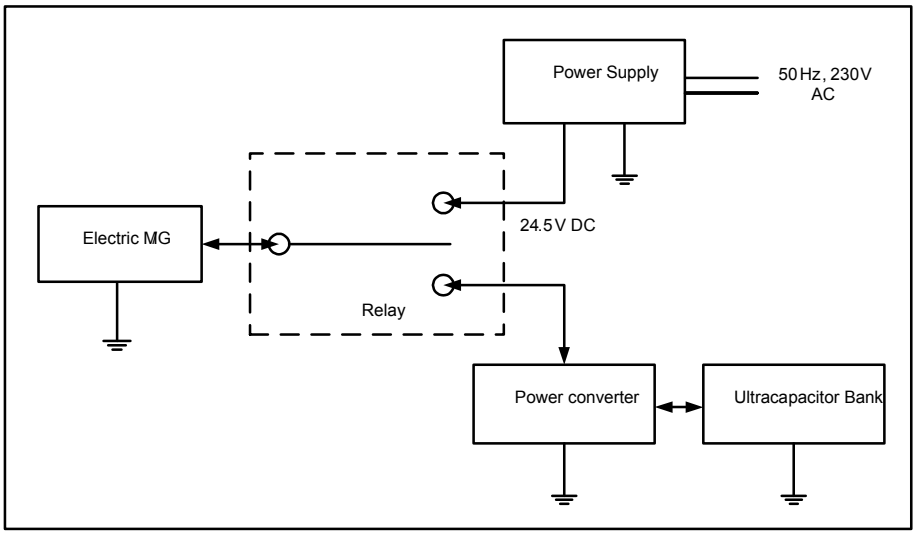

Figure 5.2: Connection diagram of the power supply

5.4 Ultracapacitor system

The ultracapacitor pack consists of ten Maxwell BCAP0350 modules connected in series to create a nominal voltage of 25 V and 35 F capacity. The maximum energy storage capacity of the ultracapacitor bank is 3 Wh (10.9 kJ). Since the available energy bandwidth of the ultracapacitor bank is six times higher than the maximum energy limit of the flywheel system, this arrangement avoids the

energy storage limitations of the system. According to [2] and [74], the stored energy in the capacitor bank during the charging process is given by 5.1

$$E_{uc} = \frac{1}{2}C(V_f^2 - V_{in}^2) \tag{5.1}$$

Where E_{uc} is the stored energy in the UC-bank during the recharging process. V_f and V_{in} are final and initial voltage of the capacitor bank in V.

A simple circuit with resistor, capacitor, switch and a constant voltage source connected in series to demonstrate the charging process of the capacitor bank 5.3. The initial voltage of the capacitor is considered as zero. When the switch is closed, applying Kirchhoff's law to the circuit yields

$$V_g = i(t)r_c + \frac{1}{C}\int_0^t i(\tau)d\tau \tag{5.2}$$

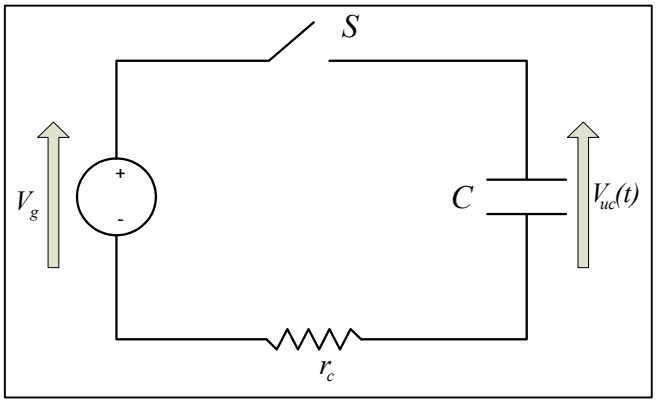

Figure 5.3: Resistor-capacitor circuit demonstrates charging of a capacitor

Where i(t) is the current flow of the circuit with respect to the time. When we take the derivative and rearrange it to obtain the first order differential equation 5.3

$$r_c C\frac{di(t)}{dt} + i(t) = 0 \tag{5.3}$$

Since the initial voltage across the capacitor is zero,5.3 yields 5.4

$$i(t) = \frac{V_g}{r_c} e^{-t/k} \tag{5.4}$$

Where $k = r_c C$ is defined as the time constant of the circuit. From 5.2 and 5.4, the voltage across the capacitor at $t = t$ yields

$$V_{uc}(t) = V_g(1 - e^{-t/k}) \tag{5.5}$$

5.4 and 5.5 provides the charging power of the capacitor as 5.6

$$P_{uc}(t) = \frac{V_g^2}{r_c}(1 - e^{-t/k})e^{-t/k} \tag{5.6}$$

Taking the derivative of 5.6 to obtain the condition for the maximum charging power of the capacitor provides

$$t = k.ln(2) \tag{5.7}$$

Therefore the maximum charging power of the capacitor is $\frac{V_g^2}{4r_c}$ and which reached at $t = k.ln(2)$. At this time the voltage of the capacitor is obtained as $V_g/2$. Applying this yields the charge acceptance characteristic of the ultracapacitor bank as 5.8

$$P_{uc} = \frac{V_g^2}{4ESR_{DC}} \tag{5.8}$$

As illustrated in the table 5.1, the ESR_{DC} of each module is 3.2m ohm. Therefore, ten modules in series configuration provides 32m ohm. The maximum

charging power of the ultracapacitor bank at the maximum terminal voltage of 24 V computes 4.5 kW. According to this the charging efficiency of the capacitor can be written as

$$\eta = \frac{P_{uc}(t)}{P_{uc}(t) + P_{res}(t)} = \frac{V_{uc}(t).i(t)}{V_g.i(t)} = \frac{V_{uc}(t)}{V_g} \tag{5.9}$$

The charging power can be further simplified as

$$P_{uc} = \eta(1-\eta)\frac{V_g^2}{r_c} \tag{5.10}$$

From 5.9 and 5.10, the figure 5.4 has been obtained for the capacitor bank, where it describes the recharging efficiency variation of the capacitor with respect to the charging power and its initial voltage. Where ,the input terminal voltage remains constant.

As illustrated in the figure, one can notice that two different charging efficiencies exist for a given charging power, which is determined by the initial voltage of the capacitor. The charging efficiency yields 50% under the maximum power charging condition. When the initial voltage of the capacitor is close to the charging terminal voltage, low power charging achieves higher charging efficiency. In this design configuration, for a maximum of 73 W charging power, the capacitor bank is more than sufficient to achieve over 99% charging efficiency. However, it is highly dependant on the initial voltage of the capacitor bank.

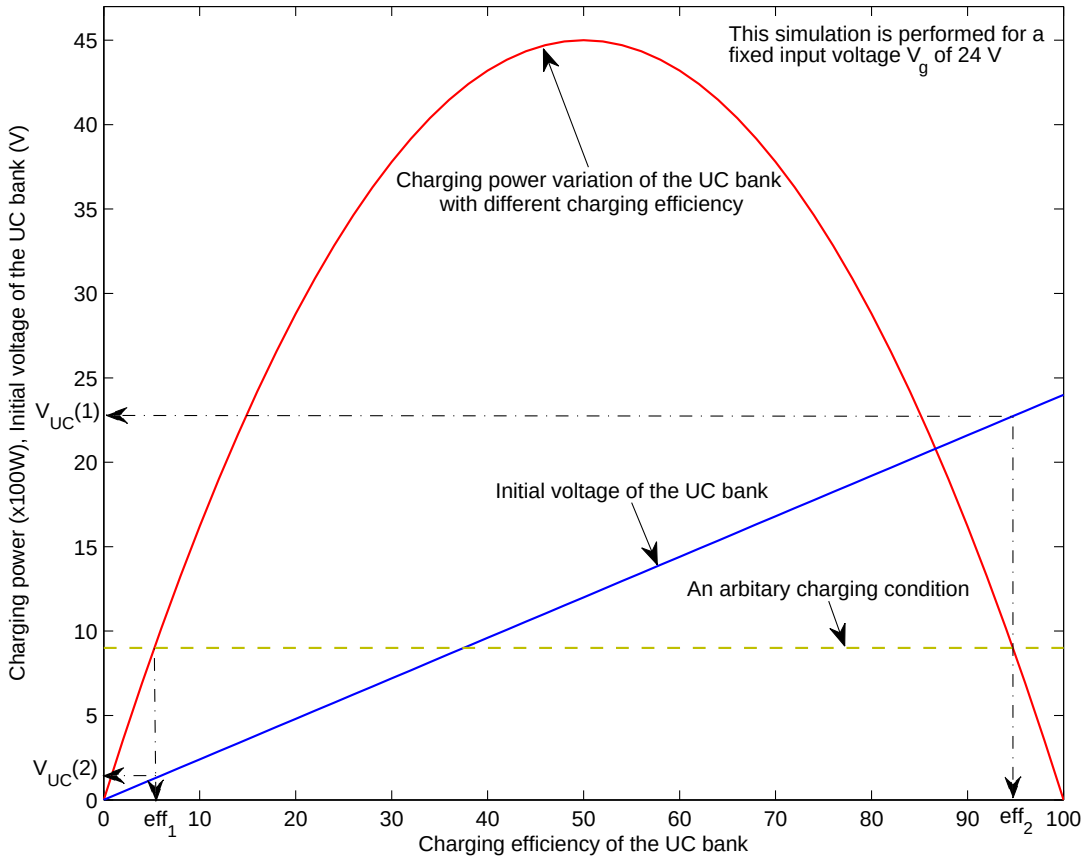

Figure 5.4: Recharging efficiency variation of the capacitor with respect to the charging power and initial voltage

5.5 Instrumentation and data acquisition

5.5.1 Voltage and Current Measurement

Terminal voltage of the electric motor and the ultracapacitor bank are the voltage measurement points of the system as depicted in figure 5.5. Due to the voltage and current limitations of the controller and data acquisition system, the actual terminal voltage reading is scaled down by a factor of 4.7 for measurement and re-scaled into the controller. A resistive potential divider with a single pole low pass filter is used for voltage measurement purposes.

Currents are measured using two CKSR 6-NP compact Fluxgate LEM current transducers. The CKSR 6-NP module is configured in the series mode to increase the output resolutions of the current reading. Both modules are powered by a +5 V DC bias voltage from an external power supply. The reading across the LEM module is scaled in the controller by a factor of 2/3, where 6A current flow produces a 4V reading in the current transducer. The circuit for the instrumentation of current and voltage measurements are illustrated in figure 5.6.

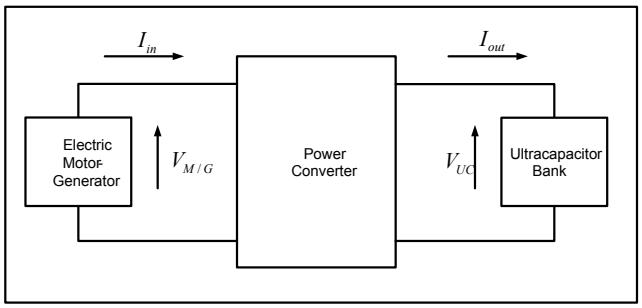

Figure 5.5: Voltage, current measurement points of the system

5.5.2 Speed Measurement

A three channel optical rotary encoder HEDS-5500/5540 module is used for the speed measurement of the flywheel system. The module is attached with the electric motor and powered by a 5V DC external power supply. Data channels are biased with 2.7k resistors to restrict the current flow in to the optic circuit. The data channel readings are decoded by the controller to obtain the speed measurement.

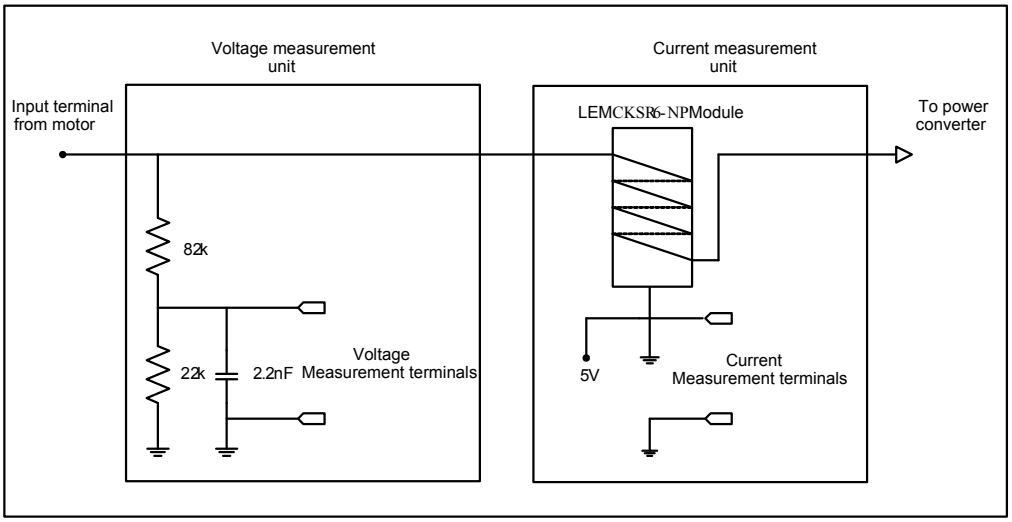

Figure 5.6: Voltage, current measuring method for the instrumentation

The circuit configuration for the speed measurement of the regenerative braking system is depicted in figure 5.7.

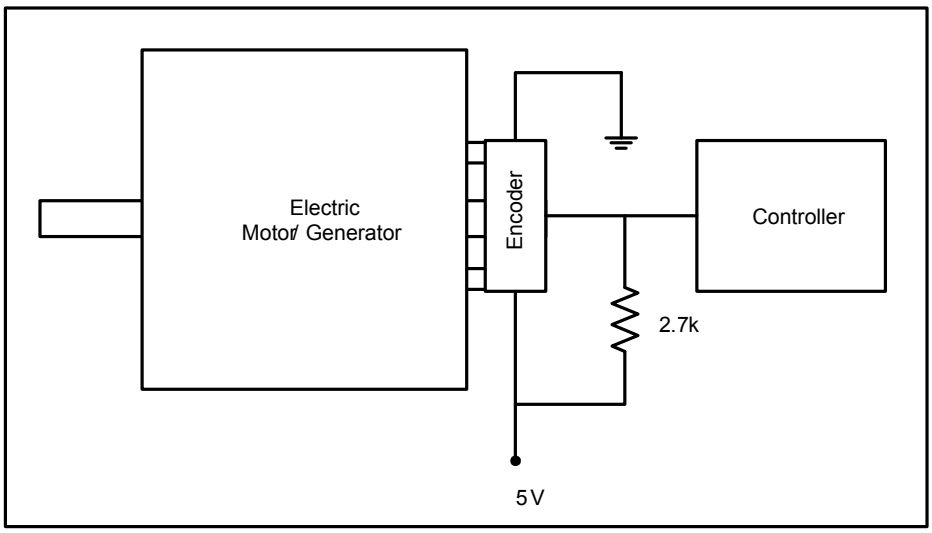

Figure 5.7: Encoder circuit Configuration

5.6 Control system

The propeller microcontroller chip is used in the control system design. A 7.5V external power supply is used to energize the controller. There are eight individual processers called cogs in the controller to perform parallel tasking and they can be

individually operated depending upon the requirements. As illustrated earlier, both the regenerative braking system and the mechanical braking system are controlled by this micro controller. The predefined braking profile is uploaded to the controller before the experiment is performed. $I_{in}, I_{out}, V_{in}, V_{out}$ and speed of the flywheel system are considered as the feed back state variables of the system to produce the control outputs. The duty cycle of the power converter is controlled for the regenerative braking system, while the position of the mechanical braking calliper is controlled for the mechanical braking system. In addition to that, the state variables and the duty cycle values of the DC-DC converter are stored in the SD card. The block diagram in figure 5.8 illustrates the input and output variables of the control system.

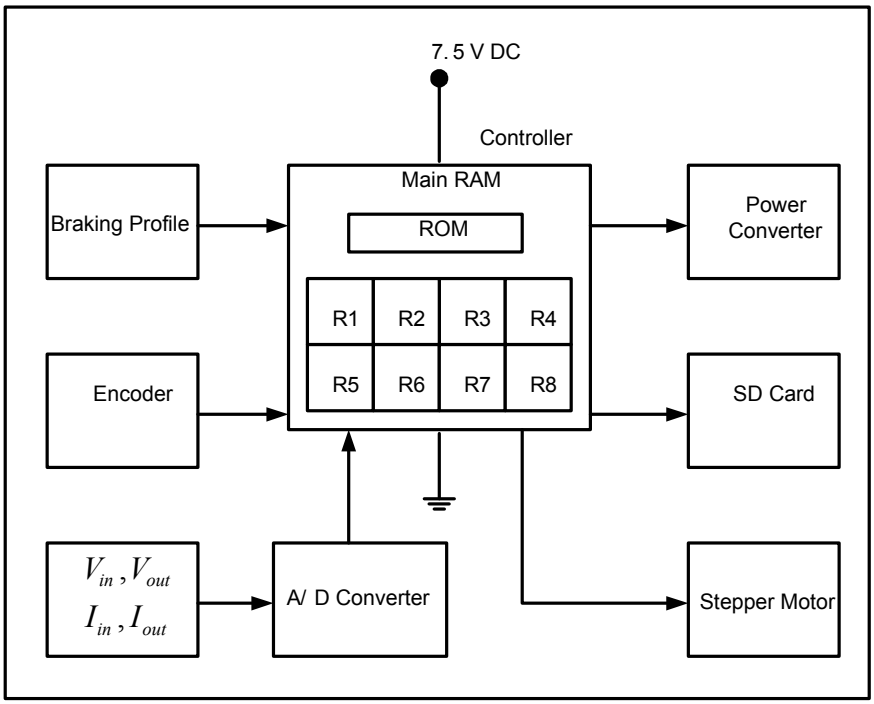

Figure 5.8: Block diagram of the controller and its connection configuration

Since there are four semiconductor switches in the power converter, it requires four PWM signals to perform the buck boost operations. A cog is dedicated to controlling the power converter switches, where a program is designed to generate a 20kHz fixed frequency on four output pins. The time period of the output is divided into 256 equal segments (each segment represents 0.195μs time period), where they can be adjusted to change the duty cycle. It is designed in such a way that the duty cycle can be adjusted independently for each of the PWM out puts,

which allows independent control of the power electronic switches. Appropriate switching and duty cycle value are decided by the main program with reference to the regenerative braking requirement and other feed-back information. An optical isolation circuit is used to prevent cross-conduction between the power electronic switches and the micro controller. The detailed circuit diagram of the power converter can be found in the appendix.

5.7 Power converter selection and design procedure

Appropriate selection of the power converter is essential to increase the efficiency of the regenerative braking system under a variety of braking circumstances. The voltage difference in between the ultracapacitor (UC) bank and the terminal voltage of the electric motor is the key factor which determines the regenerative braking performance. As illustrated in the previous chapter, the back electromotive force (E_{emf}) of the motor reduces with the velocity of the vehicle during braking. In contrast, due to the charging process, the voltage level of the ultracapacitor bank increases. As a result of this, the voltage difference between the motor and the ultracapacitor bank varies as illustrated in figure 5.9. It can be noticed from the figure that the potential difference is significant at the beginning of the braking, but this declines over time. It results in a higher current flow at the beginning of the braking and it decreases as the voltage difference decreases over time. This effect will lead to an uneven braking torque/ power distribution over time, which is not desirable for braking applications. In addition to that, due to the varying voltage differences, the charging efficiency of the ultracapacitor bank also decrease.

Another important fact that should be noticed from the figure is that, the voltage difference becomes zero at point O and after this point the current flow of the motor will become zero. As a result of this it is not possible to continue the regenerative braking after this point. Therefore the mechanical braking system needs to be engaged to supply the surplus braking power, which simply dissipates the kinetic energy of the vehicle as heat in the brake disc.

As an example, let us assume a driving case where the vehicle is cruising down hill with a constant speed and requires to engage its braking system for driving safety. Due to the constant speed cruising requirement, the motor will produce a constant voltage output (E_{emf}). At the same time, the voltage level of the capacitor bank can be $V_{uc} \lesseqgtr E_{emf}$, and under each conditions the braking scenarios explains:

- If $V_{uc} \geq E_{emf}$, it is not possible to involve the regenerative braking system. This is mainly due to the voltage limitation rather than the storage limitation (It is not a necessary condition for V_{uc} to be equal to $V_{uc}max$) of the ultracapacitor bank.
- If $V_{uc} < E_{emf}$, it is possible to engage the regenerative braking system. However, the voltage level of the capacitor bank will gradually increase due to the re-charging process. It results in the decrease of the voltage difference between the electric motor and the capacitor bank, which will deteriorate the regenerative braking torque. Due to this fact, the mechanical braking system needs to be involved to control the speed of the vehicle.

Since the mechanical braking system is actively involved in both braking circumstances, it significantly limits the kinetic energy recovery of the vehicle. Therefore, there are two problems that need to be solved to increase the involvement of the regenerative braking system to enhance the kinetic energy recovery:

- The regenerative braking system should be able to produce a wide range of braking torques (within the operating limitations of the electric motor) regardless of the voltage differences in between the capacitor bank and motor.
- It should be able to recover the kinetic energy of the vehicle during the whole braking duration.

The same theory is applicable during the acceleration of the vehicle as well, where the voltage level of the ultracapacitor will decline while the required voltage to overcome the driving resistance will increase with time. Therefore as the implementation frame work, a bidirectional buck-boost DC-DC converter is considered as the potential candidate and adopted to overcome the aforementioned

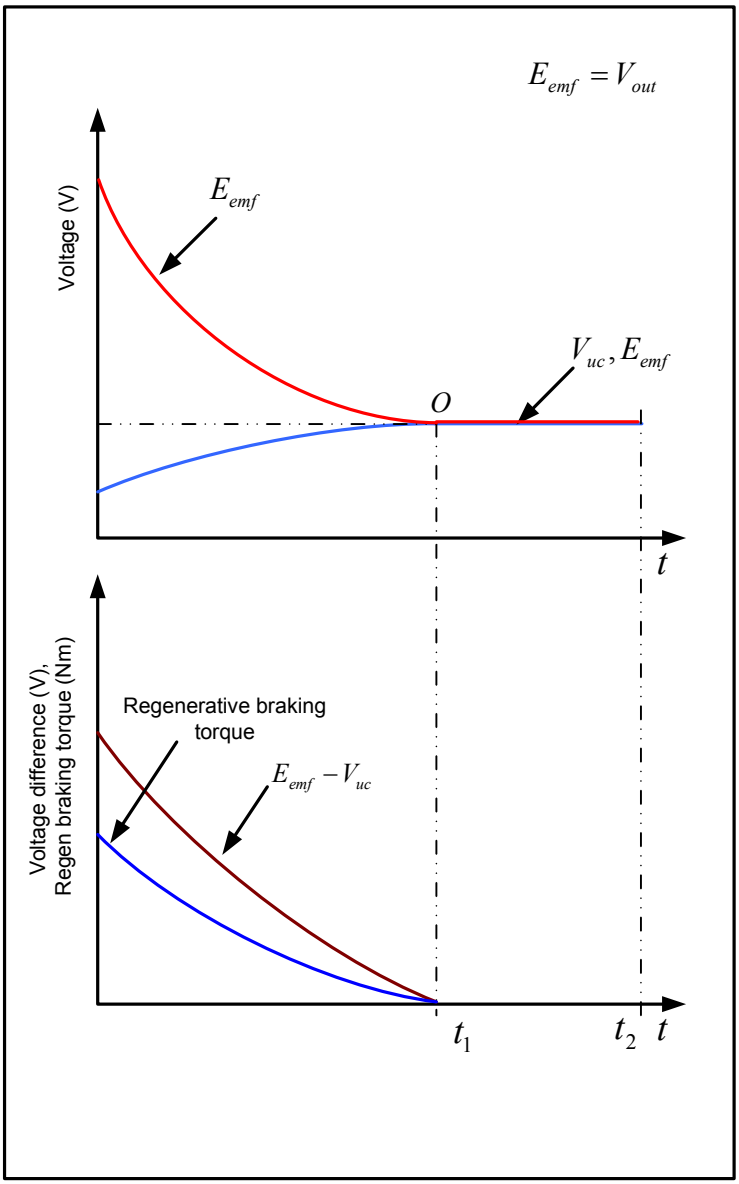

Figure 5.9: Back emf and UC bank's terminal voltage variation during the regenerative braking (without power converter)

issues. As it can boost up and step down the voltage level of both sides regardless of the voltage variation, the electric power flow can be controlled and directed to either side of the converter. Utilizing this converter control the voltage difference as illustrated in figure 5.10, which eventually controls the braking torque distribution while increasing the energy recovery in the UC bank. Since the main focus of this research is to investigate the kinetic energy recovery of the vehicle, the operating principle and sizing procedure of this power converter is illustrated

from the regenerative braking perspective.

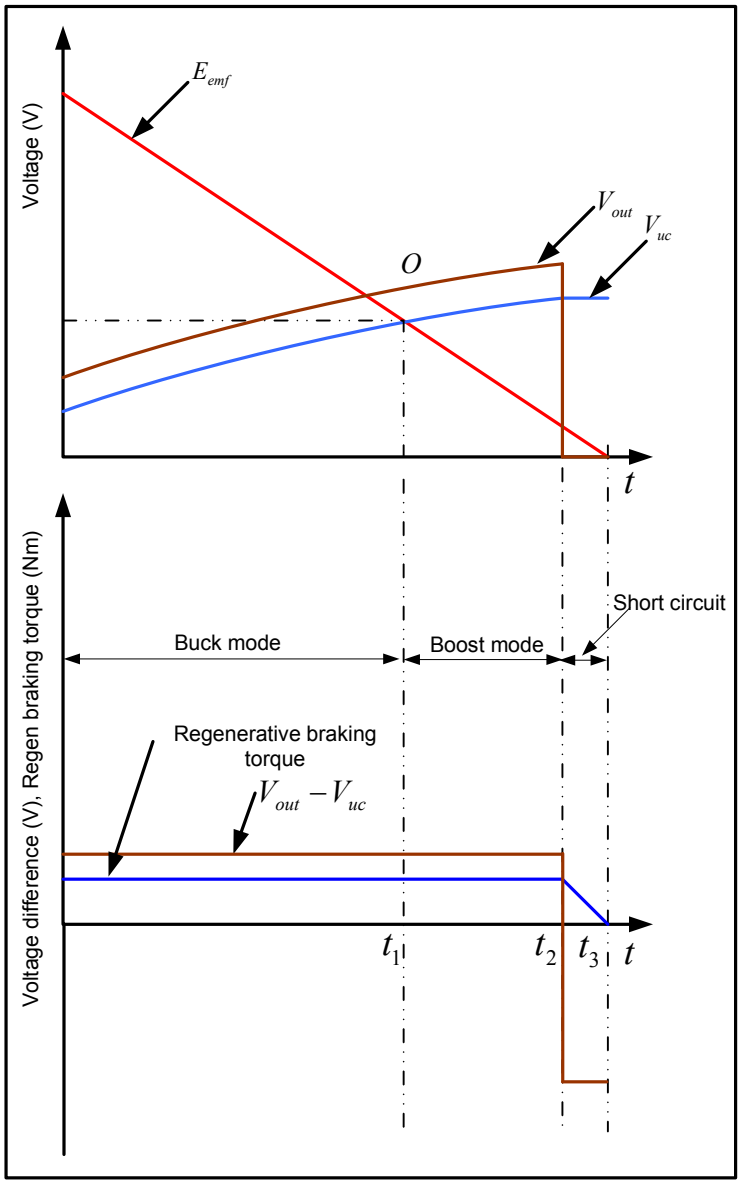

Figure 5.10: Back emf and UC bank's terminal voltage variation during the regenerative braking (with power converter)

5.7.1 Power converter topology

Figure 5.11 shows the schematic of the designed H-bridge bidirectional buck-boost power converter topology, which has been constructed for experimental purposes. Depending upon the state of the power electronic switches $S1$ to $S4$,

the power flow direction, mode of operation (buck, boost) and the power flow magnitude can be controlled. The following section describes the operational principle of this power converter.

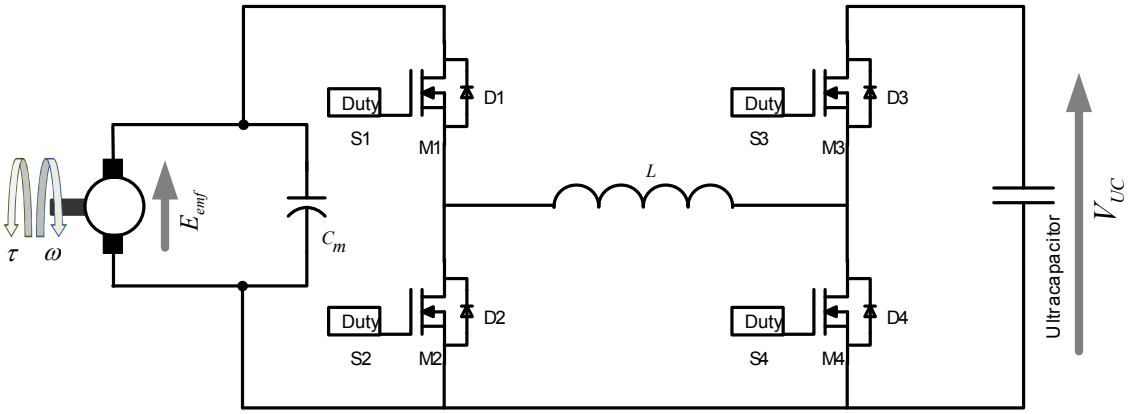

Figure 5.11: Bidirectional Buck Boost Converter

5.7.2 Operating principle

This power converter has symmetric operational behavior, where both directions are controllable for voltage step-up and step-down requirements. However as it has been emphasized earlier, the power flow characteristic of the regenerative braking system is considered in order to explain the operational principle of the power converter. Consider the regenerative braking scenario as illustrated in the figure 5.11. When the input voltage is higher than the ultracapacitor (UC) terminal voltage, the power converter operates in buck mode. It will regulate the voltage difference to control the braking torque while increasing the recharging efficiency of the UC bank. Under this operating mode, power electronic switches $S1, S3$ and the freewheeling diode $D2$ are providing the active circuit path, where $S3$ is enabled with 100 % duty while the control signal is given to $S1$.

Similarly, when the input voltage is less than the terminal voltage of the UC bank, then the power converter operates as a boost converter. Under the boost mode operation, the output voltage of the power converter will be increased to regulate the voltage difference between the power converter and UC bank. It results in a current flow that produces the braking torque and recharges the UC bank during this braking condition. As the operating principle, switches

Table 5.2: Operational specification of the DC-DC power converter

Parameter	*Notation*	Values
Maximum converter power	P_{max}	150W
Maximum current flow	I_{max}	5-6 A
U C charging voltage	V_{uc}	5-22V
Back electro motive force	V_g	24-5V
Switching frequency of the power converter	f_{sw}	20kHz
Current ripple	I_{ripple}	2.5 per

$S1$, $S4$ and the freewheeling diode $D3$ provide the active circuit path for the boost converter, where $S1$ is enabled with 100 % duty while the control signal is given to $S4$. The power switches are controlled to achieve variable duty cycle at a constant switching frequency.

As illustrated in figure 5.10, when the vehicle is braking from a higher velocity to stand still, the power converter needs to go through both the buck and boost modes of operation to achieve the expected braking requirement while ensuring the active recharging process of the UC bank. Therefore at the beginning, $S3$ is enabled with 100% duty and the control signal is given to $S1$. When the potential difference between the terminal voltage and the ultracapacitor falls bellow the required value to produce the expected braking torque, buck to boost transition switching will be directed by the controller, where $S3$ will be switched off and $S1$ will be enabled to 100% duty while $S4$ will be given the control signal. The buck boost transition is purely dependant upon the initial conditions of the UC bank, vehicle velocity and braking requirements.

5.7.3 Operational specification of the power converter

The power and energy limitations of the electric motor and the UC bank determine the operational specification of the power converter, where the power converter should be designed to cope with extreme operating requirements. Therefore, with reference to table 5.1, design specifications of the power converter are defined as listed in table 5.2.

The semiconductor switches and passive components are sized to meet the de-

sign specification of the power converter as illustrated in table 5.2. With respect to the voltage constraints of the electric motor and the ultracapacitor bank, the duty cycle range of the converter is determined. By applying the basic buck/boost circuit topology derivations, electric motor buck/boost mode operations are analyzed. Throughout this analysis, an appropriate magnetic component is sized to fulfil the maximum operating requirements of the converter.

5.7.4 Buck mode operation of the Power converter (UC-charging)

The buck mode operation of the circuit is illustrated in figure 5.12, where the inductor is charging during the interval $T_0 < t < T_0 + DT$ and it is discharging during the interval $T_0 + DT < t < T_0 + T$.

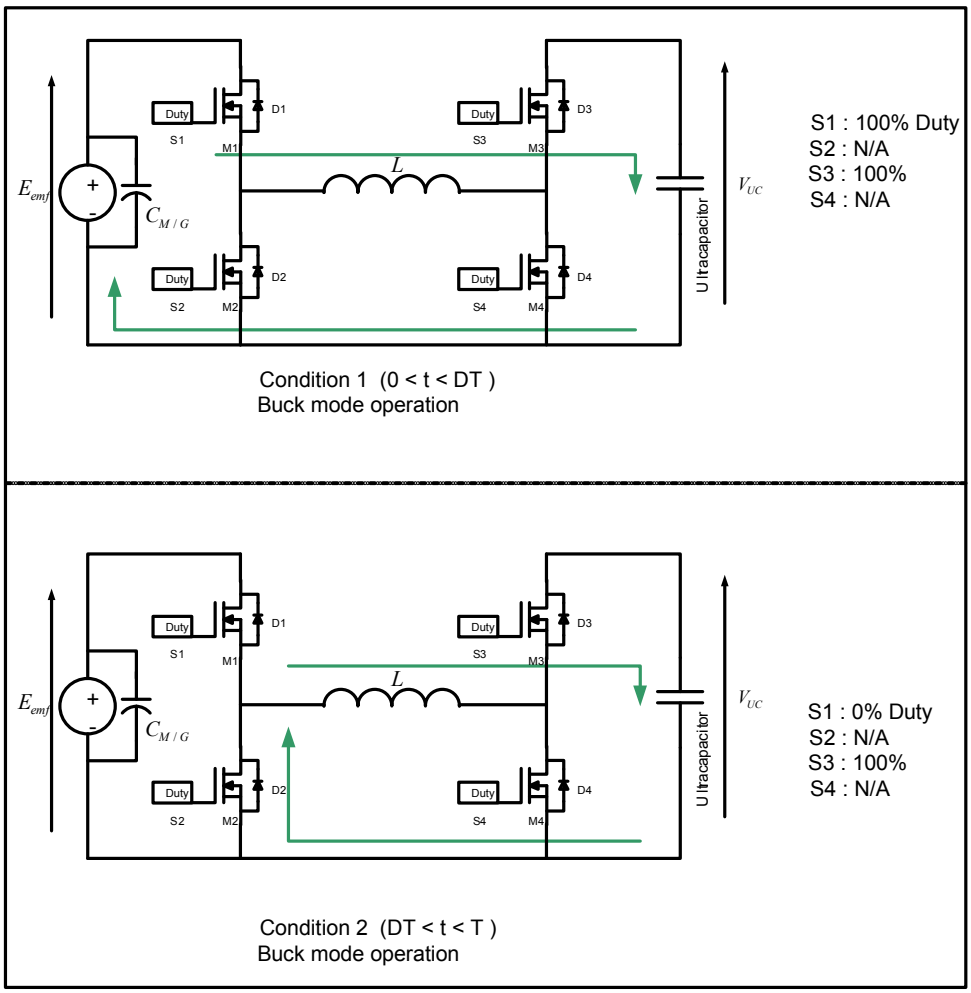

Figure 5.12: State diagram of the DC-DC converter for the buck mode operation

As emphasized earlier, to cope with the real time braking requirements, the braking torque should be controlled. As a result of this, the conditions to produce constant braking torque requirements are considered for the analysis of the converter. There are two conditions that need to be satisfied to produce constant braking torque:

- Constant current should be drawn from the motor (since τ is proportional to the current flow rate of the motor).
- Due to the constant braking torque, the velocity drop of the motor should be constant. This results in a constant rate of decrease of voltage ($\dot{V}_g$) of the motor (since velocity is proportional to the back electromotive force of the motor).

here V_g represents the E_{emf} of the electric motor ($V_g = E_{emf}$).

$$V_g = \kappa_v \omega \Rightarrow \dot{V}_g = \kappa_v \dot{\omega} \tag{5.11}$$

$$\tau = J\dot{\omega} \tag{5.12}$$

$$\tau = \kappa_i i \tag{5.13}$$

$$\dot{V}_g = \frac{\kappa_v \kappa_i i}{J} \tag{5.14}$$

let assume $\frac{\kappa_v \kappa_i}{J} = K$, then $\dot{V}_g$ can be written as,

$$\dot{V}_g = Ki \tag{5.15}$$

Applying kirchhoff's voltage low to the circuit within the time interval $T_0 < t < T_0 + DT$ provides,

$$V_g = i(r_g + r_c) + L\frac{di}{dt} + V_{uc} + \frac{1}{C}\int idt + \int \dot{V}_g dt \tag{5.16}$$

Where V_g is the initial voltage of the electric motor at time $t = T_0$, $\dot{V}_g$ is the voltage reduction rate of the motor generator due to the deceleration, r_g is the series internal resistance of the electric motor, r_c is the series internal resistance of the ultracapacitor bank, V_{uc} is the initial voltage of the capacitor at time $t = T_0$, $L\frac{di}{dt}$ is the voltage across the inductor, $\frac{1}{C}\int idt$ is the voltage increment of the ultracapacitor bank and D is the duty cycle value of the switch $S1$.

Rearranging 5.16 yields,

$$L\frac{di}{dt} = V_g - (i(r_g + r_c) + V_{uc} + \frac{1}{C}\int idt + \int \dot{V}_g dt) \tag{5.17}$$

Similarly applying kirchhoff's voltage law to the circuit within the time interval $T_0 + DT < t < T_0 + T$ provides,

$$L\frac{di}{dt} + V_{uc} + i.r_c + \frac{1}{C}\int idt + \frac{1}{C}IDT = 0 \tag{5.18}$$

Where, $\frac{1}{C}IDT$ represents the voltage increment of the UC bank during the interval $T_0 < t < T_0 + DT$

Rearranging 5.18 yields

$$L\frac{di}{dt} = -(V_{uc} + i.r_c + \frac{1}{C}\int idt + \frac{1}{C}IDT) \tag{5.19}$$

According to 5.17 and 5.19, figure 5.13 illustrates the voltage variation of the inductor and UC bank during the buck mode charging of the power converter.

Though we assumed a constant current flow in the circuit to produce constant braking torque, there will be a current ripple in the inductor during the operation of the converter. The inductor is charging in the first time interval $T_0 < t < T_0 + DT$ and discharging in the second time interval $T_0 + DT < t < T_0 + T$, therefore the net accumulated energy in the inductor becomes zero throughout a complete duty cycle of the power converter. However, inductor selection is critical to maintain a study state current flow in the circuit. Since the voltage across the inductor is a function of current ripple $\frac{di}{dt}$ and inductance value L, an appropriate sizing of the inductor value will minimize the current ripple to a negligible component. To design an inductor for this power convert application, the volt-second balance of the inductor is considered for a duty cycle interval T.

Integrating the equation 5.17 with respect to the time within the interval $T_0 < t < T_0 + DT$ yields,

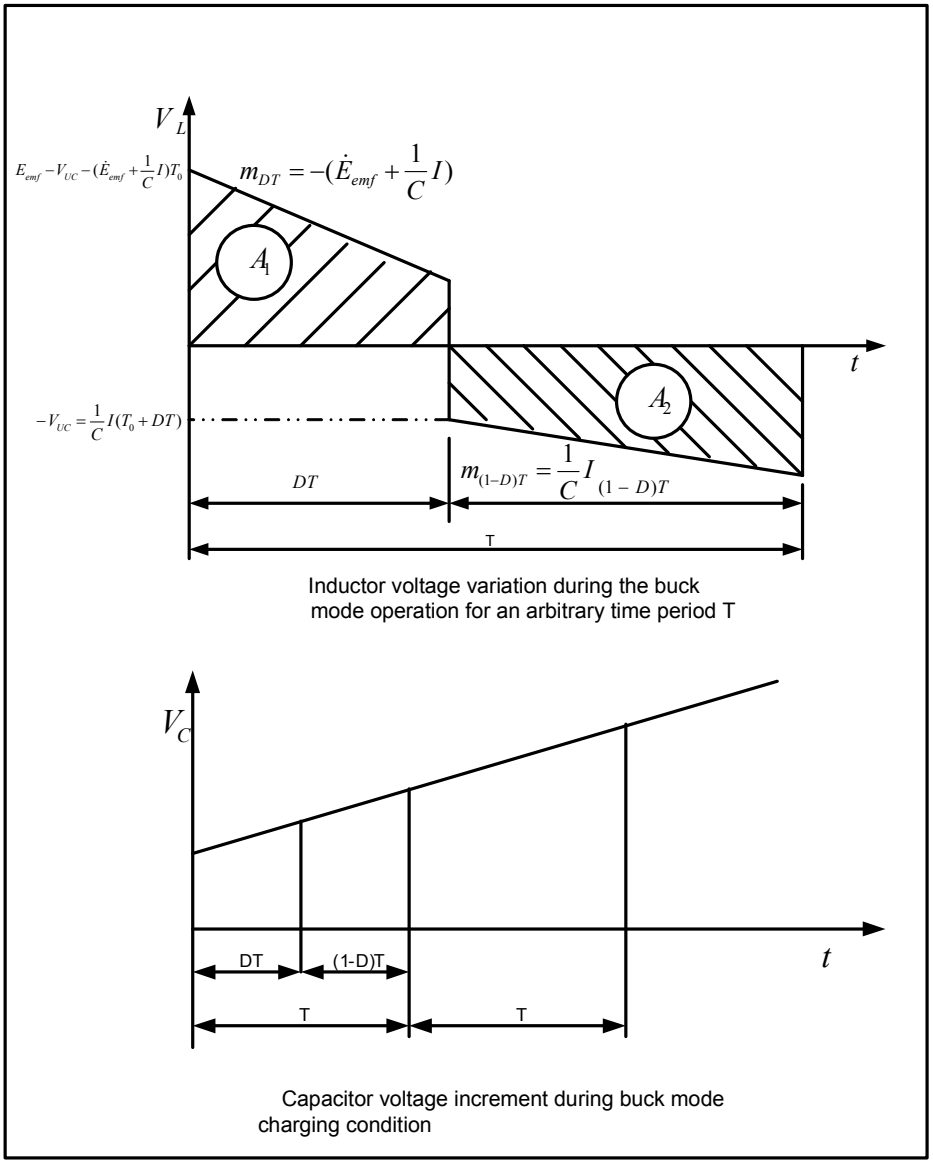

Figure 5.13: Voltage variation of the inductor and ultracapacitor during buck mode charging condition

$$L\Delta I = (V_g - (I(r_g + r_c) + V_{uc}))DT - \frac{1}{2C} I(DT)^2 - \frac{kI}{2}(DT)^2 \tag{5.20}$$

Similarly, integrating 5.19 with respect to the time within the interval $T_0 + DT < t < T_0 + T$ yields,

$$L\Delta I = -(V_{cu} + I.r_c + \frac{1}{C} IDT)(1 - D)T - \frac{1}{2C} I(1 - D^2)T^2 \tag{5.21}$$

For the volt-second of the inductor, the following should be satisfied

$$L\Delta I_{(0<t<DT)} + L\Delta I_{(DT<t<T)} = 0 \;\; where 0 < t < T \tag{5.22}$$

Therefore 5.20, 5.21 and 5.22 yields

$$(\frac{K}{2} - \frac{1}{C})ITD^2 - (V_g - I(r_g + \frac{T}{C}))D + (V_{uc} + I(r_c + \frac{T}{2C})) = 0 \tag{5.23}$$

From 5.23, the current flow of the circuit can be calculated as,

$$I = \frac{DV_g - V_{uc}}{(\frac{K}{2} - \frac{1}{C})TD^2 + (\frac{T}{C} + r_g)D + r_c + \frac{T}{2C}} \tag{5.24}$$

for smaller values of time period T, K, series resistance of the capacitor r_c and higher values of capacitance C, the internal resistance of the motor r_g, 5.24 can be further approximated as,

$$I \simeq \frac{DV_g - V_{uc}}{r_g D} \tag{5.25}$$

In addition to that, 5.21 provides the inductance value as

$$L = \{(V_{uc} + Ir_c + \frac{IT}{2C}) - D(V_{uc} + Ir_c - \frac{IT}{C}) - \frac{3ITD^2}{2C}\}\frac{T}{\Delta I} \tag{5.26}$$

Approximation and rearrangement of 5.26 and 5.25 yields the inductance value as,

$$L = \frac{(1-D)V_{uc}Tr_gD}{(DV_g - V_{uc})\zeta} \tag{5.27}$$

where ζ is the normalized ripple percentage.

According to 5.25, the worst case duty cycle will occur under minimum current, maximum V_g and minimum V_{uc} conditions. Therefore, for the minimum value of 5V V_{uc}, a simulation is carried out by varying the duty cycle value D ($0 \leq D \leq 1$) and motor voltage V_g to obtain the current flow rates and inductance requirements for different operating conditions. A 2.5% current ripple is considered as the minimum current ripple in the inductor.

As illustrated in figure 5.14, the current flow rate in the circuit increases with the increase of the duty cycle value. In contrast, the required inductance value is decreases with the increment of the duty cycle value. In addition to that, the initial voltage of the motor is also a factor, which controls the duty cycle value with respect to the current flow requirements. As depicted in the figure, 24V V_g requires only 0.22 duty while 15V V_g requires a 0.38 duty to achieve a minimum of 1A current flow in the circuit. As a comparison, to achieve a current ripple of 2.5% in the inductor, 24V V_g requires a 9mH inductance while 15V V_g requires a 5.8mH inductance. In addition to that, increasing current flow significantly minimizes the inductance requirement.

Therefore, by placing the worst case conditions such as 24V V_g and 1A current flow rate, the maximum value of 9mH inductance is obtained for the buck mode operation of the power converter

Resistive power loss during the buck mode operation can be derived as,

$$P_{loss} = \frac{I^2(r_g D + r_c)T}{T} \Rightarrow P_{loss} = I^2(r_g D + r_c) \tag{5.28}$$

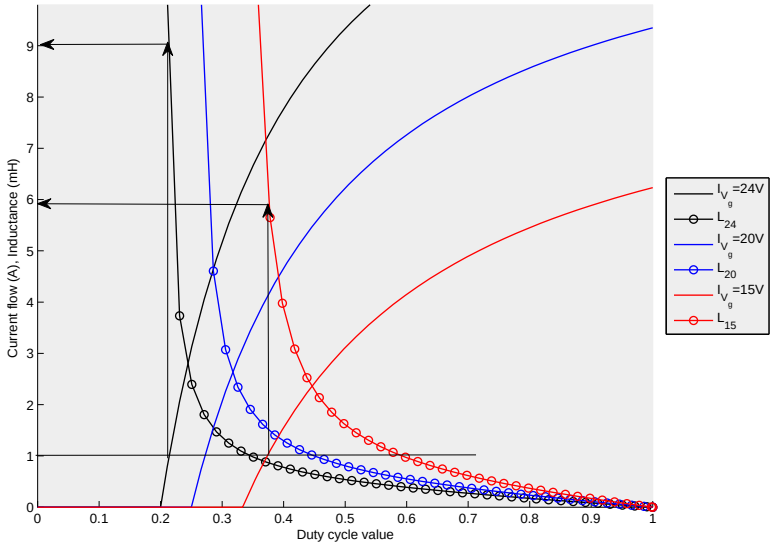

Figure 5.14: Current flow, Inductance variations with respect to the duty cycle value and initial voltage of the motor generator for the buck mode operation

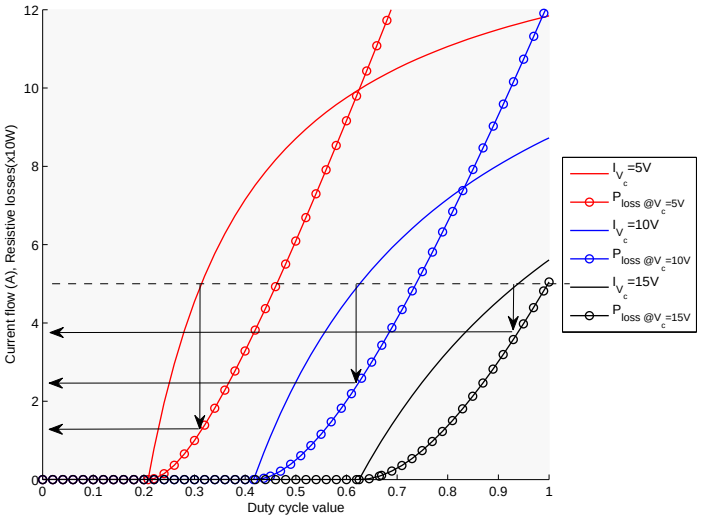

Figure 5.15: Current flow, resistive losses with respect to the duty cycle value and initial voltage of the motor generator for the buck mode operation

5.7.5 Boost mode operation of the Power converter (UC-charging)

The boost mode operation of the circuit is illustrated in figure 5.16, where the inductor is charging during the interval $T_0 < t < T_0 + DT$ and is discharging during the interval $T_0 + DT < t < T_0 + T$.

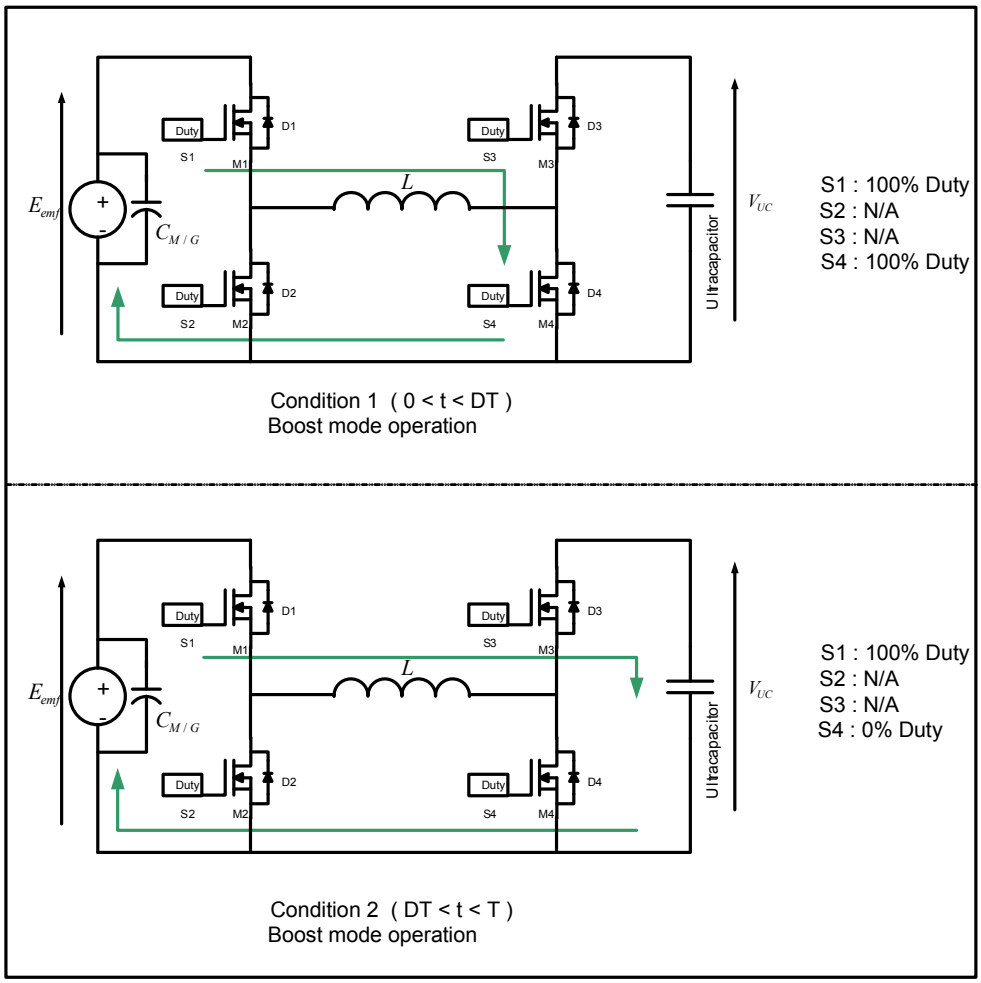

Figure 5.16: State diagram of the DC-DC converter for the boost mode operation

Applying kirchhoff's voltage law (KVL) to the circuit within the time interval $T_0 < t < T_0 + DT$ yields,

$$V_g - \int \dot{V}_g dt = ir_g + L\frac{di}{dt} \tag{5.29}$$

Rearranging 5.29 provides

$$L\frac{di}{dt} = V_g - \int \dot{V}_g dt - ir_g \tag{5.30}$$

similarly, applying KVL to the circuit within the time interval $T_0 + DT < t < T_0 + T$ yields,

$$V_g - \dot{V}_g DT - \int \dot{V}_g dt = i(r_g + r_c) + L\frac{di}{dt} + V_{uc} + \frac{1}{C}\int idt \tag{5.31}$$

Rearranging 5.31 provides

$$L\frac{di}{dt} = V_g - \dot{V}_g DT - \int \dot{V}_g dt - i(r_g + r_c) - V_{uc} - \frac{1}{C}\int idt \tag{5.32}$$

Figure 5.17 shows the voltage variation of the inductor and ultracapacitor bank during the boost mode operation of the converter.

As explained in the buck mode operation, a similar procedure is carried out to obtain the current flow rate and inductance value.

Integrating 5.30 within the time interval $T_0 < t < T_0 + DT$ yields,

$$L\Delta I = (V_g - Ir_g)DT - \frac{KI}{2}D^2T^2 \tag{5.33}$$

Similarly integrating equation 5.32 within the time interval $T_0 + DT < t < T_0 + T$ yields,

$$L\Delta I = (V_g - I(r_g + r_c) - V_{uc} - KIDT)(1 - D)T - \frac{KI}{2}(1 - D^2)T^2 - \frac{1}{2C}I(1 - D^2)T^2 \tag{5.34}$$

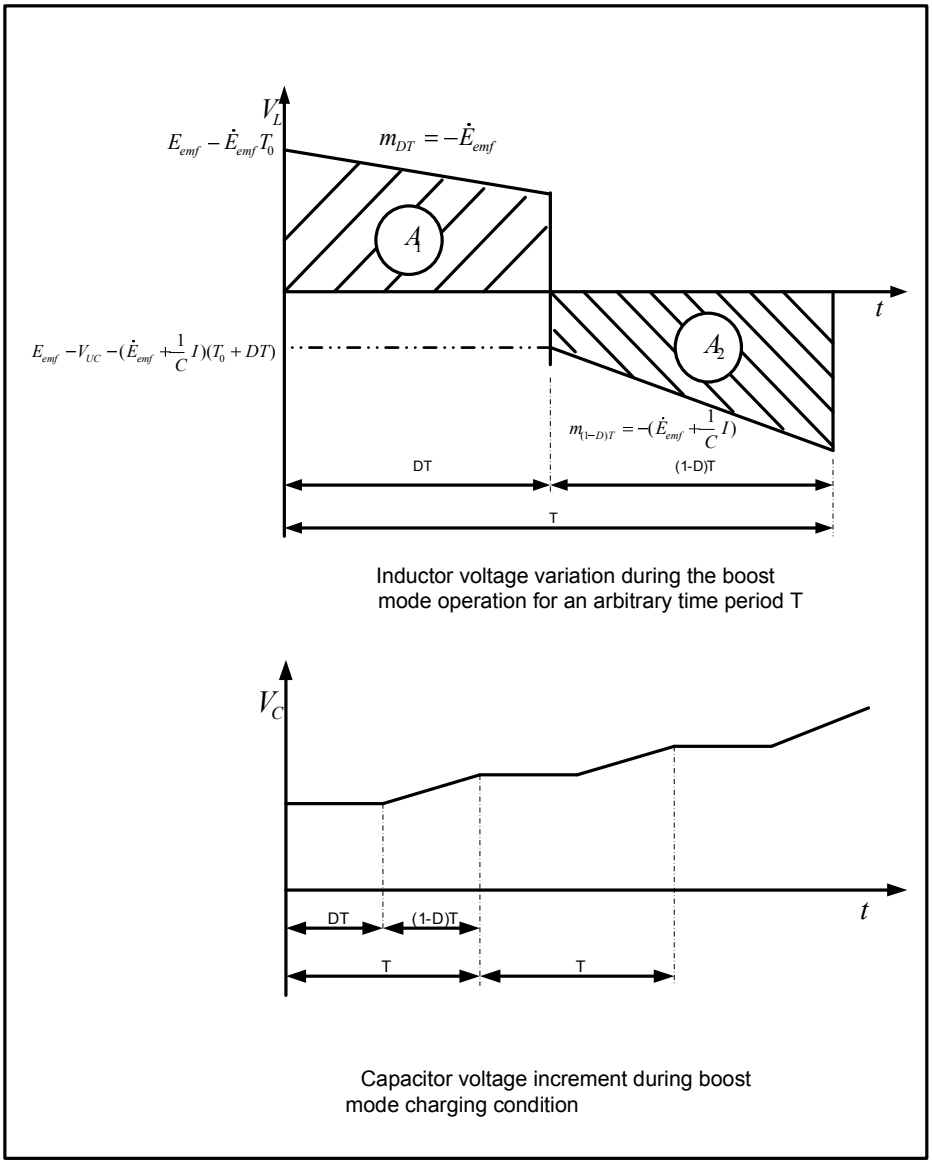

Figure 5.17: Voltage variation of the inductor and ultracapacitor during boost mode charging condition

For the volt-second balance of the inductor, $L\Delta I_{(T_0<t<T_0+DT)} + L\Delta I_{(T_0+DT<t<T_0+T)} = 0$,

Therefore 5.33 and 5.34 yields,

$$(k + \frac{1}{2C})ITD^2 - ((KT - r_c)I - V_c)D + (V_g - V_{uc} - I(r_c + r_g + \frac{KT}{2} + \frac{T}{2C})) = 0 \quad (5.35)$$

The current flow in the circuit can be calculated as,

$$I = \frac{(1-D)V_{uc} - V_g}{(k + \frac{1}{2C})TD^2 - (KT - r_c)D - (r_c + r_g + \frac{KT}{2} + \frac{T}{2C})} \tag{5.36}$$

As illustrated earlier, for a smaller value of time period T, K, the series resistance of the capacitor r_c and higher values of capacitance C, internal resistance of the motor r_g, 5.36 can be further approximated to,

$$I \simeq \frac{V_g - (1-D)V_{uc}}{r_g} \tag{5.37}$$

In addition to that, 5.33 yields the required inductance value as,

$$L = \frac{(V_g - Ir_g)DT - \frac{kI}{2}D^2T^2}{\Delta I} \tag{5.38}$$

Neglecting the higher order terms for smaller time period approximates the inductance value as,

$$L = \frac{(V_g - Ir_g)DT}{\Delta I} \tag{5.39}$$

From 5.37 and 5.39, it can be further simplified to

$$L = \frac{(1-D)V_{uc}r_gDT}{(V_g - (1-D)V_{uc})\zeta} \tag{5.40}$$

where ζ is the normalized percentage of the current ripple in the inductor.

It can be noticed from 5.40 that, increasing V_{uc} will increase the Inductance value. Apart from that, duty cycle D and motor terminal voltage V_g are also critical factors, which are significant for the inductor design. Therefore, different values of V_g are simulated by varying the duty cycle for a maximum value of $V_{uc} = 22V$.

Similar to the buck mode operation, a 2.5% current ripple is considered as the maximum current ripple in the inductor.

As illustrated in figure 5.18, to achieve a minimum current flow rate of 1A, 12.5 V V_g requires the maximum inductance value of 10.7mH. Also the inductance value is inversely proportional to the current flow rate, where higher current flow requires lower inductance values.

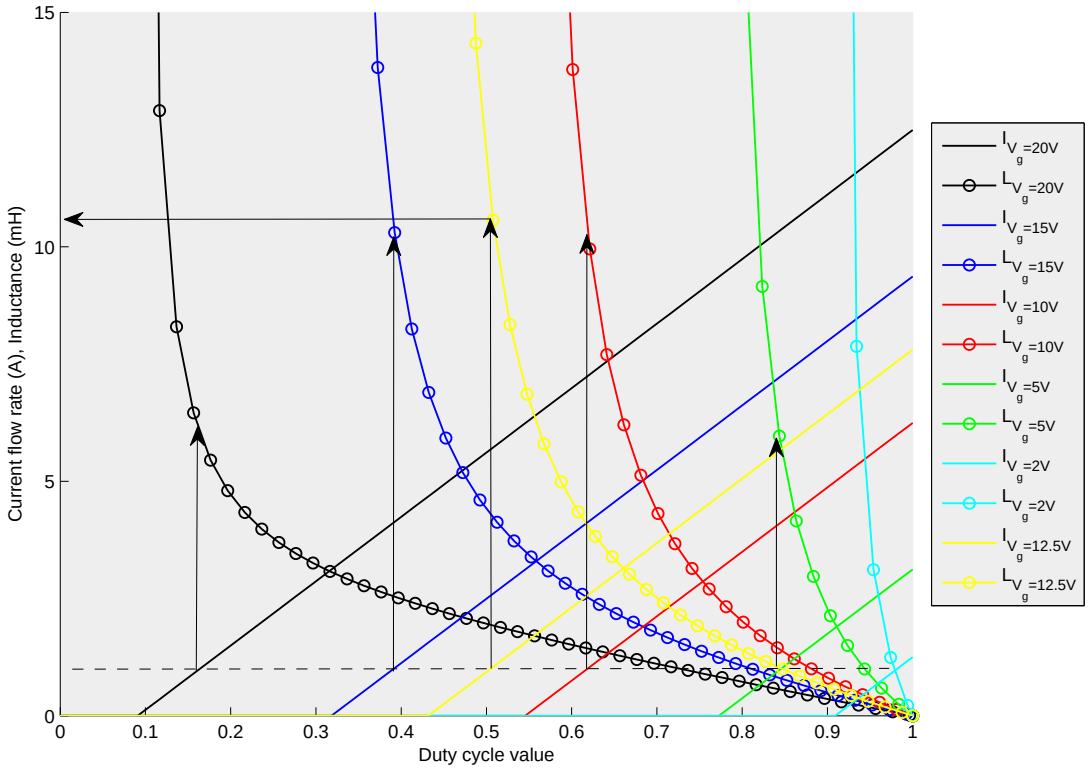

Figure 5.18: Current flow, Inductance variations with respect to the duty cycle value and initial voltage of the ultracapacitor bank for the boost mode operation

Resistive power loss during boost mode operation can be derived as,

$$P_{loss} = \frac{I^2(r_g + (1-D)r_c)T}{T} \Rightarrow P_{loss} = I^2(r_g + r_c(1-D)) \tag{5.41}$$

As depicted in figure 5.19, resistive losses are proportional to the duty cycle value and current flow rate in the converter.

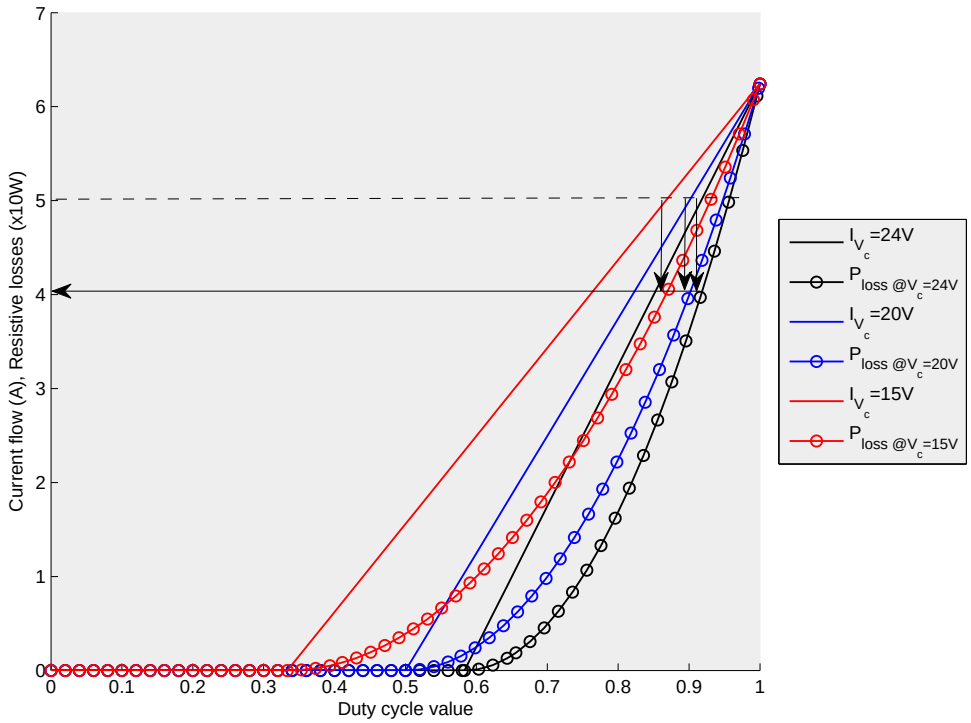

Figure 5.19: Current flow, resistive losses with respect to the duty cycle value and initial voltage of the ultracapacitor bank for the boost mode operation

From the above analysis for the buck and boost mode operation of the power converter, a design value of 10.7mH inductance is considered for the design.

5.7.6 Inductor design

The increase of inductance value significantly minimizes the current ripple Δi and switching losses by reducing the operating frequency of the converter. In contrast, the transient response of the converter will slow down with the increment of the inductance value as ($V_L = L\frac{di}{dt}$), which is not desirable for the vehicular power train application [61], [75] and [76]. Therefore the inductor should be able to handle the power requirement of the propulsion system with quick transient response and minimum energy losses. In terms of regenerative braking systems, the voltage bandwidth of the operating region for the converter appears wider than other applications. On the other hand if we narrow down the operating band width, it will constrain the kinetic energy recovery of the vehicle. As a result of

Table 5.3: Operational specification of the converter

Inductance	10.7 mH
Operating motor voltage	24 - 5 V
Operating Ultracapacitor voltage	5 - 22 V
Average current flow	5 A
Operating frequency	20 kHz
Current ripple	2.5 %

these reasons, sizing of the inverter is a compromise between operating range and current ripple [76].

This section describes the design procedure of the inductor, where the detail specifications and the design constraints are depicted in table 5.3.

The use of a ferrite core material for this design favored to minimize the copper losses in the inductor. Otherwise, as a result of the lower permeability of the air, it requires a higher number of turns to achieve the same inductance value hence a higher series resistance will increase the copper losses. EPCOS ETD 54 Ferrites core N87 material is used for the construction of the inductor. With reference to the manufacturers data sheet, 370 mT is considered as the maximum operating flux density for the design, which is always less than the saturation flux density [77].

The Inductor design was carried out based on the geometrical constraint (K_g) method as illustrated in [76]. The relationship of the geometrical properties of the core material is defined as K_g . The objective is to size an appropriate core geometry, which allows accommodation of the winding material to produce the required inductance value. Accordingly the design constraints can be given by the following mathematical inequality 5.42.

$$K_g = \frac{A_c^2 W_A}{MLT} \geq \frac{\rho L^2 I_{max}^2}{B_{max}^2 R K_u} 10^8 cm^5 \tag{5.42}$$

Where K_g is the core geometrical constraint and is obtained from the manufacturers data sheet, A_c is the cross sectional area of the magnetic core in cm^2. W_A

is the core window area available for the winding in cm^2, MLT is the mean length per turn in cm and these parameters are the geometrical constraints of the core material.

The design specification for the inductor is specified in the right hand side of the inequality, where ρ is the resistivity of the winding wire in $\Omega - cm$, L is the required inductance value in H. I_{max} is the peak winding current in A, B_{max} is the maximum operating flux density in T, R is the series winding resistance in Ω and K_u is the winding fill factor.

Therefore the geometrical constraints of the core material yields

$$K_g = \frac{380^2 \times 330}{70} \times 10^{-5} \quad cm^5 = 6.8cm^5 \tag{5.43}$$

As a design constraint, 0.2 Ω internal resistance is considered, which is approximately 14% of the internal resistance of the electric motor. According to the design guidelines given in [76], 0.5 is considered as the value of winding fill factor K_u. Under these specifications, the inequality for K_g yields,

$$K_g \geq \frac{1.724 \times 10^{-6} \times 10700^2 \times 10^{-12} \times 1^2}{370^2 \times 10^{-6} \times 0.2 \times .5} \times 10^8 \quad cm^5 = 1.4 \quad cm^5 \tag{5.44}$$

The comparison shows that the inequality is satisfied, therefore the chosen core material is appropriate for the application.

As the second stage of the design procedure, the turns ratio n is calculated by the following equation

$$L = A_L n^2 10^{-9} \Rightarrow n = 42 \quad turns \tag{5.45}$$

Where A_L is obtained from the manufactures data sheet and which is 5800 nH.

Since the internal resistance is a known parameter, the cross sectional area of the copper wire for the winding is obtained from 5.47

Table 5.4: Design specification and actual value comparison of the inductor

Parameter	Final value
Inductance	10.4 mH
Number of turns	42
Series internal resistance	0.08Ω

$$A_w = \rho \frac{n(MLT)}{R} = 1.724 \times 10^{-6} \frac{42 \times 7}{0.2} = 2.5 \times 10^{-3} cm^2 \tag{5.46}$$

The obtained A_w value and turn ratio are used to recalculate the core window area W_A to cross check the space availability for the winding. As it calculated, the selected coil requires only 3.2% of the available space. Therefore, it is possible to increase the cross sectional areas of the copper wire, which will further minimize the internal resistance of the inductor. As a design decision, 10.5% of the core window area is utilized for the winding purposes. Therefore 42 turns of 18 AWG wire was wound on the former to construct the inductor, which minimizes the internal resistance of the inductor to 0.07Ω.

Due to the series resistance, the power loss of the inductor can be derived as

$$P_L = I_L^2 R_L \tag{5.47}$$

Where P_L is the resistive loss in the inductor, I_L is the DC current and R_L is series resistance of the inductor.

The inductor core geometry and the sectional view of the core assembly are depicted in figure 5.20.

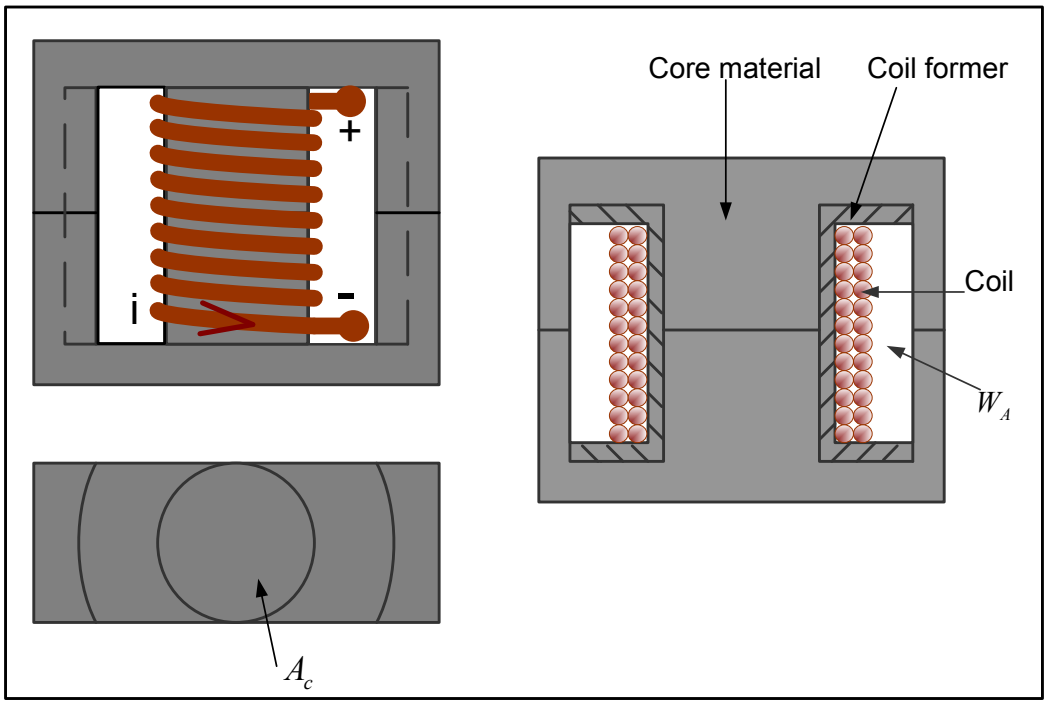

Figure 5.20: Symmetric of the inductor core geometry and sectional view of the core assembly

5.7.7 Summary

The hardware description of the experimental frame work is discussed in this chapter. The analysis, design, and construction procedure of the hardware system is detailed step by step. To simplify the implementation, a flywheel vehicle model is introduced and its characteristics are correlated with the real vehicle system from the view point of regenerative braking energy. Following that, the operating principle of the hardware system and data acquisition methods and control system design are described. The charging characteristics of the UC bank and its connection configuration is analyzed to fulfil the current, voltage and power requirements of the system. Consequently, the power converter topology selection procedure is presented based on the operating requirement of the system. The operating principle of the proposed bidirectional buck/ boost DC-DC converter is also described. Based on that, the analysis and design procedure for the power electronics and inductor is addressed. Detailed circuit diagrams and photographs of the experimental test bench can be seen in the appendix.

Chapter 6

Experiment Procedure, Results and Discussion

6.1 Introduction

The experiments and their results are presented in this chapter. Initially the calibration procedure of the mechanical braking system is presented. Subsequently, an experiment is conducted to verify the correlation between the kinetic energy recovery and deceleration rate. Here two different operating conditions of the regenerative braking systems were tested such as constant torque and constant power operating mode. In constant torque mode operation five different torque rates are experimented and compared to understand the effect of braking torque on kinetic energy recovery. Consequently, four different constant power flow rate braking scenarios are also investigated. Finally Heavy braking scenarios are investigated that make use of combined braking actuation. An issue related to the kinetic energy recovery in heavy braking events is explained based on braking distance and potential time duration for energy recovery. As were described in chapter 4, a discrete braking profile is examined that achieves the same braking distance with different state conditions throughout the braking process. Results are compared to explain the answers to the question "why net recovered energy varies for different deceleration profiles?" To increase the kinetic energy recovery, a novel brake sharing strategy is employed and results are compared. Six different braking scenarios are tested and results are compared and analyzed.

6.2 Calibration of the mechanical braking system

Calibration of the mechanical braking system is essential for the control of the braking system. As illustrated in the previous chapter, the mechanical braking

system is activated by a stepper motor. Therefore each step of the stepper motor exerts a braking force in the brake disk. Due to the vibration and nonlinear operating behavior of the calliper actuator mechanism, the mechanical braking system does not hold a linear relation-ship between the step angle and braking force. Repeatability and reliability are important factors, which must be ensured before performing experiments.

Therefore by increasing the rotor angle of the stepper motor, the relevant braking force distribution is obtained and the mechanical braking system is calibrated. For the repeatability assessment, the same procedure is carried out five times and the obtained data are compared. Figure 6.1 illustrates the data captured in each of the experiments and the average braking torque and percentage deviation of them with respect to the rotor angle variation of the stepper motor. It should be noted from the table that, the maximum percentage deviation of the braking torque is 3.4%, which shows the mechanical braking system is repeatable within a minimum error bandwidth. Correlation between the step angle variation and calibrated braking torque is depicted in figure 6.2 and it is utilized for the experiments.

6.3 Experimental procedure

The flowchart in the figure 6.3 illustrates the experimental procedure. Initially the flywheel is charged by the external power supply. When the flywheel reaches a speed of 1220 rpm, the external power supply is disconnected from the system. Meanwhile a predefined braking profile is exported to the controller. The controller activates the braking system when the speed of the flywheel reaches 1210 rpm. Therefore as the flywheel speed drops below 1210 rpm by aerodynamic and transmission resistance, the braking system is activated by the controller. Since the initial speed of the flywheel and the second moment of inertia of the system are known parameters, stored energy is obtained by the following mathematical equation

$$E_{FW} = \frac{1}{2} J (\frac{2\pi N_f}{60})^2 \tag{6.1}$$

Step Angle x0.05625 deg	Exp 1		Exp 2		Exp 3		Exp4		Exp 5		Average
	Tor(mNm)	% dev	Tor(mNm)	% dev	Tor(mNm)	% dev	Tor(mNm)	% dev	Tor(mNm)	% dev	
180	179	1.4	187	3.0	184	1.3	176	3.1	182	0.2	181.6
190	610	1.3	590	2.1	602	0.1	614	1.9	596	1.1	602.4
200	918	0.7	893	3.4	927	0.3	934	1.0	951	2.9	924.6
210	1018	2.9	1023	2.4	1054	0.6	1071	2.2	1074	2.5	1048.0
220	1136	3.1	1167	0.5	1179	0.5	1192	1.6	1190	1.5	1172.8
230	1298	2.1	1305	1.6	1335	0.6	1346	1.5	1348	1.6	1326.4
240	1374	2.3	1389	1.3	1402	0.3	1436	2.1	1433	1.9	1406.8
250	1476	1.8	1486	1.2	1519	1.0	1537	2.2	1501	0.2	1503.8
260	1615	1.4	1608	1.9	1635	0.2	1652	0.8	1682	2.7	1638.4
270	1694	1.2	1696	1.0	1723	0.5	1738	1.4	1718	0.2	1713.8
280	1771	1.9	1795	0.6	1805	0.0	1830	1.4	1827	1.2	1805.6
290	1890	1.8	1917	0.4	1934	0.4	1899	1.4	1987	3.2	1925.4
300	2009	0.8	2009	0.8	2017	0.4	2032	0.4	2057	1.6	2024.8
310	2083	1.2	2065	2.0	2120	0.6	2135	1.3	2137	1.4	2108.0
320	2154	1.7	2181	0.5	2183	0.4	2214	1.0	2225	1.5	2191.4
330	2304	1.3	2317	0.8	2334	0.0	2348	0.6	2370	1.5	2334.3
340	2408	1.3	2422	0.7	2439	0.0	2452	0.5	2476	1.5	2439.4
350	2513	1.2	2527	0.7	2543	0.0	2557	0.5	2582	1.5	2544.4
360	2617	1.2	2633	0.6	2648	0.1	2661	0.4	2689	1.5	2649.4
370	2722	1.2	2738	0.6	2752	0.1	2765	0.4	2795	1.5	2754.4
380	2826	1.2	2843	0.6	2857	0.1	2870	0.4	2901	1.5	2859.4
390	2931	1.1	2948	0.5	2961	0.1	2974	0.3	3007	1.5	2964.5
400	3035	1.1	3054	0.5	3066	0.1	3079	0.3	3114	1.4	3069.5

Figure 6.1: Average braking torque and percentage deviation with respect to the step angle variation of the stepper motor

where J is the equivalent second moment of inertia of flywheel system, N_f is speed of the flywheel system in *rpm*

Feed-back information about the system such as the speed of the flywheel, current flow rate of the electric motor and UC-bank are utilized for the control of the power converter and mechanical braking system. During the braking process, voltage variation of the electric motor and UC-bank, duty cycle variation of the power converter and braking distance are also recorded in the data acquisition system for analysis.

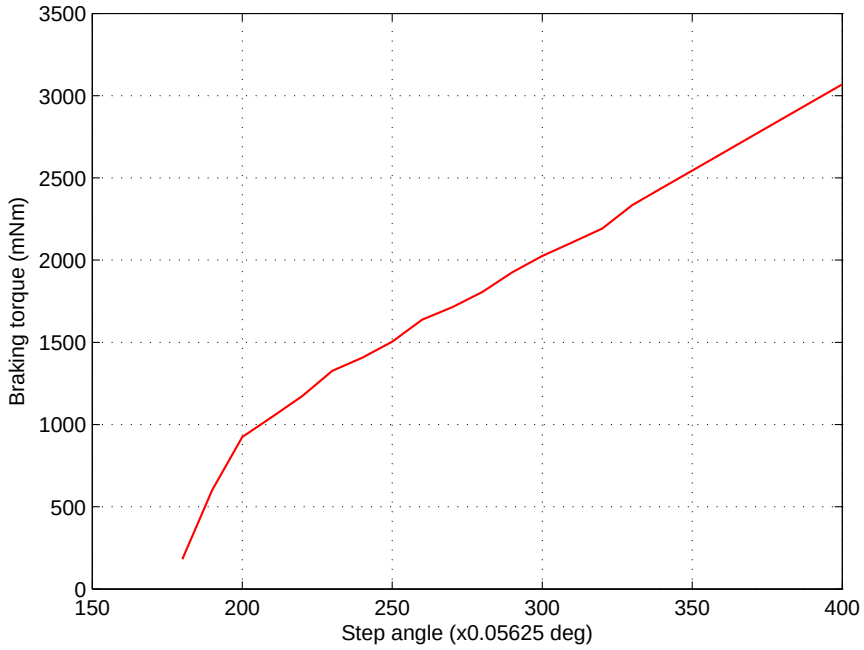

Figure 6.2: Step angle variation and calibrated braking torque

6.4 Experiment 1 : Constant torque braking scenario

The main purpose of this experiment is to understand the constraints which appear as the limiting factors on the kinetic energy recovery of the system. Results of this experiment can be utilized to design an appropriate braking strategy to increase the kinetic energy recovery of the electric drive train.

6.4.1 Procedure

The experiment was conducted using the designed hardware illustrated in chapter 6. As illustrated in the previous section, each test was performed with the same initial condition of the flywheel system (where the braking process starts when the flywheel system reached or fell to a speed of 1210 rpm). Since the torque can be written as a function of the torque constant of the motor and current flow rate, appropriate choice of the current flow rate controls the torque produced by the motor. Applying this concept, five different torque values were evaluated and

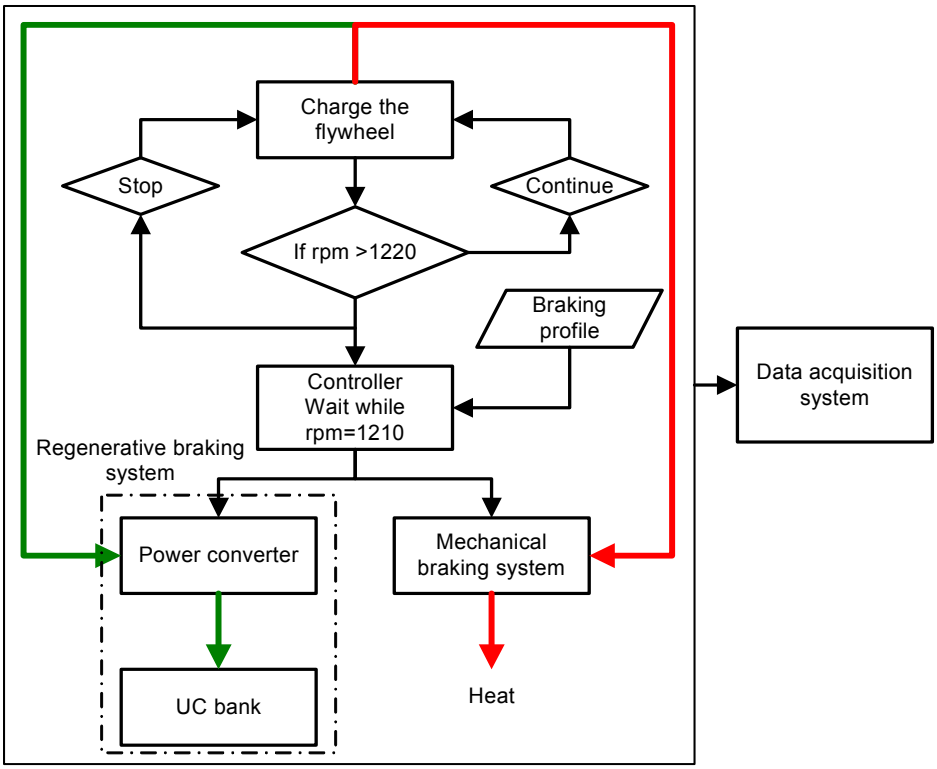

Figure 6.3: Experimental procedure

the recovered energy, braking distance, velocity profile, torque profile, voltage variation of the electric motor, UC-bank and variation of the duty cycle value were analyzed.

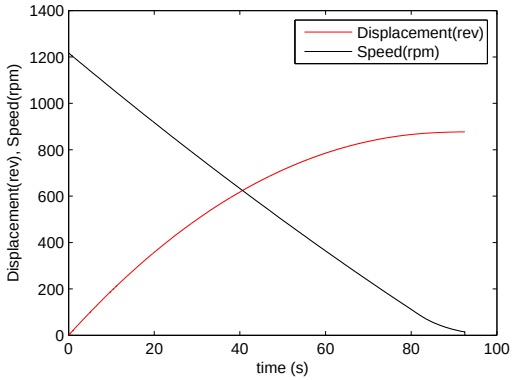

(a) Speed, braking distance Vs time

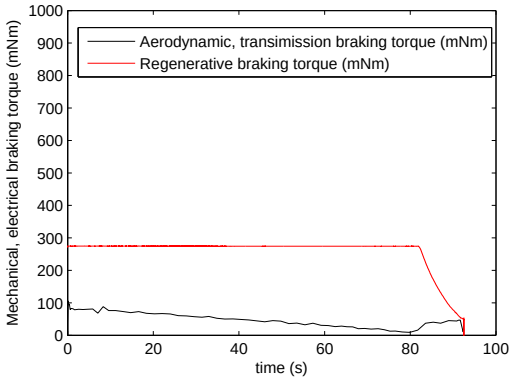

(b) Braking torque Vs time

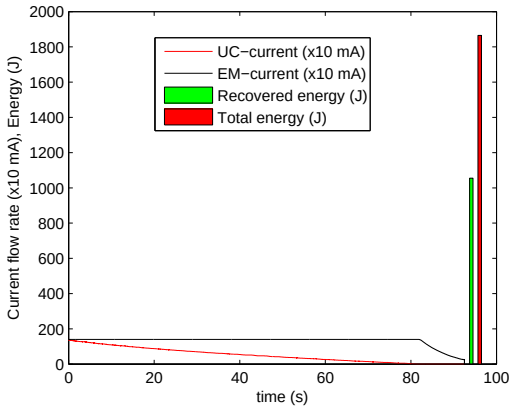

(c) Current flow rate Vs time, energy

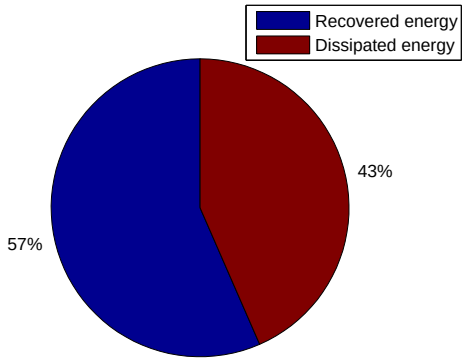

(d) Percentage share of recovered energy on total energy

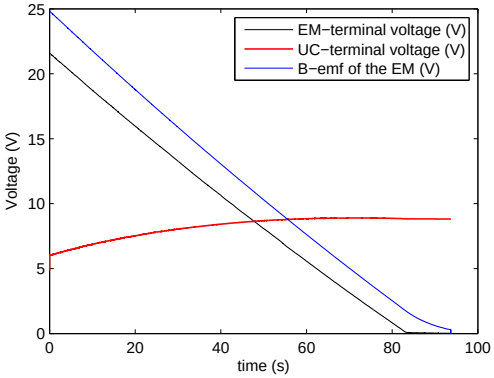

(e) Voltage Vs time

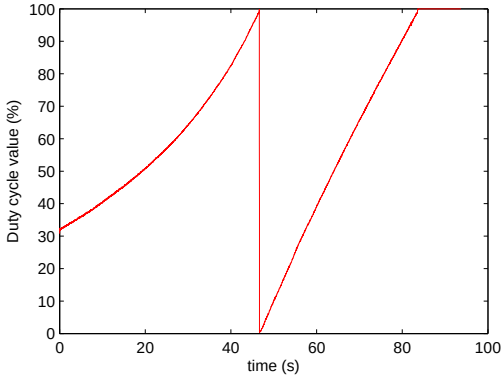

(f) Duty cycle variation of the power converter Vs time

Figure 6.4: Constant Torque braking scenario 1: 270 mNm

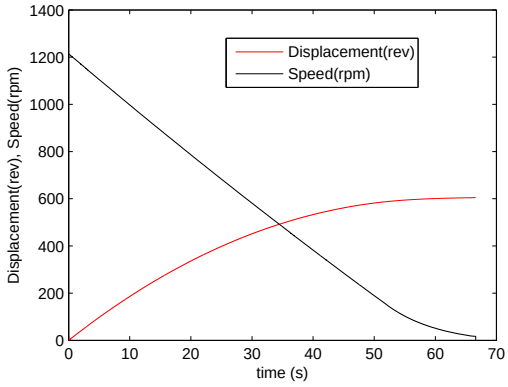

(a) Speed, braking distance Vs time

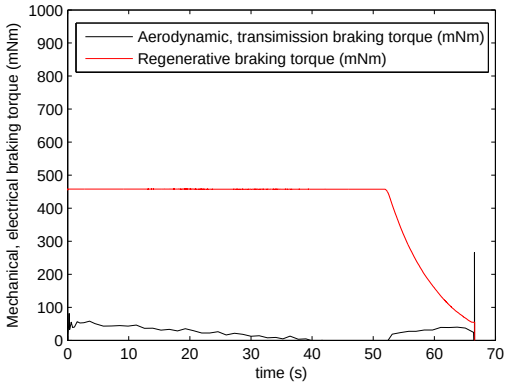

(b) Braking torque Vs time

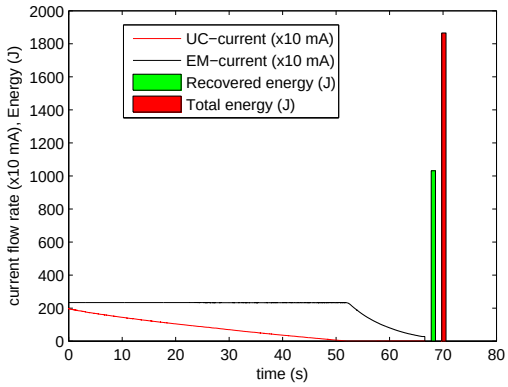

(c) Current flow rate Vs time, energy

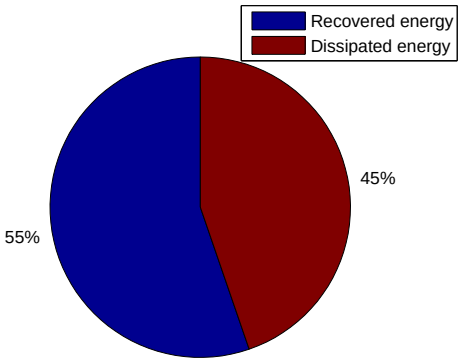

(d) Percentage share of recovered energy on total energy

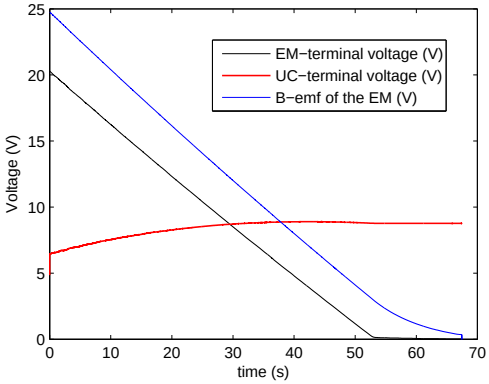

(e) Voltage Vs time

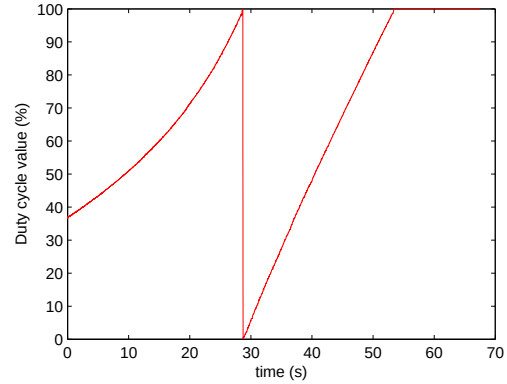

(f) Duty cycle variation of the power converter Vs time

Figure 6.5: Constant Torque braking scenario 2: 455 mNm

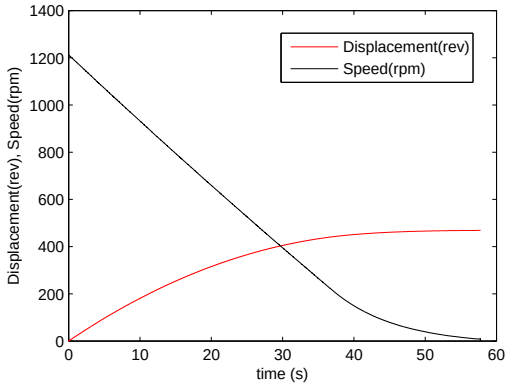

(a) Speed, braking distance Vs time

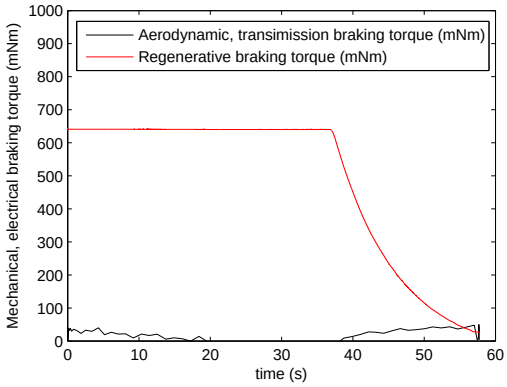

(b) Braking torque Vs time

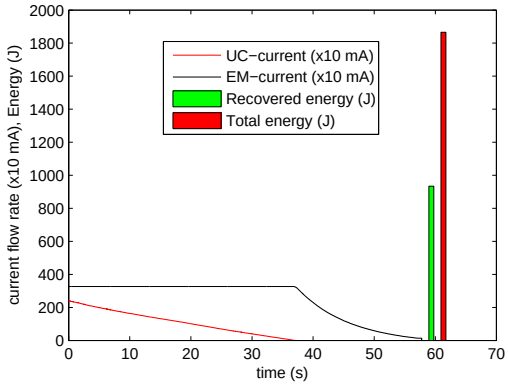

(c) Current flow rate Vs time, energy

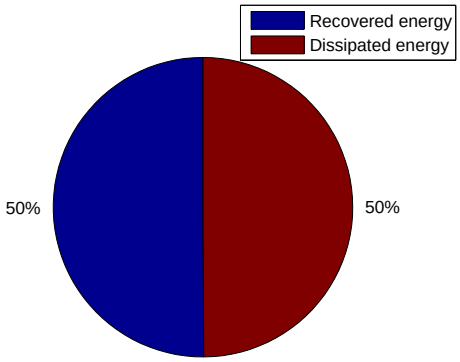

(d) Percentage share of recovered energy on total energy

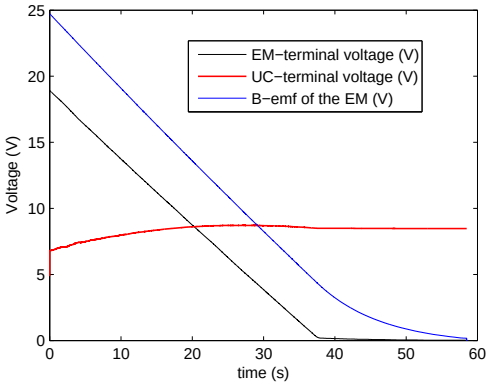

(e) Voltage Vs time

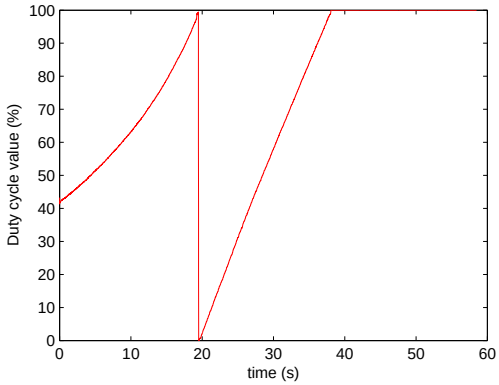

(f) Duty cycle variation of the power converter Vs time

Figure 6.6: Constant Torque braking scenario 3: 640 mNm

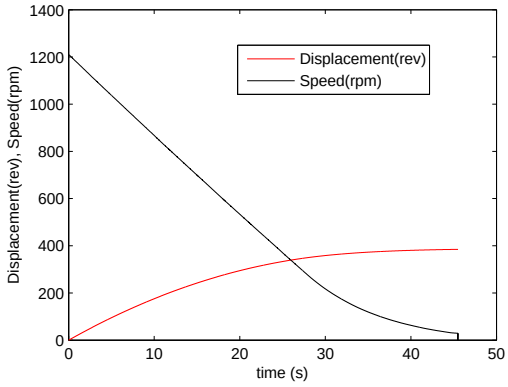

(a) Speed, braking distance Vs time

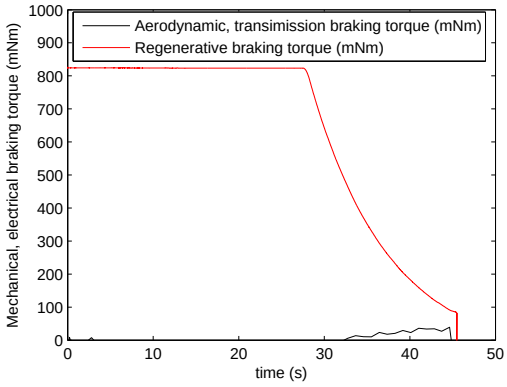

(b) Braking torque Vs time

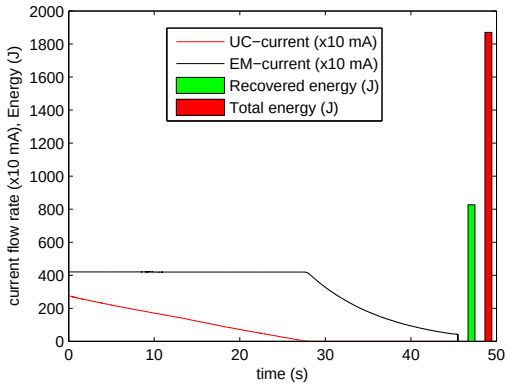

(c) Current flow rate Vs time, energy

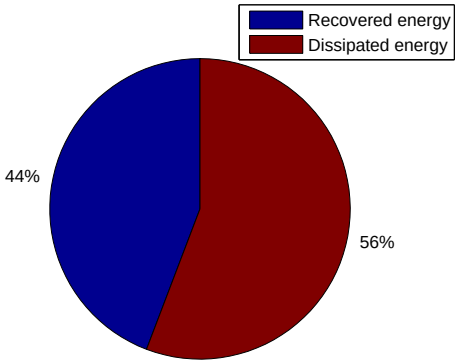

(d) Percentage share of recovered energy on total energy

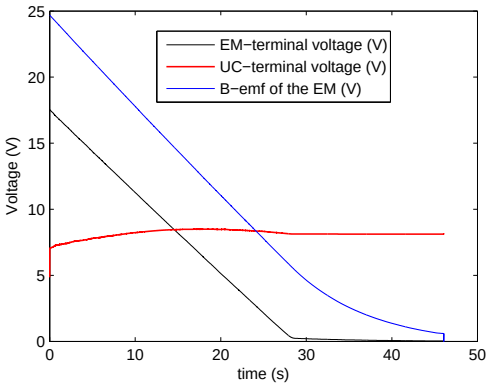

(e) Voltage Vs time

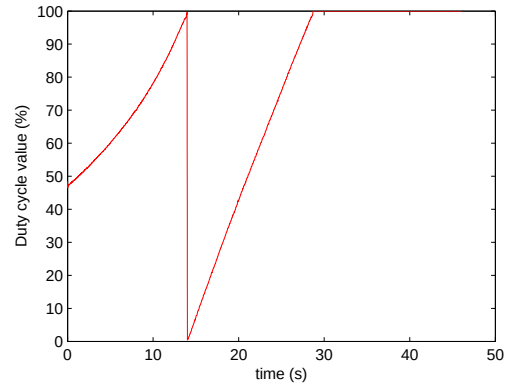

(f) Duty cycle variation of the power converter Vs time

Figure 6.7: Constant Torque braking scenario 4: 825 mNm

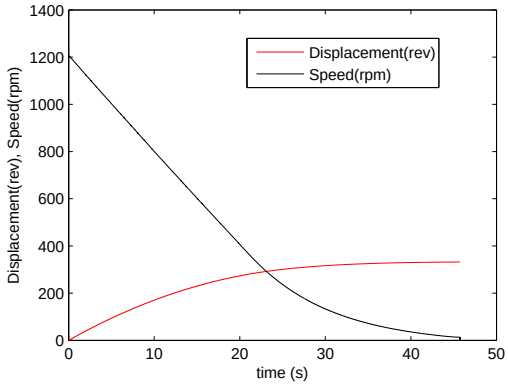

(a) Speed, braking distance Vs time

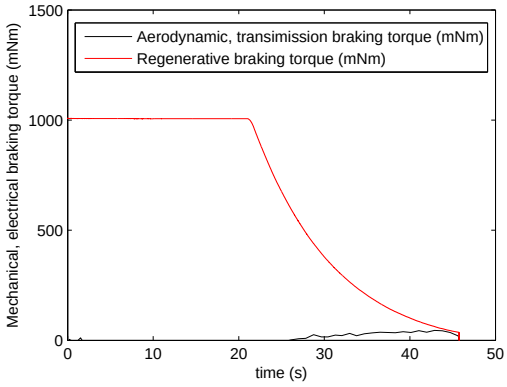

(b) Braking torque Vs time

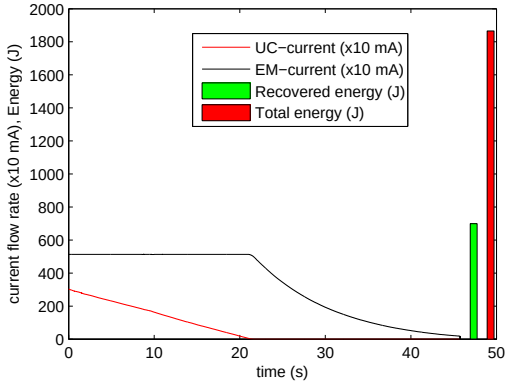

(c) Current flow rate Vs time, energy

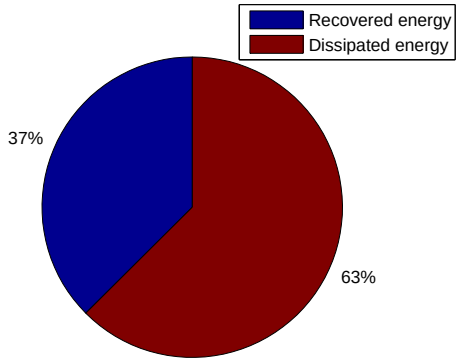

(d) Percentage share of recovered energy on total energy

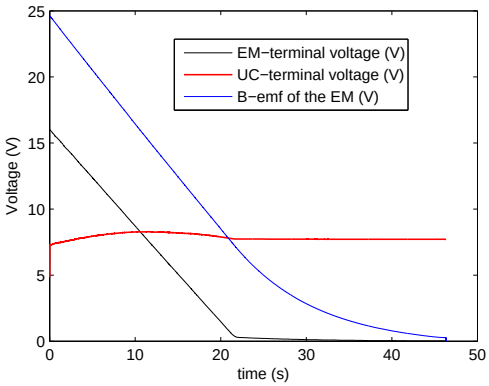

(e) Voltage Vs time

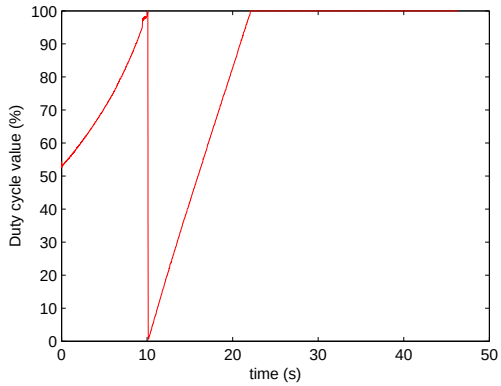

(f) Duty cycle variation of the power converter Vs time

Figure 6.8: Constant Torque braking scenario 5: 1005 mNm

6.4.2 Discussion

Figure 6.4 shows the results obtained for a 270 mNm maximum braking torque event. Figure 6.4.a depicts the speed variation and the angular displacement of the flywheel system with respect to the time throughout the braking duration. Figure 6.4.b shows the braking torque distribution over the time period, where the torque due to the aerodynamic and transmission resistance as well as the regenerative braking torque are shown. As it can be noticed from the figure that up to 83 sec the regenerative braking torque remains constant and declines after that. As described in chapter 4, due to the speed variation and internal resistance of the electric motor, sufficient B-emf could not produced by the motor to generate the predefined torque below the speed of 100 rpm for this condition. At the same time the torque due to the aerodynamic and transmission resistance also contributes to the braking process. Lower braking torque distribution result in a higher angular displacement and longer braking period for this case.

Figure 6.4.c shows the current flow rate of the electric motor and UC-bank. Although there is a current flow from the electric motor for the entire braking duration, the current flow into the UC-bank stopped after 80 sec. Also it should be noted here that, the current flow into the UC-bank declines due to the decreasing regenerative braking power flow of the system. As emphasized earlier, insufficient B-emf and internal resistance of the motor generator result in zero current flow in the UC-bank after 80 sec. The total energy stored in the flywheel at the beginning of the braking process and recovered energy are depicted in figure 6.4.c 6.4.d. Almost 57% of the stored energy is recovered in the UC-bank in this braking scenario.

Figure 6.4.e shows the terminal voltage of the electric motor and UC-bank. The back-emf of the electric motor is calculated by multiplying the speed of the motor with the back-emf constant, which is obtained from the manufactures data-sheet. As can be seen, there is a significant voltage difference between the measured and the calculated back-emf voltage of the EM. This is explained by the voltage drop inside the electric motor, which is eventually dissipated as heat by internal resistance.

Figure 6.4.f illustrates the variation of the duty cycle value of the power converter. The first half of the duty cycle variation explains the buck mode operation

of the power converter. Once it reaches a value of 100% in the buck mode operation, it switches to the boost mode operation which gradually increases the duty cycle to 100% duty cycle value. At the same time when duty cycle value reaches 100% in boost mode operation, there is no current flow into the UC-bank and the electric motor is short circuited. Therefore all the available energy in the flywheel system after this point is simply dissipated as heat in the internal resistance of the electric motor and in the transmission system.

Figure 6.5 shows the results obtained for a 455 mNm constant braking torque scenario. The results show some similarity with the previous experiment; however braking distance, braking duration and recovered energy quantity are different compared with the above. With the increase of the current, the recovered energy quantity is reduced to 55% in this braking condition.

Similarly, results depicted in Figure 6.6, 6.7 and , 6.8 are also can be explained. It should be noticed from these results that, increasing the current significantly affects the kinetic energy recovery of the flywheel system. Here a considerable amount of voltage drop occurs in the electric motor with increasing current. For this reason, a significant amount of energy cannot be recaptured in higher current conditions. In addition to that, higher current causes the power converter to saturate the duty cycle faster than lower current. As a comparison, when we consider figure 6.4 and 6.8, there is a current flow into the UC-bank until a two volts of back-emf in the first case while there is no charge current flow into the UC-bank after the back-emf reached a value of seven volts. Moreover, the net recovered energy varies by 20% between the above two cases. This fact demonstrates that higher braking torque is not desirable for the kinetic energy recovery of the electric propulsion system. However in reality, there are a variety of braking scenarios a vehicle should undergo depending upon the driving circumstances, which includes higher, medium and lower braking cases. This implies that the kinetic energy recovery is a compromise.

It should also be noticed from the figure that, just after the duty cycle value reached 100% in the power converter, the braking system looses its controllability. Therefore, the mechanical braking system should be engaged to ensure the complete controllability of the drivetrain system in low speed braking scenarios.

As illustrated in the figures, increasing the current flow of the motor increases the current flow into the UC-bank. These effects quicken the energy recovery

process within a short time frame (otherwise it requires a longer time period). However, there are braking events, where the braking period and braking distance are shorter than above (heavy braking events). Therefore this fact can be effectively utilized to increase the energy recovery in such braking scenarios.

6.5 Experiment 2 : Constant power braking

This experiment serves as a platform to understand the issues related to braking the drivetrain system by drawing a constant power flow rate. This experiment also illustrates the operating limitations of the drivetrain system, which restrict the kinetic energy recovery. These results are compared with the constant torque braking scenario to understand the difference in operating behavior.

6.5.1 Procedure

This experiment was also performed with the same initial condition of the flywheel system (where the braking process starts when the flywheel system reaches a speed of 1210 rpm). With respect to the speed of the flywheel system, braking torque of the motor has been changed (it has been achieved by modifying the reference duty cycle value of the power converter with respect to the speed variation of the flywheel system). As a safety requirement, the maximum current was limited to 5.8A, which is close to the maximum current which can be measured by the current transducer. Four different braking power conditions are tested and the recovered energy, braking distance, velocity profile, torque profile, voltage variation of the electric motor, UC-bank and variation of the duty cycle value were analyzed.

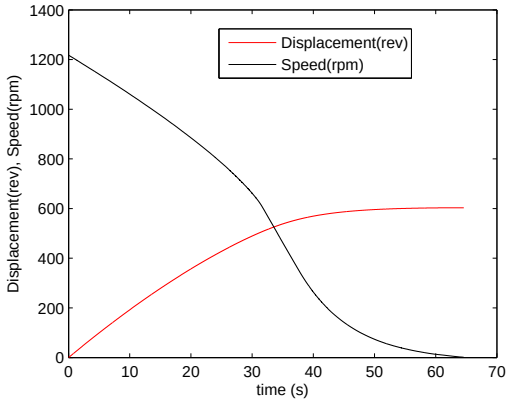

(a) Speed, braking distance Vs time

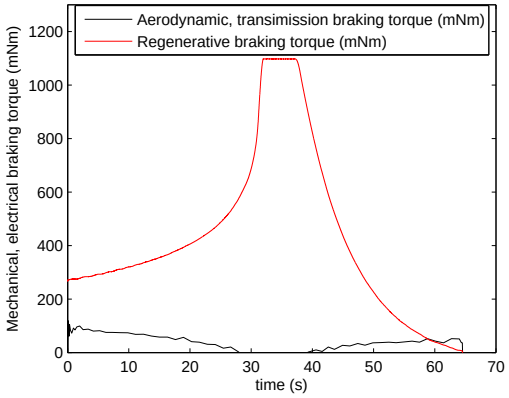

(b) Braking torque Vs time

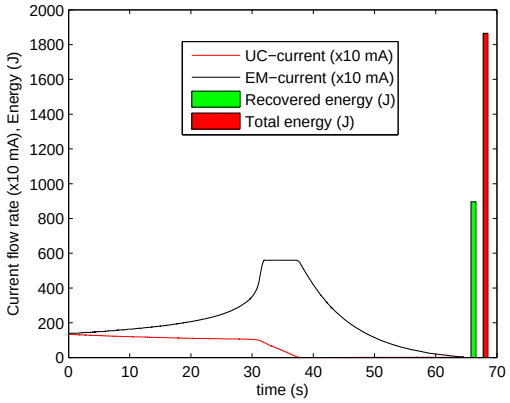

(c) Current flow rate Vs time, energy

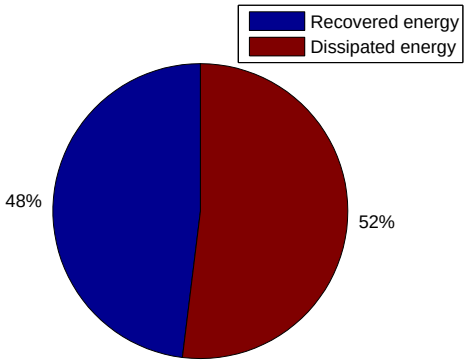

(d) Percentage share of recovered energy on total energy

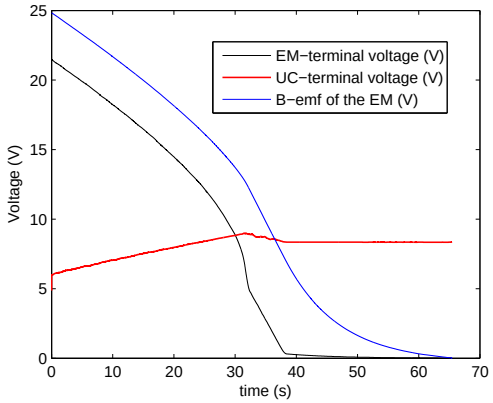

(e) Voltage Vs time

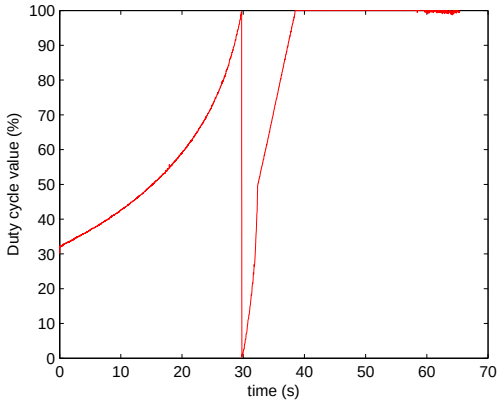

(f) Duty cycle variation of the power converter Vs time

Figure 6.9: Constant Power flow braking scenario 30W

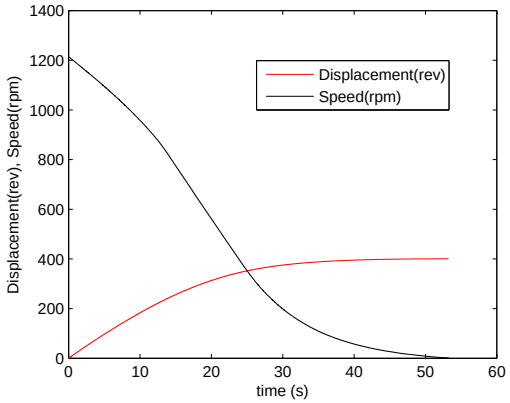

(a) Speed, braking distance Vs time

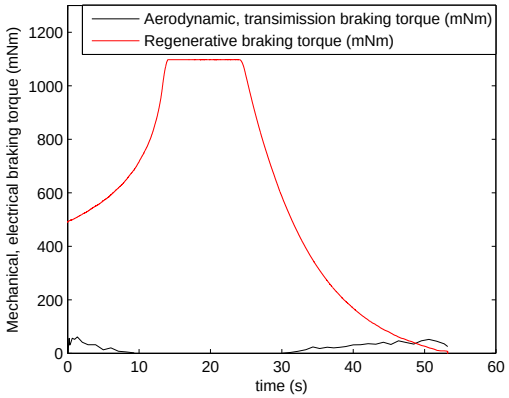

(b) Braking torque Vs time

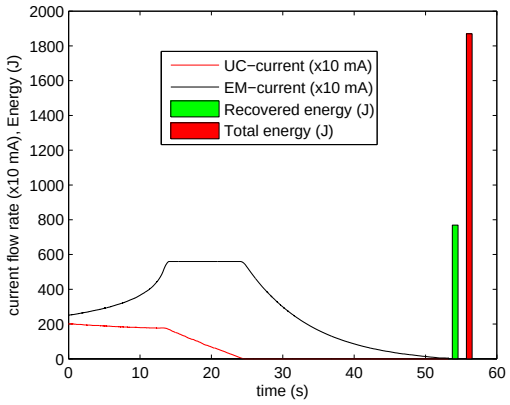

(c) Current flow rate Vs time, energy

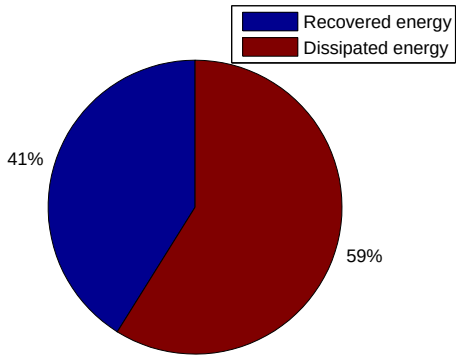

(d) Percentage share of recovered energy on total energy

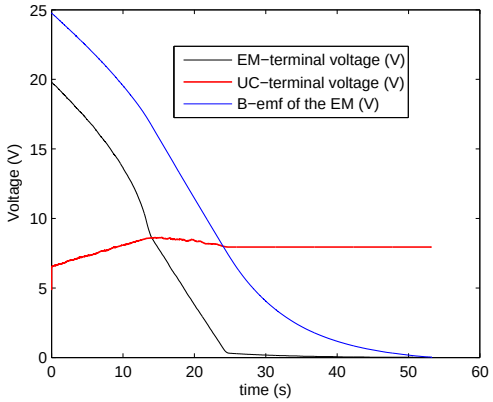

(e) Voltage Vs time

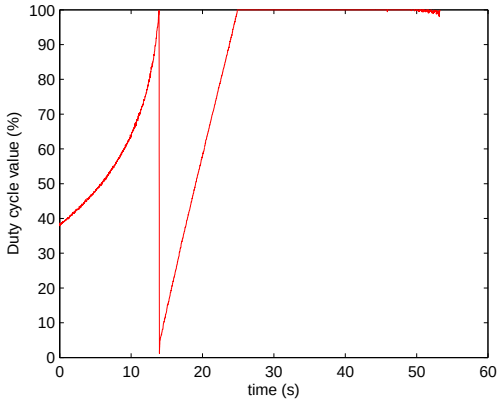

(f) Duty cycle variation of the power converter Vs time

Figure 6.10: Constant Power flow braking scenario 65W

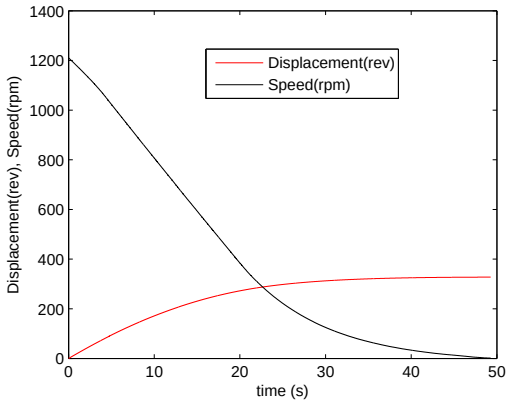

(a) Speed, braking distance Vs time

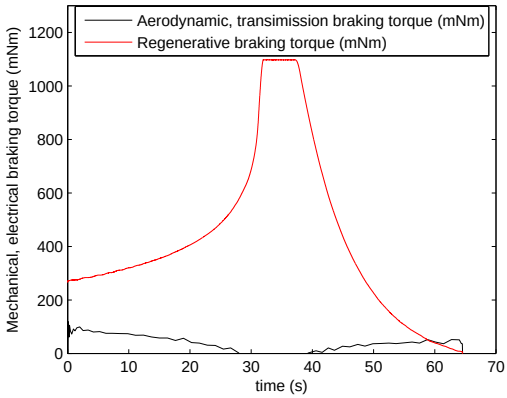

(b) Braking torque Vs time

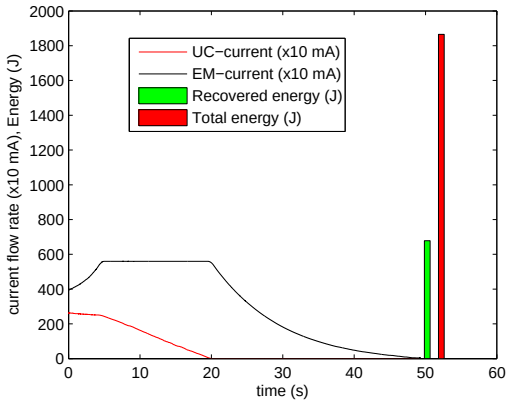

(c) Current flow rate Vs time, energy

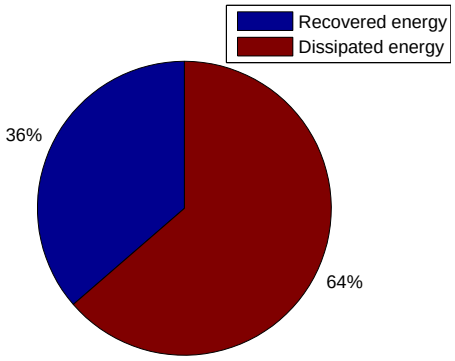

(d) Percentage share of recovered energy on total energy

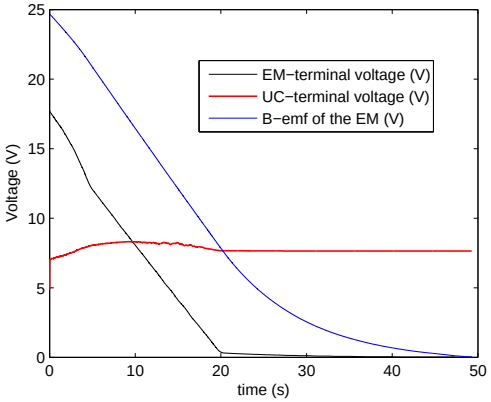

(e) Voltage Vs time

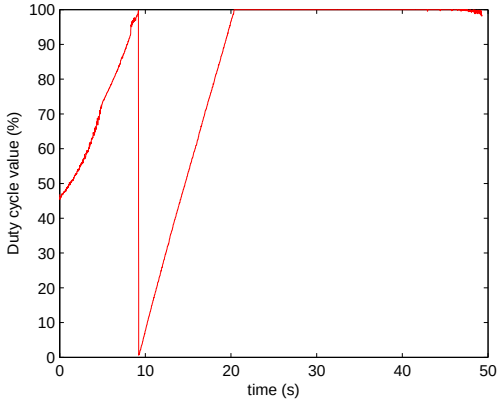

(f) Duty cycle variation of the power converter Vs time

Figure 6.11: Constant Power flow braking scenario 96W

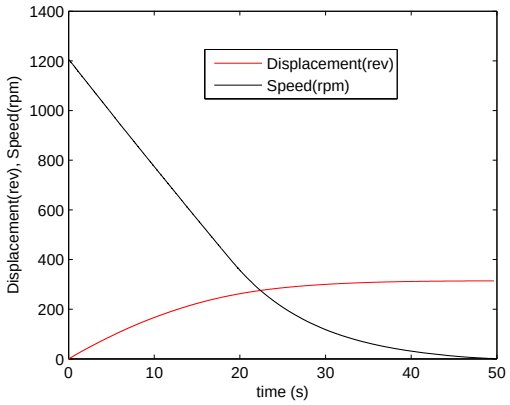

(a) Speed, braking distance Vs time

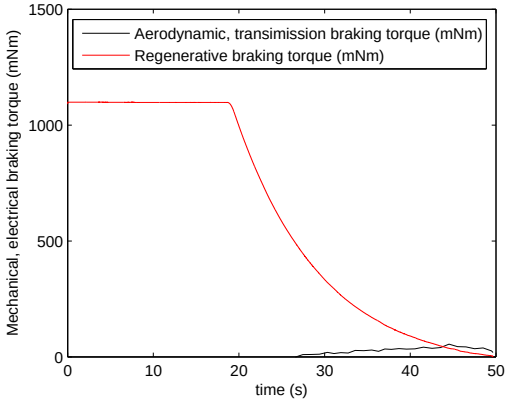

(b) Braking torque Vs time

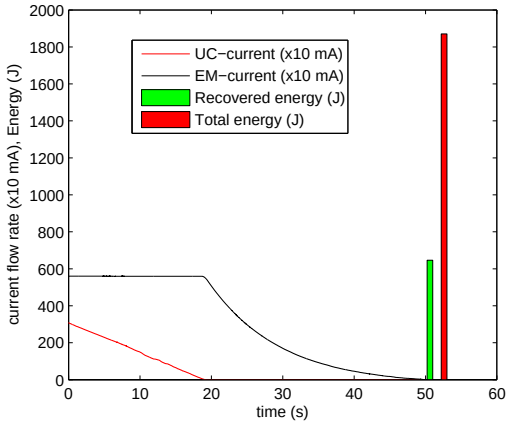

(c) Current flow rate Vs time, energy

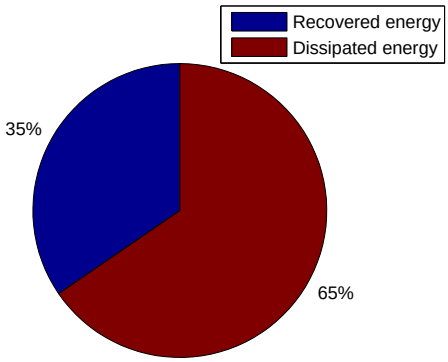

(d) Percentage share of recovered energy on total energy

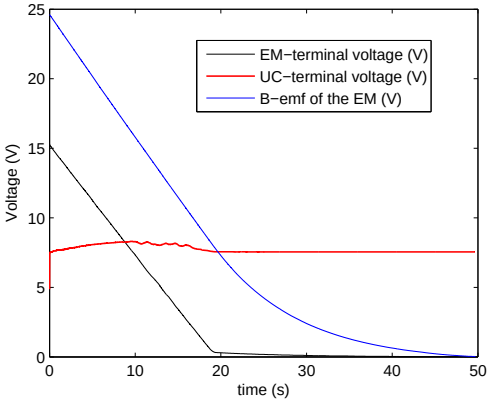

(e) Voltage Vs time

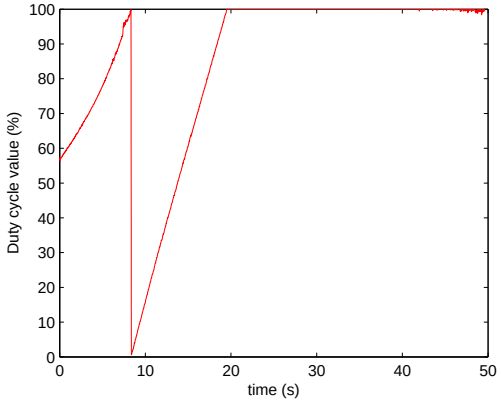

(f) Duty cycle variation of the power converter Vs time

Figure 6.12: Constant Power flow braking scenario 130W

Table 6.1: Comparison of recovered energy percentage of the constant torque and constant power braking events for fixed braking distance

CBT(mNm)	% Energy	CBP (W)	% Energy	Braking distance
455 mNm	55%	30 W	48%	600 rev
825 mNm	44%	65 W	41%	400 rev
1005 mNm	37%	96 W	36%	320 rev

6.5.2 Discussion

Figure6.9 shows the results obtained for a 30W constant power braking scenario. As shown in figure 6.9.a and 6.9.b a constant power braking scenario produces an uneven braking torque and velocity profile, this is inappropriate for the control requirement of the braking. Since the braking torque increases with the decreasing speed of the flywheel system, the current flow rate of the electric motor increases in low speed braking conditions. Therefore, there was a significant voltage drop in the electric motor as depicted in figure 6.9.f, which limits the kinetic energy recovery of the system. As a comparison when we consider figure 6.5 and 6.9, both braking scenarios achieve the same braking distance as 600 complete revolutions while constant torque braking recovers 7% more energy compared to the constant power braking event. This clearly shows that constant torque braking is more efficient than the constant power braking. Figure 6.9.e and 6.9.f shows that the duty cycle of the boost mode operation saturates to 100% when the back-emf of the motor reaches 8V. However as emphasized in the previous section, the constant torque braking event continues to transfer the power until the back-emf reaches a value of 3V. Similarly when comparing the recovered energy percentage for the constant torque and constant power braking events for fixed braking distance scenarios as depicted in table 6.1, constant torque braking recovers more energy than the constant power braking.

This shows that, constant torque braking is more efficient for kinetic energy recovery than constant power braking. In addition to that, the velocity profile of the constant torque braking scenario is more linear and controllable than the constant power braking regime.

The following conclusions were drawn from the constant torque, constant power braking experiments:

- Higher braking torque reduces the kinetic energy recovery of the drivetrain compared with the lower braking torque.
- Since constant power braking includes a range of current flow rates throughout the braking process and constant torque braking maintains consistency of current flow rate, constant torque braking is desirable to increase the kinetic energy recovery for a given braking requirement (braking distance).
- Constant torque braking results in a more controllable and uniform deceleration profile than the constant power braking regime.

As addressed in chapter 4, in reality, there are braking scenarios which cannot be achieved by the regenerative braking system alone. In addition to that, even a pure regenerative braking system looses its controllability at low speed. Therefore, a combination of regenerative braking and secondary braking systems should be engaged to fulfil these braking requirements. Apparently involvement of the secondary braking system will deteriorate the kinetic energy recovery of the electric propulsion system. However, appropriate torque sharing of the dual braking will increase the energy recovery percentage.

Further to this, as explained in chapter 4, a given braking distance can be achieved with variety of braking profiles. This fact can also be effectively employed to increase the kinetic energy recovery by increasing the efficient operating range and time duration of the regenerative braking system. The following section investigates heavy braking scenarios and the effect of them on kinetic energy recovery.

6.6 Experiment 3 : Heavy braking scenarios

The primary constraints of kinetic energy recovery in heavy braking scenarios and different braking torque sharing techniques were investigated in this experiment. The observations which are made in previous experiments were effectively used to design the braking torque sharing techniques. The braking distance is considered as the primary objective and to achieve a fixed braking distance, two different braking profiles were designed and investigated with different combinations of brake sharing ratios. Results were compared to illustrate the difference in kinetic energy recovery.

6.6.1 Procedure

The initial condition of this experiment was also identical to the above experiments, where the braking process starts when the flywheel system reached a speed of 1210 rpm as in previous experiments. Three sets of experiments were conducted to achieve an approximate value of 117 complete revolutions of the flywheel as the braking distance constraint. Each experiment is described bellow:

Fixed braking ratio Initially a braking profile is designed, where electrical and mechanical braking torques were shared in a fixed ratio. To maximize the utilization of the regenerative braking system, 900 mNm of torque was provided by the electric braking system while 1900 mNm of torque was supplied by the mechanical braking system.

Variable braking ratio: 1 Here different mechanical braking torques were applied with respect to the velocity variation of the system. Until the speed of the flywheel reaches a value of 950 rpm, as the maximum of 2500 mNm torque was supplied by the mechanical braking torque. Within the speed range of 950 to 450 rpm, the mechanical braking torque was reduced to 1400 mNm. From 450 to the standstill, again the mechanical braking torque was increased as 2500 mNm. However, the electric braking torque was maintained at a fix value of 900 mNm throughout the entire braking duration. This ensures that the electric braking system maintains consistency with the above experiment.

Variable braking ratio: 2 The first two parts of this experiment are identical to the above experiment. However, the third part was slightly modified and mechanical braking torque was increased to 2800 mNm. At the same time regenerative braking torque was reduced to 450 mNm. The basic reason for this modification is to employ the observation, that was obtained from the constant torque braking experiment. Until the motor reaches a lower back-emf value, kinetic energy can be recaptured in the low torque braking scenario while it was not true for higher torque braking condition. Therefore, by considering braking distance, braking duration and velocity variation of the flywheel system, regenerative braking torque has been modified and investigated.

Similar to previous experiments, braking distance, velocity profile, torque profile, voltage variation of the electric motor, UC-bank and variation of the duty cycle value were captured and analyzed.

6.6.2 Discussion (case-1)

Figure 6.13.a illustrates the velocity variation and angular displacement of the flywheel with respect to time. It shows that the complete braking duration to achieve the angular displacement of 117 revolution required only 11.5 sec. The average braking torque exerted by the electrical and mechanical braking systems are depicted in figure 6.13.b. It should be noted here that the braking torque given by the mechanical braking system was twice as high as the regenerative braking torque.

The terminal voltage across the electric motor and UC bank are shown in figure 6.14.a. The duty cycle variation of the power converter is also depicted in the figure to show the energy recovery time duration. The current flow rate of the electric motor and the UC-bank are depicted in figure 6.14.b, which also illustrates that, there is no recharging current flow into the capacitor bank after 8 sec while there is a current flow in the electric motor. Apparently, the area occupied by the UC-bank current flow in figure 6.14.b provides the voltage increment of the UC-bank. Therefore, based on the initial and final voltage of the UC-bank, the recovered energy quantity was calculated. In this experiment only a fraction of 13.66% of the energy was recovered in the UC-bank.

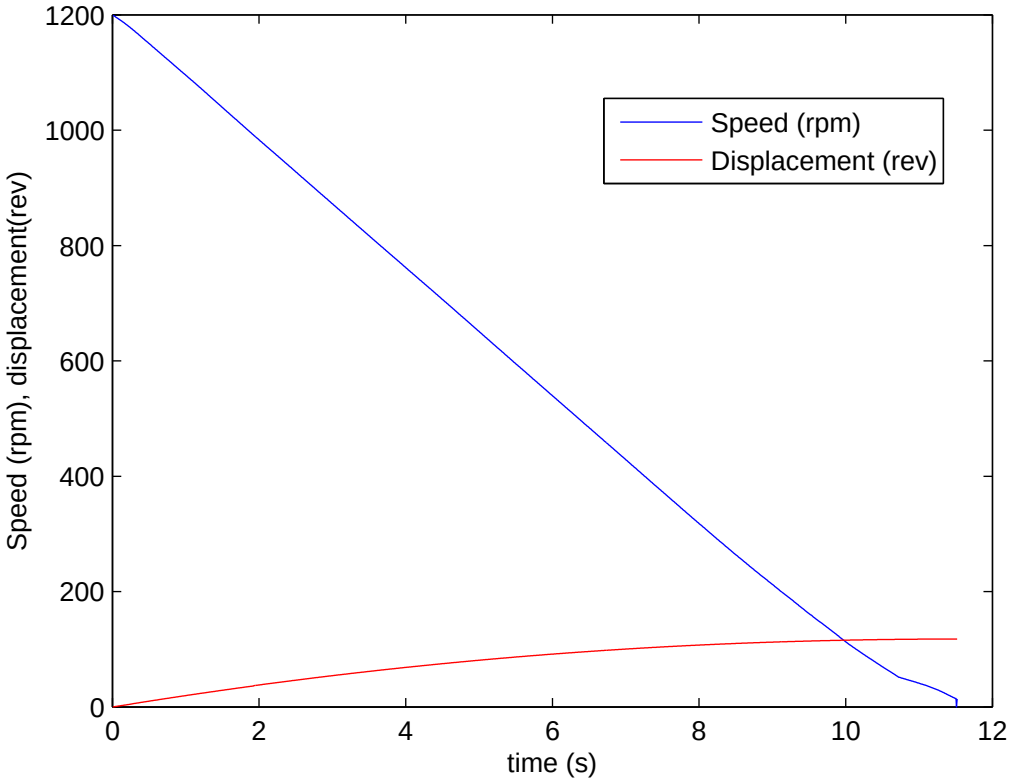

(a) Speed, braking distance Vs time

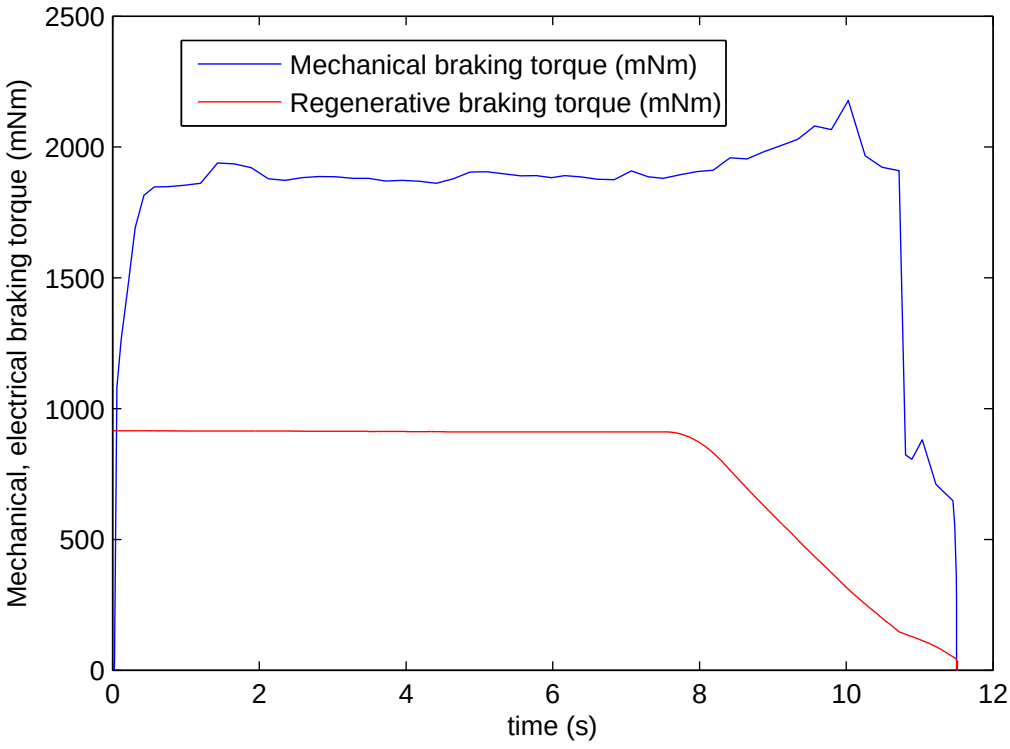

(b) Electric, mechanical braking torque Vs time

Figure 6.13: Fixed braking ratio

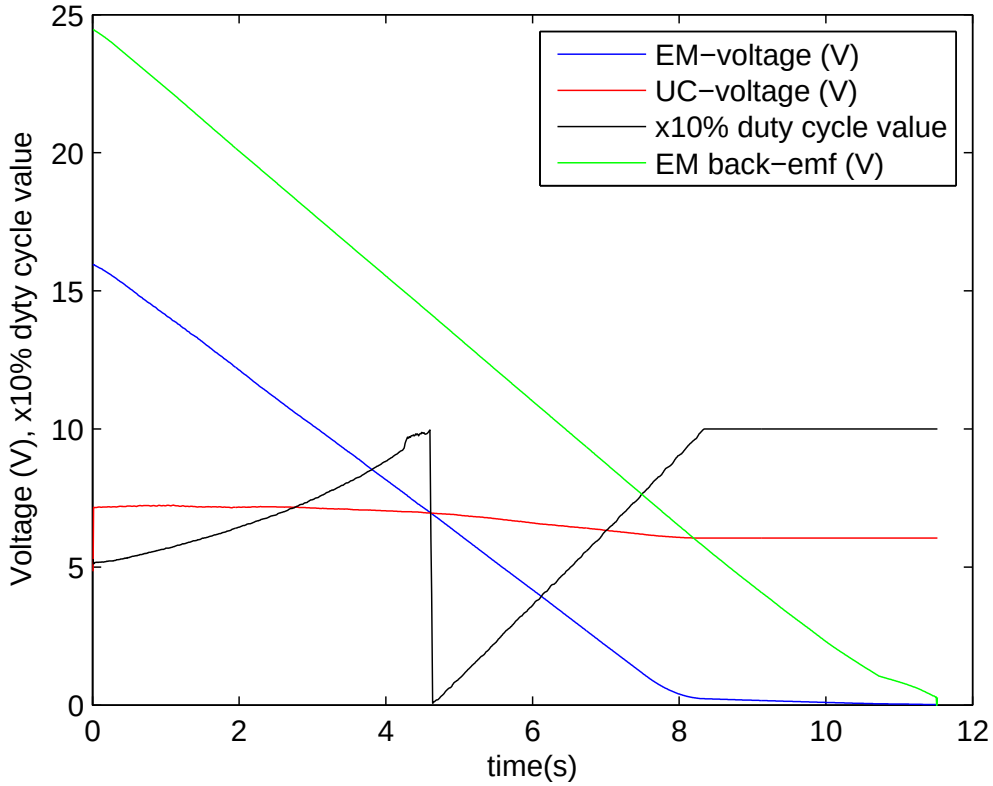

(a) UC, EM terminal voltage, duty cycle variation Vs time

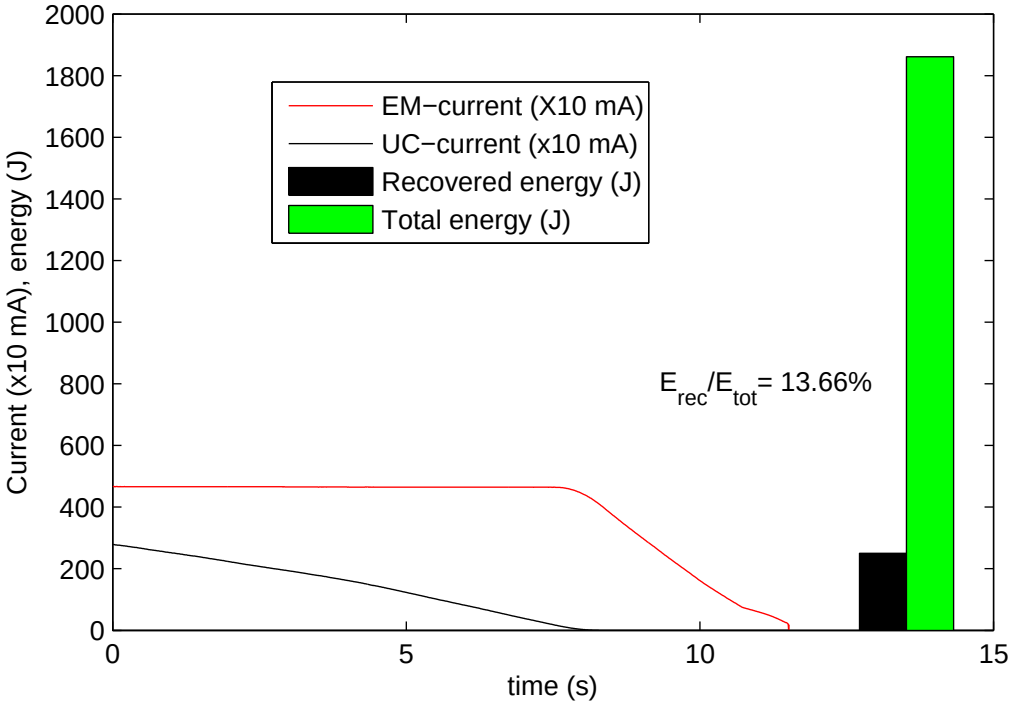

(b) UC, EM current flow rates Vs time and recovered and total energy percentage

Figure 6.14: Fixed braking ratio

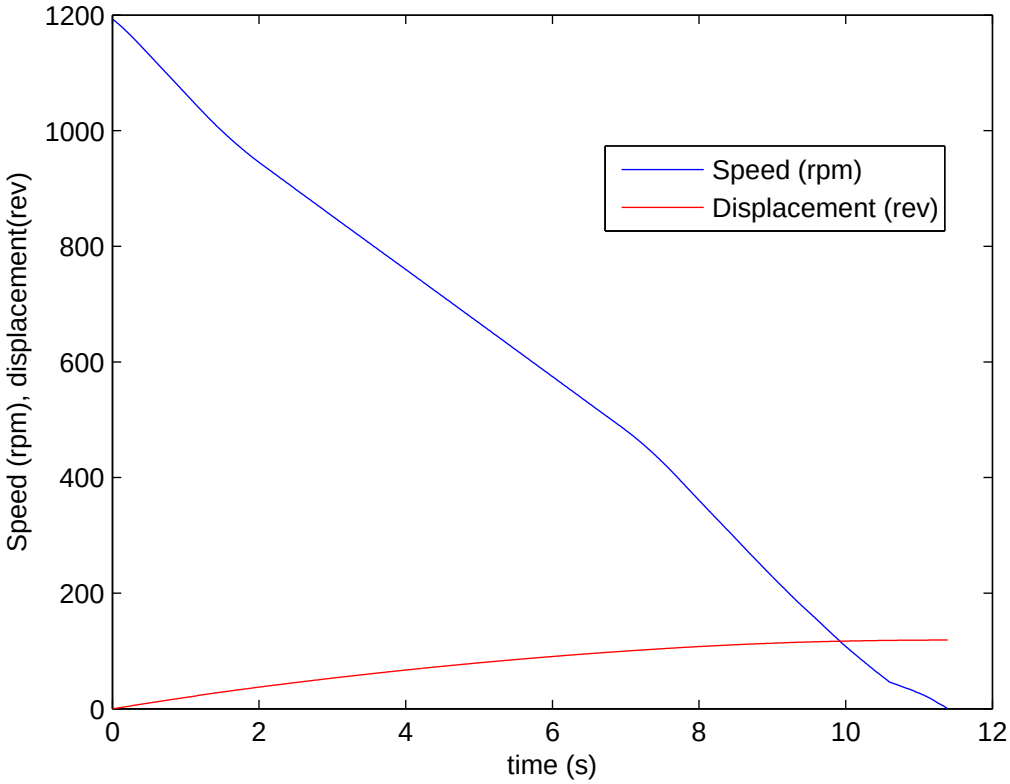

(a) Speed, braking distance Vs time

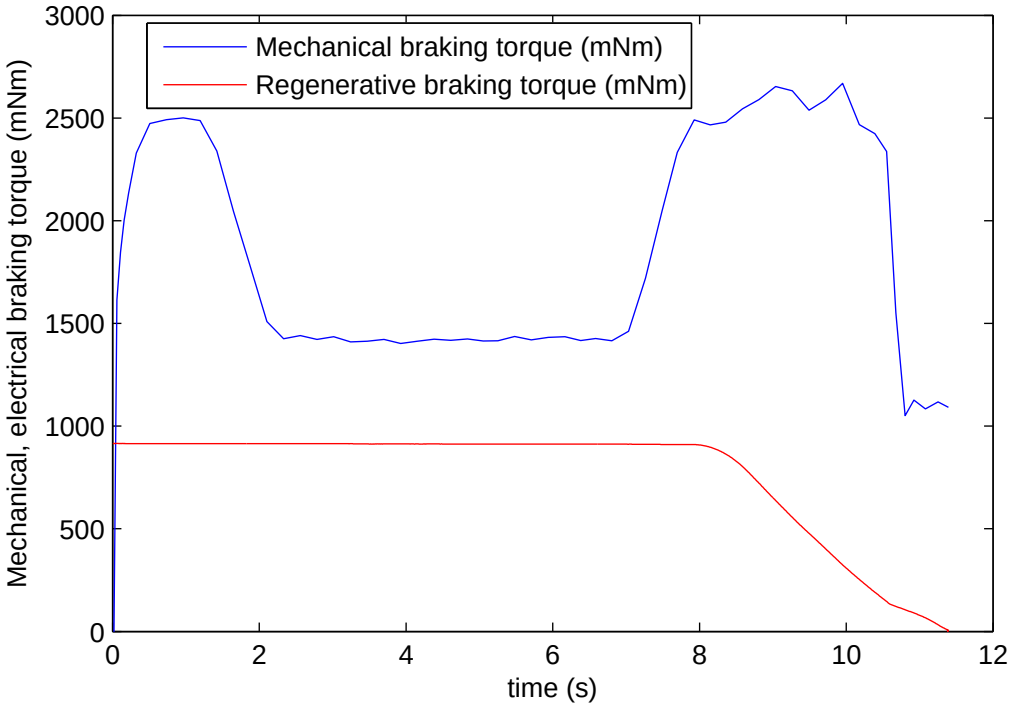

(b) Electric, mechanical braking torque Vs time

Figure 6.15: Variable braking ratio: 1

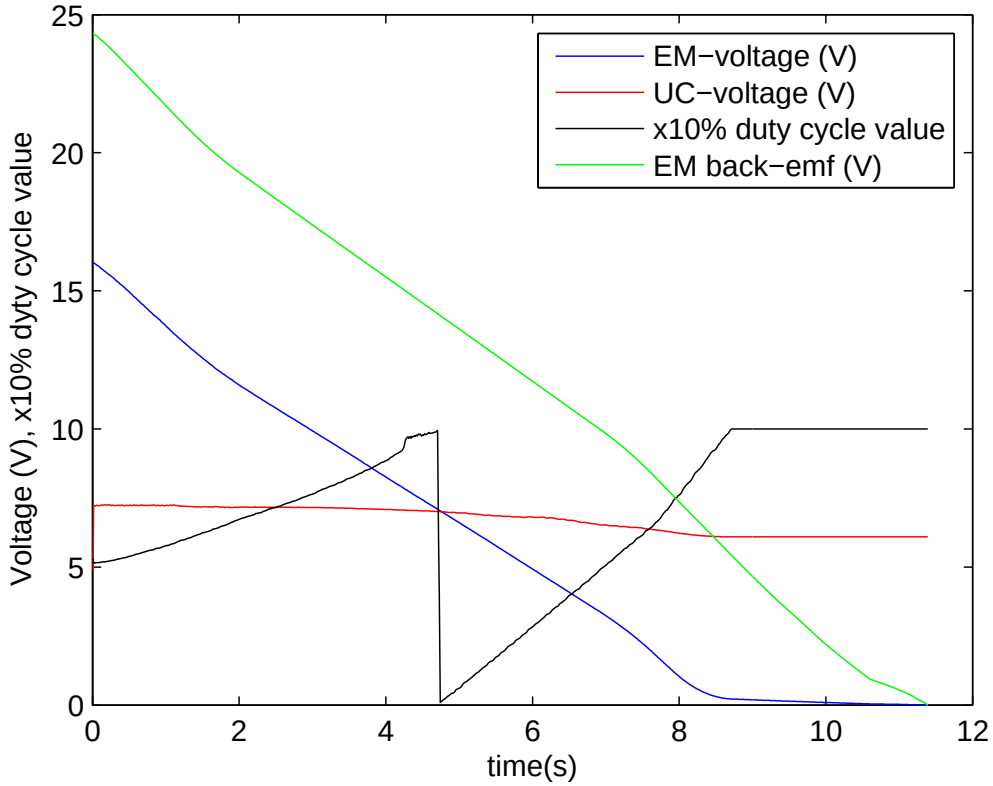

(a) UC, EM terminal voltage, duty cycle variation Vs time

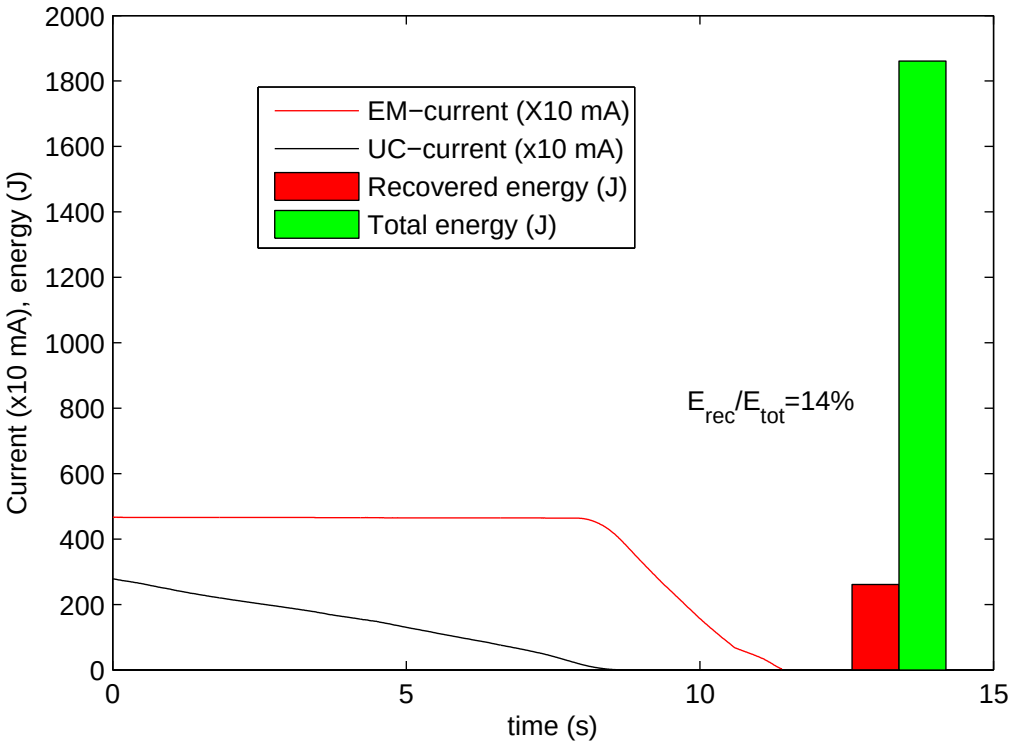

(b) UC, EM current flow rates Vs time and recovered and total energy percentage

Figure 6.16: Variable braking ratio: 1

6.6.3 Discussion (case-2)

Figure 6.15.a also illustrates the velocity variation and angular displacement of the flywheel with respect to time. It should be noticed here, that the velocity profile shows a more discrete nature than the above. However, this braking scenario also achieves an angular displacement of 117 revolution within 11.4 sec. Discrete variation of the mechanical braking torque and constant regenerative braking torque distribution are depicted in figure 6.15.b.

Figure 6.16.a illustrates the terminal voltage variation of the electric motor and UC-bank. It should be noted here that the effect of the velocity profile variation was reflected on the terminal voltage across the electric motor and UC bank. In addition to that, the energy recovery process has been extended to 8.5 sec in this case, which can be noticed from the duty cycle variation of the power converter. Figure 6.16.b describes the current flow rate of the electric motor and the UC-bank. As the energy recovery time period extended by 0.5 sec, the current of the UC-bank in figure 6.16.b occupies more area then the previous experiment. This directly translates in a voltage increment for this braking case, which is higher than the previous. This results in an increase of the kinetic energy recovery of 14%, which is almost 0.4% higher than the previous experiment.

6.6.4 Discussion (case-3)

The above two experiments did not capture the energy after the point there the back-emf of the motor fell below 7 volts. However, it has been observed from constant torque braking experiment, that low torque braking recaptures the energy until the back-emf reaches a much lower voltage than the high torque braking scenario. Therefore, this experiment was conducted to increase the energy recovery of the regenerative braking system by effectively employing the above observation. As an illustrative example, regenerative braking torque was minimized to half the previous value during the low speed braking. Therefore, until the back-emf reached a value of 8V, the regenerative braking system was engaged with its maximum capacity. Once the back-emf reached 8V, the regenerative braking system was engaged with 450 mNm torque.

Due to the reduction in regenerative braking torque supply, braking perfor-

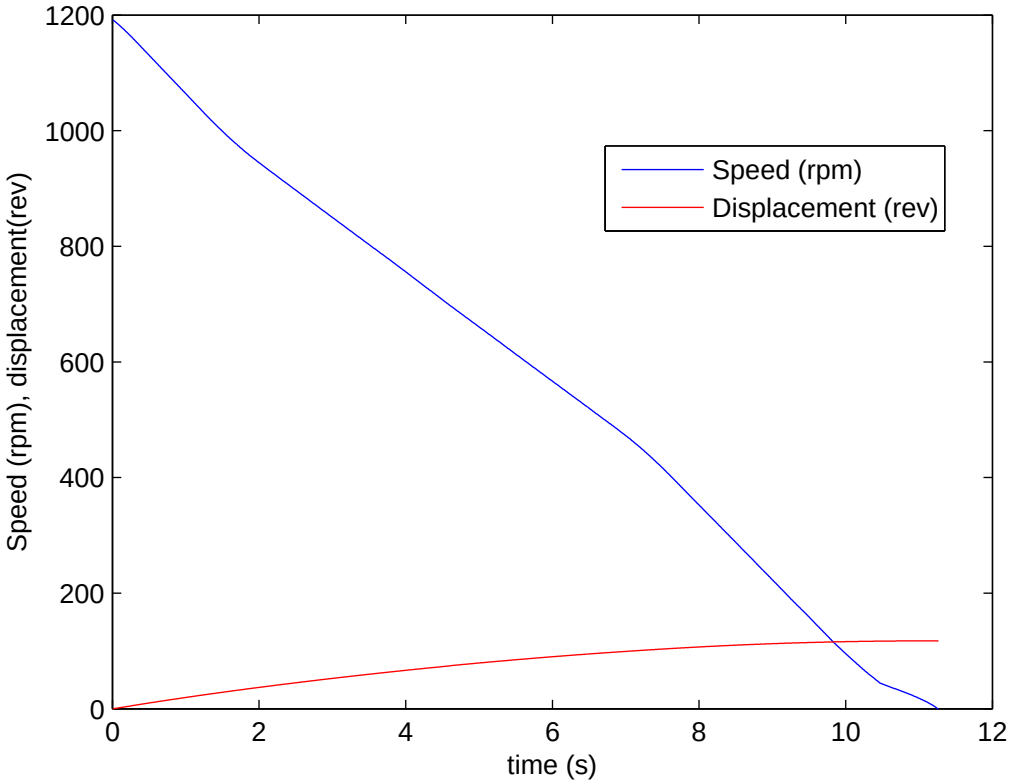

(a) Speed, braking distance Vs time

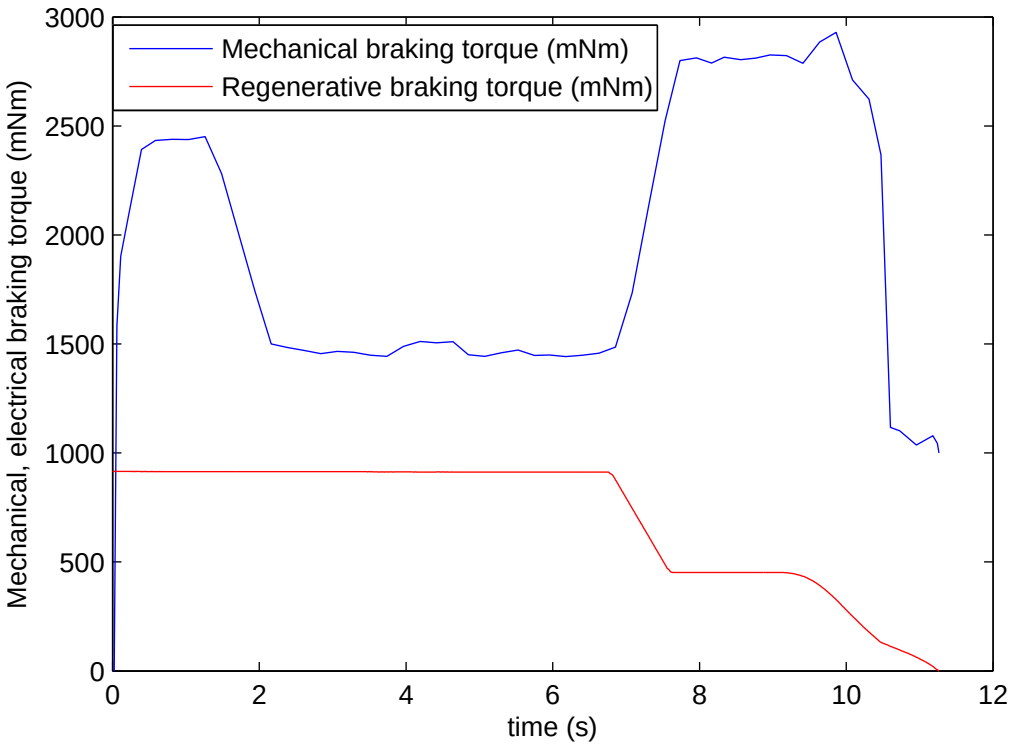

(b) Electric, mechanical braking torque Vs time

Figure 6.17: Variable braking ratio: 2

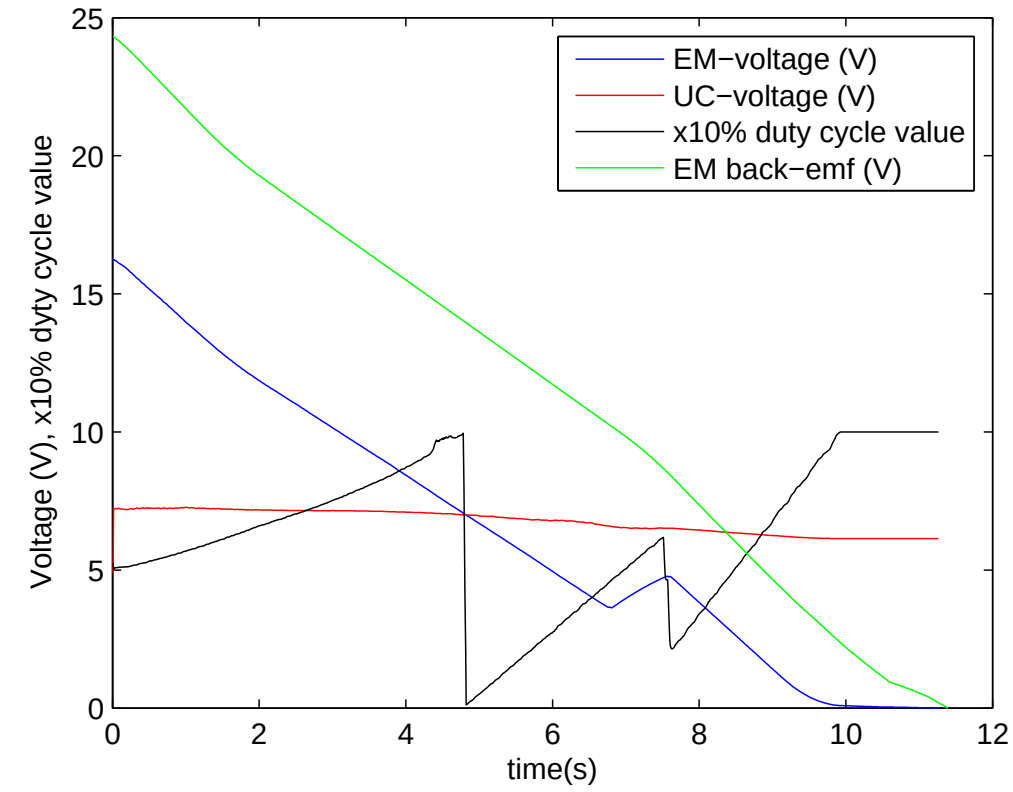

(a) UC, EM terminal voltage, duty cycle variation Vs time

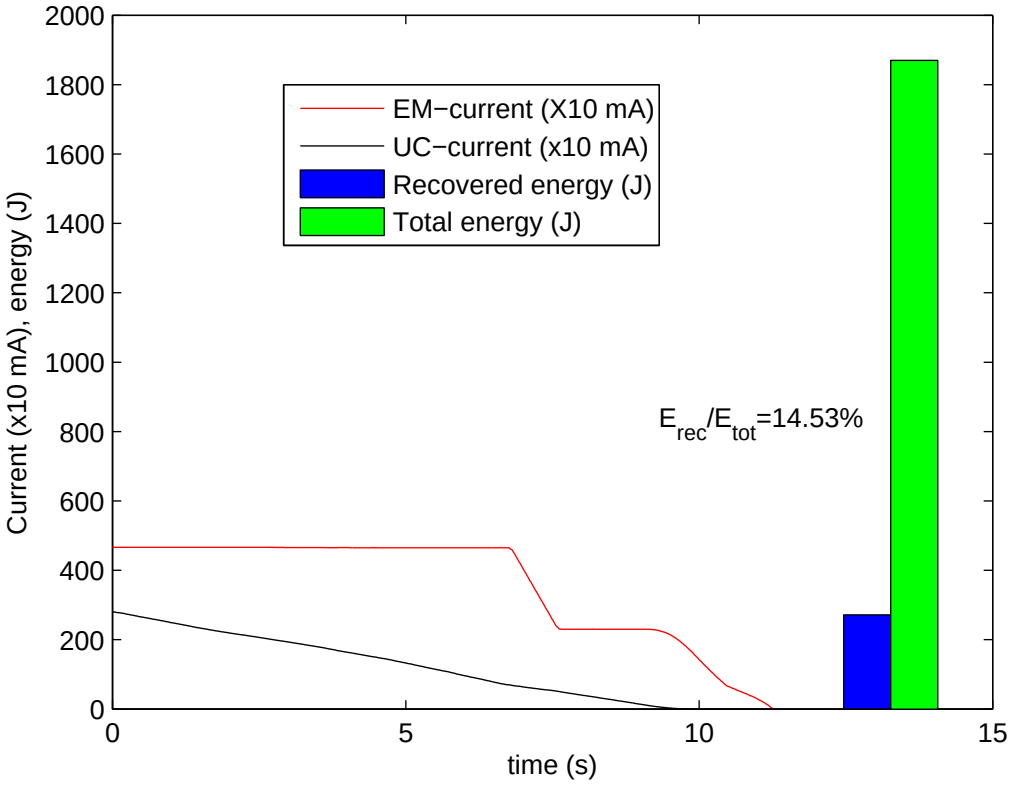

(b) UC, EM current flow rates Vs time and recovered and total energy percentage

Figure 6.18: Variable braking ratio: 2

mance will be affected. This will lead to an increase in the total braking distance. Therefore, the mechanical braking torque was increased to ensure the torque balance of the system, which resulted in achieving the fixed braking distance as per the previous experiment. It can be noticed from figure 6.15.b, 6.17.b that, the first two sections of the graphs are almost identical while the third section shows slightly different torque blending ratios. Only 2500 mNm average torque was supplied by the mechanical braking system in the first case while 2800 mNm torque was supplied in the second case.

It should be noted here that the velocity profiles of both braking cases were almost identical while the torque distribution ratio differs significantly. As depicted in figure 6.18.a, the energy recovery process is occurs until the back-emf reached a value of 3V here, but it was terminated in the above case just after the back-emf value was 7 volts. This torque blending technique enables the regenerative braking system to actively increase the kinetic energy recovery of the system. Figure 6.18.b depicts the current flow rate of the electric motor and UC-bank. It illustrates that, the UC-current flow curve occupies more area than the previous two experiments. The correlation between this area and the recovered energy is described by following equations [2].

$$Q = \int idt \tag{6.2}$$

$$Q = \int Cdv \tag{6.3}$$

$$E = \frac{1}{2}C.V^2 = \frac{1}{2C}.Q^2 \tag{6.4}$$

where Q is the charge accumulated in the capacitor in As, C is the capacitance in F, and E is the stored energy in J

A maximum energy recovery of 14.53% was recorded in this experiment, which is more than a 0.53% increase compared with the previous experiment.

Figure 6.19 shows the comparison of above three braking scenarios in the same figure to clearly depict the effect of the braking profile on kinetic kinetic energy recovery enhancement. This test illustrates that, the kinetic energy recovery can significantly be improved by employing an appropriated braking blending ratio between regenerative and mechanical braking systems. Controversial to the general thinking, this example illustrates that, the appropriate brake blending technique enhances regenerative energy recapture more than pure regenerative braking in low speed braking conditions.

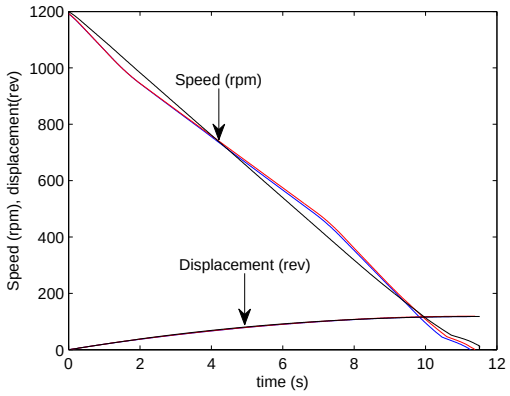

(a) Speed, braking distance variation Vs time

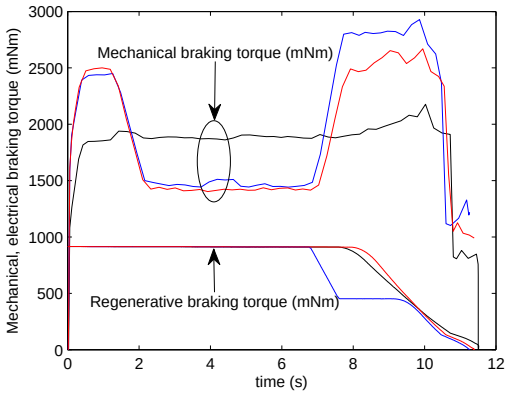

(b) Electric, mechanical braking torque Vs time

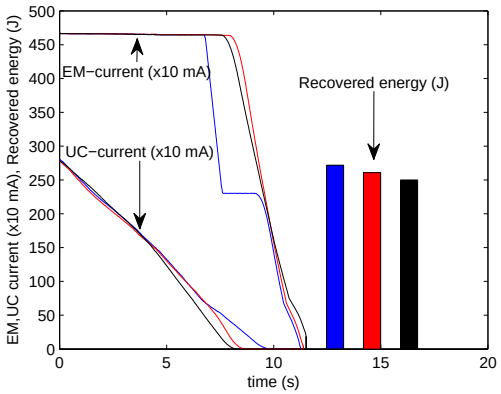

(c) UC, EM current flow rates Vs time and recovered and total energy percentage

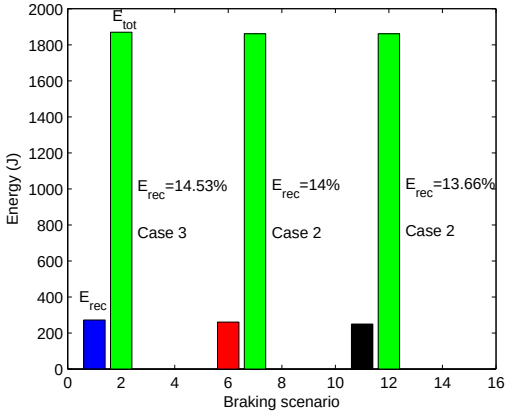

(d) Comparison of recovered energy percentage in each braking scenarios

Figure 6.19: Comparison of the effect of different braking profiles : 1 (117 revolution braking distance)

Following this experiment, five different heavy braking scenarios were investigated to illustrate the repeatability of this hypothesis. 140, 157, 205, 220 and 250 complete revolutions of the flywheel were considered as the target braking distances. The results obtained from each experiment agreed and have been compared in the figures bellow.

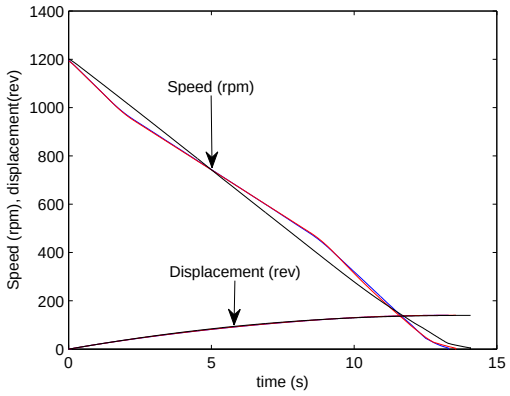

(a) Speed, braking distance variation Vs time

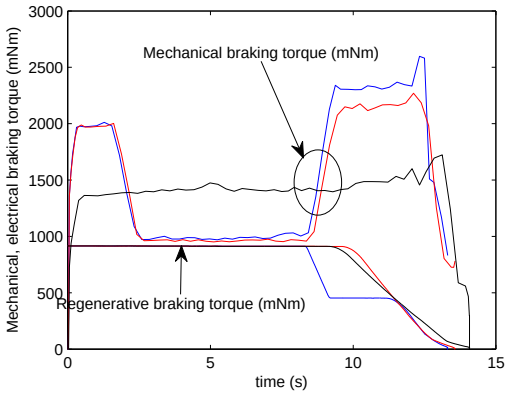

(b) Electric, mechanical braking torque Vs time

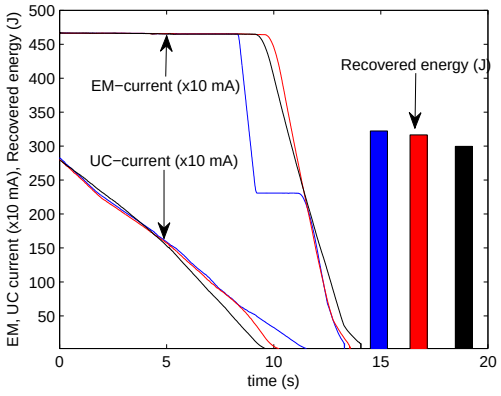

(c) UC, EM current flow rates Vs time and recovered and total energy percentage

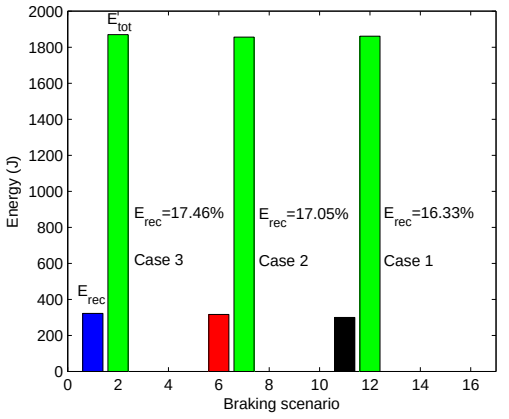

(d) Comparison of recovered energy percentage in each braking scenarios

Figure 6.20: Comparison of the effect of different braking profiles : 2 (140 revolution braking distance)

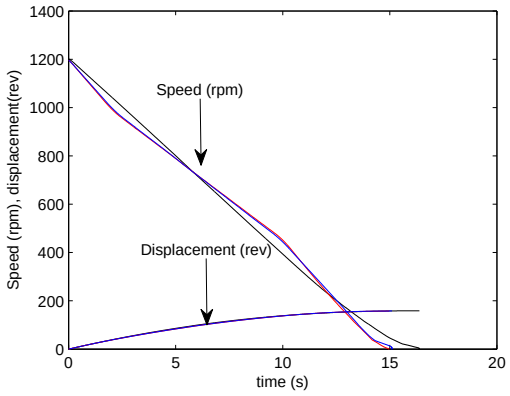

(a) Speed, braking distance variation Vs time

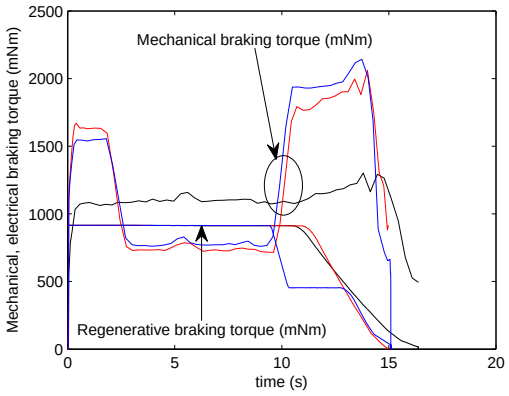

(b) Electric, mechanical braking torque Vs time

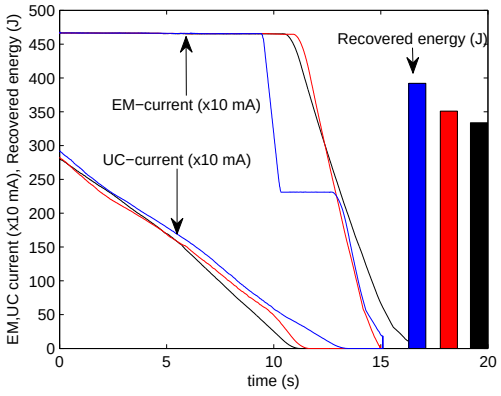

(c) UC, EM current flow rates Vs time and recovered and total energy percentage

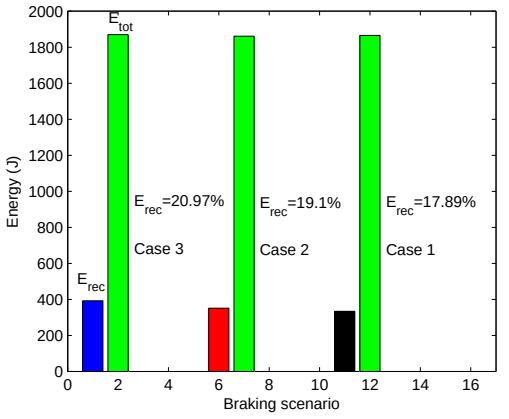

(d) Comparison of recovered energy percentage in each braking scenarios

Figure 6.21: Comparison of the effect of different braking profiles: 3 (157 revolution braking distance)

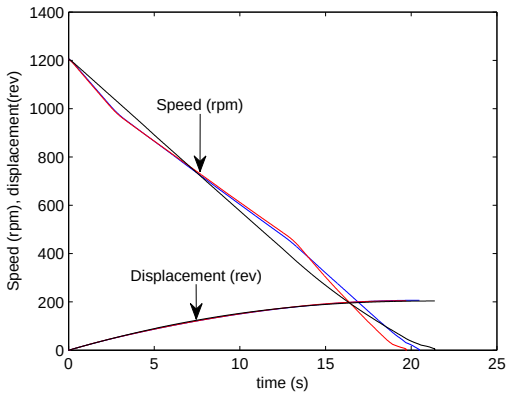

(a) Speed, braking distance variation Vs time

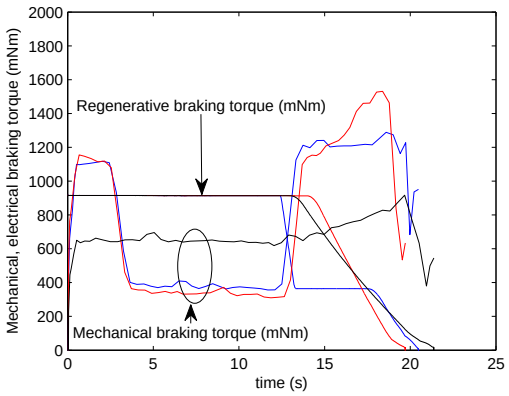

(b) Electric, mechanical braking torque Vs time

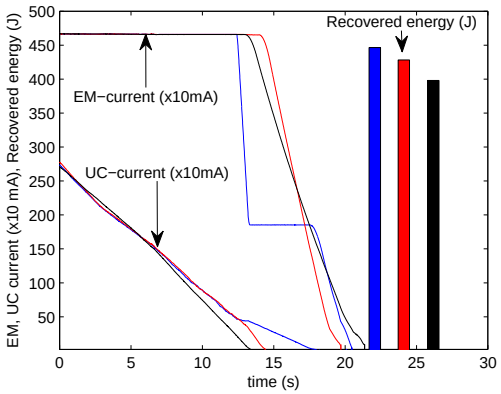

(c) UC, EM current flow rates Vs time and recovered and total energy percentage

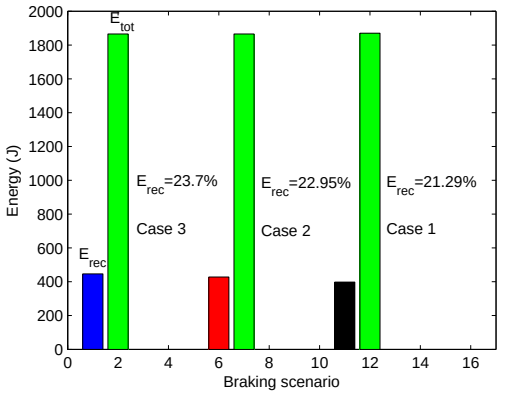

(d) Comparison of recovered energy percentage in each braking scenarios

Figure 6.22: Comparison of the effect of different braking profiles : 4 (205 revolution braking distance)

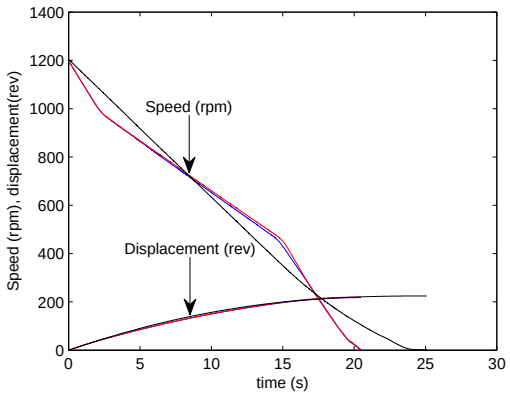

(a) Speed, braking distance variation Vs time

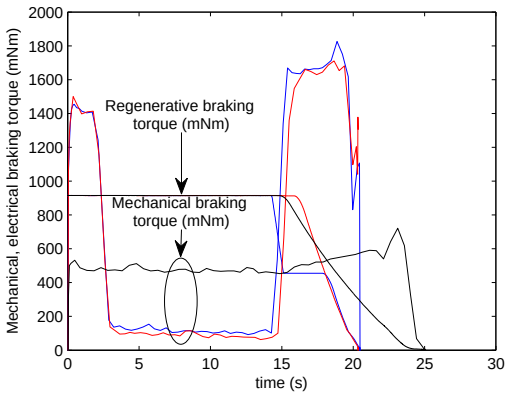

(b) Electric, mechanical braking torque Vs time

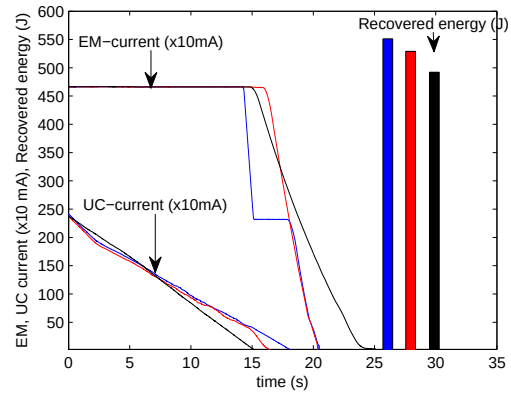

(c) UC, EM current flow rates Vs time and recovered and total energy percentage

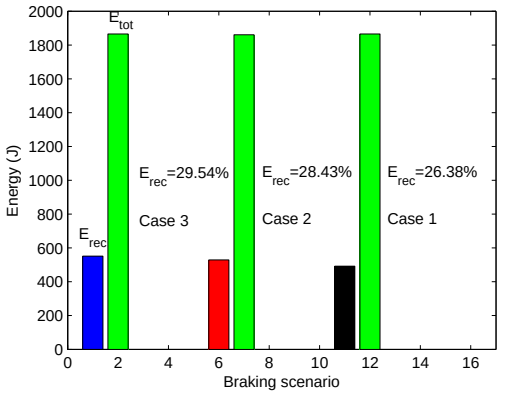

(d) Comparison of recovered energy percentage in each braking scenarios

Figure 6.23: Comparison of the effect of different braking profiles : 5 (220 revolution braking distance)

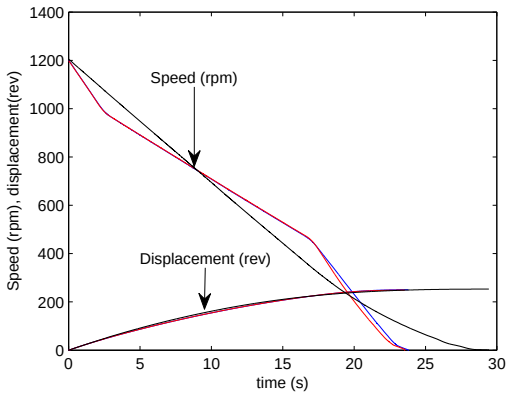

(a) Speed, braking distance variation Vs time

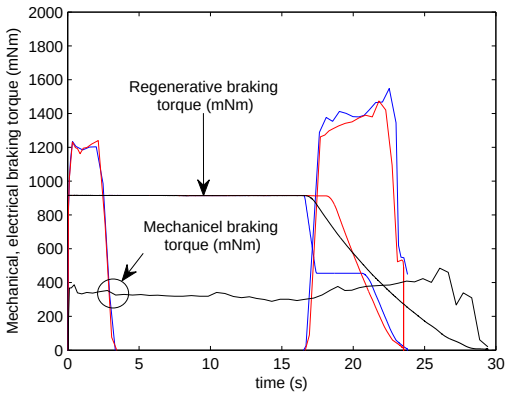

(b) Electric, mechanical braking torque Vs time

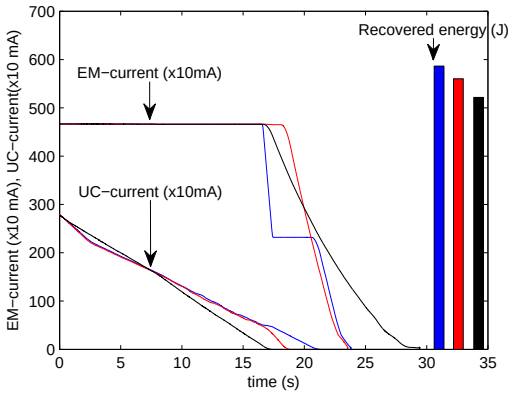

(c) UC, EM current flow rates Vs time and recovered and total energy percentage

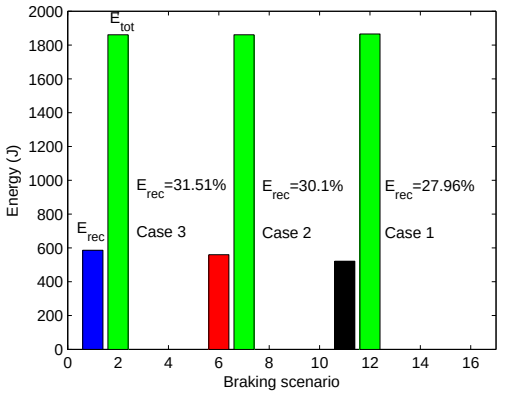

(d) Comparison of recovered energy percentage in each braking scenarios

Figure 6.24: Comparison of the effect of different braking profiles : 6 (250 revolution braking distance)

Table 6.2: Comparison of the kinetic energy recovery variation with respect to the braking distance and employed braking method

Dist (rev)	RKE% fixed BR	RKE% variable BR-1	RKE% variable BR-2
117	13.66	14	14.53
140	16.33	17.05	17.46
157	17.89	19.1	20.97
205	21.29	22.95	23.7
220	26.38	28.43	29.54
250	27.96	30.1	31.51

To achieve different braking requirements, three different braking methods are applied as illustrated in the above section (fixed braking ratio, variable braking ratio-1, variable braking ratio-2) and they have been compared. Figure 6.20 shows the braking scenario, where the flywheel is braking from 1210 rpm to stand still within 140 complete revolution. It can be noticed from the figure 6.20(a), that all three braking methods achieve the same braking distance of 140 rev in different time frame. However, their velocity profile is different. Figure 6.20(b) depicts the mechanical and regenerative braking torque blending differences with respect to the applied braking method. Figure 6.20(c) illustrates the current flow rate of the electric motor and current flow rate into the ultracapacitor during each braking method. Similar to the above experiment, it can be noticed that, the variable braking ratio-2 occupy more current-time area than the variable braking ratio-1 and the variable braking ratio-1 occupy more current-time area than the fixed braking ratio. Due to this effect, variable braking ratio-2 recover more energy than variable braking ratio-1 and variable braking ratio-1 recover more energy than fixed braking ratio. Recovered kinetic energy percentage of the above three braking methods are compared in figure 6.20(d). In summary, although all three braking methods achieve the same braking distance, their energy recovery percentage varies significantly with respect to the employed braking method. As we can noticed from the figure, the fixed braking profile achieve 16.33% kinetic energy recovery while the variable braking ratio-1 achieve 17.05% kinetic energy recovery. In addition to that, the variable braking ratio-2 achieve 17.46% kinetic energy recovery. Similarly figure 6.21, 6.22, 6.23 and 6.24 also can be explained.

Table 6.2 shows the recovered kinetic energy (RKE) percentage with respect to the braking distance and the applied braking methods such as fixed braking ratio (BR), variable braking ratio-1 (BR-1) and variable braking ratio-2 (BR-2). As a common tendency, it can be noticed from the table that, variable braking ratio-2 recover more energy than the variable braking ratio-1 and variable braking ratio-1 recover more energy than the fixed braking ratio. Required braking distance is another critical factor, which significantly influence the kinetic energy recovery performance. Decreasing braking distance minimizes the recovered percentage of the kinetic energy. Since the electric propulsion system is limited to its power and torque handling capability, higher amount of braking torque is supplied by the mechanical braking system to achieve shorter braking distances. However, when the braking distance increases, regenerative braking system can be effectively employed to increase the kinetic energy recovery. Based on these results, following conclusions are drawn:

1. Modification of the braking profile enables the regenerative braking system to be actively involved with the kinetic energy recovery of the drivetrain system for heavy braking scenarios. This fact has been illustrated by the first two experiments in this section.

2. Varying the brake blending ratio with respect to the operating conditions of the drive train system also significantly contributes to increasing the regenerative braking efficiency.

3. In low speed braking conditions, combined braking techniques capture more energy than the pure regenerative braking.

4. Kinetic energy recovery is inversely proportional to the braking distance.

Chapter 7

Conclusions and Future Work

This chapter is divided into three sections and the first section describes the main findings and contribution to knowledge of this research work. Following that, limitation of this work are presented for readers information. At the end, future work are highlighted to further investigate this research work.

7.1 Main findings and contributions to knowledge

A holistic approach to the problem of kinetic energy recovery enhancement during various braking conditions in electric propulsion systems is presented in this document. The effect of braking profile on energy recovery was demonstrated theoretically as well as experimentally.

An extensive literature survey in this field was performed to understand the state of the art in this research domain. Problems associated with the stability criteria of vehicles, braking power sharing strategies, control methods, power and energy management methods, limitations of energy storage systems and their hybrid arrangements, and power converter topologies which are employed in electric propulsion systems were revisited in this review. Most of the work in the literature divides the research into many isolated problems and investigates them individually rather than approaching it in a holistic manner. The integrated nature of many subsystems and their direct and indirect interaction with each other was emphasized in this review to illustrate the need to approach this problem by considering the larger picture. Key findings of this research study and contributions to knowledge are summarized as follows:

- Problems associated with dynamic force transfer during braking and the requirement of dual braking systems to handle various braking objectives are described in chapter 3. The implications of the dynamic force transfer problem on kinetic energy recovery are rarely considered in the literature.

The objective of this analysis was to understand the influence of the external factors on the kinetic energy recovery of the vehicle. It also investigates the effects of drivetrain configuration on energy recovery during braking. The analysis in this section shows that the energy recovery not only relies on the electric drivetrain's power handling capability, but also other factors such as road conditions and braking requirements. Also it was shown that, front wheel drive vehicles recover more energy than rear wheel drive vehicles under various braking conditions. These research findings significantly contribute to understanding the realistic issues on the kinetic energy recovery problem in electric/hybrid electric vehicle research.

- Problems associated with dynamic force transfer during braking and the requirement of dual braking systems to handle various braking objectives are described in chapter 3. The implications of the dynamic force transfer problem on kinetic energy recovery are rarely considered in the literature. The objective of this analysis was to understand the influence of the external factors on the kinetic energy recovery of the vehicle. It also investigates the effects of drivetrain configuration on energy recovery during braking. The analysis in this section shows that the energy recovery not only relies on the electric drivetrain's power handling capability, but also other factors such as road conditions and braking requirements. Also it was shown that, front wheel drive vehicles recover more energy than rear wheel drive vehicles under various braking conditions. These research findings significantly contribute to understanding the realistic issues on the kinetic energy recovery problem in electric/hybrid electric vehicle research.

- Most of the review on previous and ongoing research work considers standard driving cycles as a benchmark for performance requirements. As a result of this, many of them develop their algorithms to fulfil this requirement. In contrast, the study in this dissertation viewed this problem differently. In reality, it is unlikely that most drivers follow the same driving pattern as the standard driving cycles. As described in [20], driving patterns vary with several factors such as age, emergency requirements, and road conditions. To understand this problem, study in this dissertation included a wide range of braking scenarios for investigation. The outcome of this analysis reveals that, the kinetic energy recovery varies significantly with braking objectives.

Due to this reason changes in driving cycle affects the regenerative braking performance. Therefore, it is hard to say exactly what percentage of the kinetic energy of the vehicle can be recovered by the regenerative braking process.

- Rather than finding a solution for a given braking cycle, the objective of the braking event was defined from the view point of braking distance, initial, and final velocity. The possibility of achieving this objective with various intermediate state conditions (velocity and deceleration rate) were mathematically formulated. It was then demonstrated that the braking power distribution can be varied by changing the intermediate state conditions. In general, mechanical and regenerative braking systems work together to achieve heavy braking objectives. Due to the involvement of a mechanical braking system, kinetic energy recovery is significantly limited during these braking events. The possibility of choosing the intermediate state conditions, which were shown to control the braking power distribution to increase the regenerative braking performance was then investigated within the operating constraints of the electric motor. Here the strategy is designed in such a way, where it increases the kinetic energy recovery by increasing the efficient operating duration of the regenerative braking system while achieving the expected braking objective. The simulation study presented in chapter 4 provides compelling results to validate the effectiveness of the proposed braking strategy. This novel braking strategy can be also applied to various industrial automation machinery applications.

- This research does not only provide theoretical analysis to explain the issues related with kinetic energy recovery and braking profile, but also an experimental study was presented and verified. This was found to be lacking in previous research works and hence provides a significant contribution to this comprehensive problem. Obtained results from this experimental study explained the limitations of the electric propulsion system for kinetic energy recovery during braking. Due to the internal resistance, a significant amount of energy is dissipated in the motor during heavy braking scenarios (even for the case of pure regenerative braking). The study presented in chapter 6 also demonstrates that light braking events achieve higher energy recovery than heavy braking events. The proposed novel braking strategy is

tested using the experimental rig for achieving different braking objectives. Three different braking power sharing strategies were designed to achieve a fixed braking distance and they were investigated with the hardware system. Comparison of the results presented in each experiment showed that the proposed braking strategy in chapter 4 recovers more of the kinetic energy of the system. Many different braking distances were investigated to verify the concept in a wide operating range.

In summary, this research study reveals that the braking cycles significantly affect the kinetic energy recovery of the vehicle. Regenerative braking performance varies with different factors such as power handling capability of the electric propulsion system, drivetrain configuration, road condition, and braking requirements. Different braking profiles have different brake power distributions and this property can be effectively employed to increase the kinetic energy recovery.

7.2 Limitations of the work

Few limitations of this experimental framework are highlighted bellow for readers information.

- Although the effect of braking profile on kinetic energy recovery is analyzed by this experimental study, scalability is another important issue, which is not considered here. In reality, depending upon the employed electric propulsion system and its power-torque handling capability, its operating characteristic vary in a nonlinear scale. Therefore, it is difficult to extrapolate the accurate information from this experimental test bench for different drivetrain systems. However, the fundamental issues analyzed by this experimental setup is valid for all kinds of electric propulsion systems. This effect also can be clearly seen from the simulation study presented in chapter 4, where a different electric propulsion system is considered for the analysis.
- Operating characteristic of the electric propulsion system varies with respect to its operating temperature. Since there are multiple subsystems such as electric motor, power electronic switches and UC bank are involving in the

electric propulsion system, it is hard to analyze their changing behavior with respect to the temperature variation. Due to this complexity, temperature analyzes is not considered in this work. However, since all experiments are performed in the same environment, the effect of temperature on operating efficiency of the electric propulsion system is assumed to be consistent.

- Switching losses in the power converter is another important issue, which significantly minimize the efficiency of the power converter. However, since the objective of this experimental study is to demonstrate the influence of braking profiles on kinetic energy recovery, the efficiency of the power converter is not considered as a major issue.

Although the major objectives set out for this research project have been accomplished, there are several issues that need further investigation. The following section presents the potential future work for the continuation of this research.

7.3 Future work

The effect of braking profile on kinetic energy recovery is clearly demonstrated in this thesis. However, there are various other issues that also need to be investigated to further improve the effectiveness of the kinetic energy recovery process, which will lead to enhanced fuel economy. To continue with this research, the following issues are highlighted by the author.

- This study revels that, different braking profiles provide different quantities of kinetic energy recovery to achieve the same braking objective. However, to optimize the kinetic energy recovery, the braking profile needs to be optimized to achieve the objectives of kinetic energy recovery and braking performance enhancement. Therefore, further study needs to be carried out to achieve this goal. Moreover, Control systems play a vital roll on braking power management and kinetic energy recovery processes. Due to the involvement of various systems in electric vehicles, optimum operating efficiency of the drivetrain system needs to be ensured to maximize the kinetic energy recovery. Therefore, possibility of employing optimal control methods are suggested to achieve these goals

- Due to the involvement of human psychology in manned vehicles, varying braking profiles may affect the passenger comfort during braking. Therefore, further research needs to be carried out to investigate the ergonomic issues related to man-machine interfacing.

- Due to the dynamic force transfer of the vehicle (as emphasized in chapter 3), involvement of the regenerative braking system during the braking process is limited in single axle drive train systems (front, rear wheel drive vehicles). The possibility of employing a novel transmission system to integrate front and rear axles with the regenerative braking system is suggested. This will increase the operating envelop of the energy recovery potential of the vehicle.

- With respect to the decreasing vehicle speed, power handling capability of the electric motor also decreases. However, this effect can be eliminated by employing a continuously variable transmission (CVT) system in between the electric motor and drive axle. This provides a great flexibility to control the power/torque characteristic of the electric motor regardless of the vehicle speed variation. Since the output voltage can be mechanically controlled by varying the speed of the motor, a fixed voltage can be input to the power converter throughout the braking duration. This results in an increase in the operating efficiency of the power converter. However, the operating efficiency of the continuously variable transmission is another issue, which needs to further clarified. A comparison study needs to be performed in a holistic manner to understand the benefits and drawbacks of the involvement of CVT.

- There are few research studies investigating the possibility of employing flywheel systems to store the mechanical energy (rather than convert and store it as an electrical energy). The primary advantages of such systems are that, they are free from drivetrain topology and they can be even integrated with conventional vehicles. However, there are not sufficient studies performed yet to highlight the holistic picture of this energy recovery process. Therefore further research needs to be performed to investigate the benefits and drawbacks of such systems and a comparison study with the electric energy storage mechanism also need to be carried out to draw the possible

conclusions.

7.4 List of publications

- P. Suntharalingam, J.T. Economou, and K. Knowles, "Electric Propulsion System and Braking Strategy Design for the Hybrid Electric Vehicle", Vehicle Power and Propulsion Conference, 2010. VPPC '10. IEEE. Lille, France (Paper accepted)
- P. Suntharalingam, J.T. Economou, and K. Knowles, "Effect of Braking Profile on Regenerative Energy EnhancementŠ VPPC conference", Vehicle Power and Propulsion Conference, 2010. VPPC '10. IEEE. Lille, France (Paper accepted)
- P. Suntharalingam, J.T. Economou, and K. Knowles, "Effect on Regenerative Braking Efficiency with Deceleration Demand and Terrain Condition", Power Electronics, Machines and Drives (PEMD 2010), 5th IET International Conference, Issue Date: 19-21 April 2010. Brighton, UK
- P. Suntharalingam, J.T. Economou,and K. Knowles, "Gear locking mechanism to extend the consistent power operating region of the electric motor to enhance acceleration and regenerative braking efficiency in hybrid electric vehicles", Vehicle Power and Propulsion Conference, 2009. VPPC '09. IEEE. Dearborn, MI, USA
- P. Suntharalingam, J.T. Economou, and K. Knowles, "NEDC Based Compensated Forward Simulation Approach with Energy Management for Parallel Hybrid Electric Vehicles", UKACC Control Conference. Sep 2008. Manchester, UK. (Invited Paper)

References

[1] C. Chan, "The state of the art of electric, hybrid, and fuel cell vehicles," *Proceedings of the IEEE*, vol. 95, no. 4, pp. 704 –718, april 2007.

[2] J. Miller, *Propulsion Systems for Hybrid Vehicles*. IEE Power and Energy Series 45, 2003.

[3] J. Wong, *Theory of Ground Vehicles*. John Wiley and Sons, 1993.

[4] W. Page, *Eurostat Web Link*, Eurostat, *http : //www.ec.europa.eu/eurostat*, 2008.

[5] ——, *EERE Web Link*, EERE, *http : //www.eere.energy.gov/informationcenter*, 2010.

[6] S. McCluer and J. Christin, "Comparing data centre batteries, flywheels, and ultracapacitors," Transportation Research Part D: Transport and Environment, Tech. Rep., 2008.

[7] W. Page, *UQM Web Link*, UQM, *http : //www.uqm.com*, 2009.

[8] P. Clarke, T. Muneer, and K. Cullinane, "Cutting vehicle emissions with regenerative braking," *Transportation Research Part D: Transport and Environment*, vol. 15, pp. 160–167, 2010.

[9] L. Chu, M. Shang, Y. Fang, J. Guo, and F. Zhou, "Braking force distribution strategy for hev based on braking strength," in *International Conference on Measuring Technology and Mechatronics Automation*, vol. 1, 2010, pp. 759–764.

[10] K. Henry, J. A. Anderson, M. Duoba, and R. Larsen, "Engine start characteristics of two hybrid electric vehicles hevs, honda insight and toyota prius," in *SAE Future Transportation Technology Conference and Exposition*, no. 2492, Aug 2001.

[11] K. Chau and Y. Wong, "Overview of power management in hybrid electric vehicles," *Energy Conversion and Management*, vol. 43, pp. 1953 – 1968, 2002.

[12] M. Panagiotidis., G. Delagrammatikas., and D. Assanis., "Development and use of a regenerative braking model for a parallel hybrid electric vehicle," in *SAE Technical Paper Series*, March 2000.

[13] H. Yeo and H. Kim, "Hardware-in-the-loop simulation of regenerative braking for a hybrid electric vehicle," *Proceedings of the Institution of Mechanical Engineers, Part D: Journal of Automobile Engineering*, vol. 216, pp. 855 – 864, 2002.

[14] D. Kim, C. Kim, S. Hwang, and H. Kim, "Hardware in the loop simulation of vehicle stability control using regenerative braking and electro hydraulic brake for hev," in *The international federation of automatic control*, vol. 17, 2008.

[15] X. Yu, T. Shen, G. Li, and K. Hikiri, "Regenerative braking torque estimation and control approaches for a hybrid electric truck," in *Proceedings of the 2010 American Control Conference*, 2010, pp. 5832–5837.

[16] M. Shang, L. Chu, J. Guo, Y. Fang, and F. Zhou, "Braking force dynamic coordinated control for hybrid electric vehicles," in *Proceedings of the IEEE International Conference on Advanced Computer Control*, vol. 4, 2010, pp. 411–416.

[17] F. Wang and B. Zhuo, "Regenerative braking strategy for hybrid electric vehicles based on regenerative torque optimization control," *Proc. IMechE,Part D: J. Automobile Engineering*, vol. 222, pp. 499 – 513, January 2008.

[18] N. Mutoh, Y. Hayano, H. Yahagi, and K. Takita, "Electric braking control methods for electric vehicles with independently driven front and rear wheels," *IEEE Transactions on Industrial Electronics*, vol. 54, no. 2, pp. 1168 –1176, April 2007.

[19] C. Mi, H. Lin, and Y. Zhang, "Iterative learning control of antilock braking of electric and hybrid vehicles," *IEEE Transactions on Vehicular Technology*, vol. 54, pp. 486–494, 2005.

[20] J. Bray, G. Walker, A. Simpson, M. Greaves, and B. Guymer, "Brake system performance requirements of a lightweight electric hybrid rear wheel drive vehicle," *International Journal of Vehicle Autonomous Systems*, vol. 1, pp. 436–448, 2003.

[21] C. Yu and K. Chau, "Thermoelectric automotive waste heat energy recovery using maximum power point tracking," *Energy Conversion and Management*, vol. 50, pp. 1506–1512, 2009.

[22] V. Beldjajev, T. Lehtla, and H. Maţlder, "Influence of regenerative braking to power characteristics of a gantry crane," in *Procedings of Electric Power Quality and Supply Reliability Conference*, 2010, pp. 73–77.

[23] H. Seki, K. Ishihara, and S. Tadakuma, "Novel regenerative braking control of electric power-assisted wheelchair for safety downhill road driving," *IEEE Transactions on Industrial Electronics*, vol. 56, pp. 1393–1400, 2009.

[24] A. Brahma, Y. Guezennec, and G. Rizzoni, "Optimal energy management in series hybrid electric vehicles," in *Proceedings of the American Control Conference, 2000*, vol. 1, Sep. 2000, pp. 60 –64.

[25] S. Delprat, T. Guerra, G. Paganelli, J. Lauber, and M. Delhom, "Control strategy optimization for an hybrid parallel powertrain," in *Proceedings of the American Control Conference, 2001.*, vol. 2, 2001, pp. 1315 –1320 vol.2.

[26] C.-C. Lin, H. Peng, J. Grizzle, and J.-M. Kang, "Power management strategy for a parallel hybrid electric truck," *IEEE Transactions on Control Systems Technology*, vol. 11, pp. 839 – 849, November 2003.

[27] S. Delprat, J. Lauber, T. Guerra, and J. Rimaux, "Control of a parallel hybrid powertrain: optimal control," *IEEE Transactions on Vehicular Technology*, vol. 53, pp. 872 – 881, May 2004.

[28] P. Pisu and G. Rizzoni, "A comparative study of supervisory control strategies for hybrid electric vehicles," *IEEE Transactions on Control Systems Technology*, vol. 15, pp. 506 –518, May 2007.

[29] H. Zhong, F. Wang, G. Q. Ao, J. X. Qiang, L. Yang, B. Zhuo, and X. J. Mao, "An optimal torque distribution strategy for an integrated starter-generator parallel hybrid electric vehicle based on fuzzy logic control," *Proceedings of the Institution of Mechanical Engineers, Part D: Journal of Automobile Engineering*, vol. 222, pp. 79–92, 2008.

[30] A. Fuhs, *Hybrid Vehicles and the Future of Personal Transportation*. CRC Press, 2009.

[31] B. Baumann, G. Washington, B. Glenn, and G. Rizzoni, "Mechatronic design and control of hybrid electric vehicles," *IEEE/ASME Transactions on Mechatronics*, vol. 5, pp. 58 –72, Mar. 2000.

[32] F. Syed, D. Filev, and H. Ying, "Real time advisory system for fuel economy improvement in a hybrid electric vehicle," in *Annual Meeting of the North American, Fuzzy Information Processing Society, 2008.*, May 2008, pp. 1 –6.

[33] K. Huang, X. Tzeng, T. Jeng, and C. Cen, "Integration mechanism for a parallel hybrid vehicle system," *Applied Energy*, vol. 82, pp. 133 – 147, 2005.

[34] H. Hannoun, D. Diallo, and C. Marchand, "Energy management strategy for a parallel hybrid electric vehicle using fuzzy logic," in *International Symposium on Power Electronics, Electrical Drives, Automation and Motion, 2006.*, May 2006, pp. 229 –234.

[35] N. Schouten, M. Salman, and N. Kheir, "Fuzzy logic control for parallel hybrid vehicles," *IEEE Transactions on Control Systems Technology*, vol. 10, pp. 460 –468, May 2002.

[36] M. Ehsani., Y. Gao., G. Sebastien E, and A. Emadi., *Modern Electric, Hybrid electric, and Fuel Cell Vehicles Fundementals, Theory and design*. CRC presss, 2004.

[37] R. Langari and J.-S. Won, "Intelligent energy management agent for a parallel hybrid vehicle-part i: system architecture and design of the driving situation identification process," *IEEE Transactions on Vehicular Technology*, vol. 54, pp. 925 – 934, May 2005.

[38] P. Rodatz, G. Paganelli, A. Sciarretta, and L. Guzzella, "Optimal power management of an experimental fuel cell/supercapacitor-powered hybrid vehicle," *Control Engineering Practice*, vol. 13, pp. 41 – 53, 2005.

[39] M. Kim and H. Peng, "Power management and design optimization of fuel cell/battery hybrid vehicles," *Journal of Power Sources*, vol. 165, pp. 819 – 832, 2007.

[40] E. Ericsson, "Variability in urban driving patterns," *Transportation Research Part D: Transport and Environment*, vol. 5, pp. 337 – 354, 2000.

[41] L. Guzzella and A. Amstutz, "Cae tools for quasi-static modeling and optimization of hybrid powertrains," *IEEE Transactions on Vehicular Technology*, vol. 48, pp. 1762 –1769, Nov. 1999.

[42] X. Li and S. Williamson, "Efficiency analysis of hybrid electric vehicle (hev) traction motor-inverter drive for varied driving load demands," in *Twenty-Third Annual IEEE Applied Power Electronics Conference and Exposition, 2008.*, Feburary 2008, pp. 280 –285.

[43] R. Nelson, "Power requirements for batteries in hybrid electric vehicles," *Journal of Power Sources*, vol. 91, pp. 2 – 26, 2000.

[44] M. Steiner and J. Scholten, "Energy storage on board of dc fed railway vehicles pesc 2004 conference in aachen, germany," in *35th Annual IEEE Power Electronics Specialists Conference, 2004.*, vol. 1, June 2004, pp. 666 – 671 Vol.1.

[45] W. Page, *BMW Web Link*, BMW, *http : //www.bmw.co.uk*, 2009.

[46] ——, *Toyota Web Link*, Toyota, *http : //www.toyotapriusbattery.com*, 2008.

[47] A. Chu and P. Braatz, "Comparison of commercial supercapacitors and high power lithium ion batteries for power assist applications in hybrid electric vehicles: I. initial characterization," *Journal of Power Sources*, vol. 112, pp. 236 – 246, 2002.

[48] R. L. L.T. Lam, "Development of ultra-battery for hybrid-electric vehicle applications," *Journal of Power Sources*, vol. 158, pp. 1140 – 1148, 2006.

[49] F. V. Conte, "Battery and battery management for hybrid electric vehicles: a review," *Elektrotechnik and Informationstechnik*, vol. 123, pp. 424–431, 2006.

[50] M. Ehsani, Y. Gao, and J. Miller, "Hybrid electric vehicles: Architecture and motor drives," *Proceedings of the IEEE*, vol. 95, no. 4, pp. 719–728, 2007.

[51] M. Ye, S. Jiao, and B. Cao, "Energy recovery for the main and auxiliary sources of electric vehicles," *Energies*, vol. 3, pp. 1673–1690, 2010.

[52] J. Dixon and M. Ortuzar, "Ultracapacitors + dc-dc converters in regenerative braking system," *IEEE Aerospace and Electronic Systems Magazine*, vol. 17, pp. 16 – 21, Aug. 2002.

[53] J.-S. Lai and D. Nelson, "Energy management power converters in hybrid electric and fuel cell vehicles," *Proceedings of the IEEE*, vol. 95, pp. 766 –777, April 2007.

[54] R. Schupbach and J. Balda, "Comparing dc-dc converters for power management in hybrid electric vehicles," in *IEEE International Electric Machines and Drives Conference, 2003.*, vol. 3, June 2003, pp. 1369 – 1374 vol.3.

[55] A. Drolia, P. Jose, and N. Mohan, "An approach to connect ultracapacitor to fuel cell powered electric vehicle and emulating fuel cell electrical characteristics using switched mode converter," in *The 29th Annual Conference of the IEEE Industrial Electronics Society, 2003.*, vol. 1, Nov 2003, pp. 897 – 901.

[56] A. Ohkawa, "Electric power control system for a fuel cell vehicle employing electric double-layer capacitor," in *SAE Technical Paper Series*, 2004.

[57] K. Jin, X. Ruan, M. Yang, and M. Xu, "A hybrid fuel cell power system," *IEEE Transactions on Industrial Electronics*, vol. 56, pp. 1212 –1222, April 2009.

[58] D. Feroldi, M. Serra, and J. Riera, "Design and analysis of fuel-cell hybrid systems oriented to automotive applications," *IEEE Transactions on Vehicular Technology*, vol. 58, pp. 4720–4729, 2009.

[59] X. Ruan, J. Wei, Y. Xue, and L. Zhou, "Voltage-sharing of the divided capacitors in nonisolated three-level converters," in *Nineteenth Annual IEEE Applied Power Electronics Conference and Exposition, 2004.*, vol. 3, 2004, pp. 1725 – 1729.

[60] D. Sable, F. Lee, and B. Cho, "A zero-voltage-switching bidirectional battery charger/discharger for the nasa eos satellite," in *Seventh Annual Conference Proceedings on Applied Power Electronics Conference and Exposition, 1992.*, Feburary 1992, pp. 614 –621.

[61] K. Jin, M. Yang, X. Ruan, and M. Xu, "Three-level bidirectional converter for fuel-cell/battery hybrid power system," *IEEE Transactions on Industrial Electronics*, vol. 57, pp. 1976 –1986, June 2010.

[62] M. Camara, H. Gualous, F. Gustin, A. Berthon, and B. Dakyo, "Dc/dc converter design for supercapacitor and battery power management in hybrid vehicle applicationspolynomial control strategy," *IEEE Transactions on Industrial Electronics*, vol. 57, pp. 587–597, 2010.

[63] I. D. Vlieger, D. D. Keukeleere, and J. G. Kretzschmar, "Environmental effects of driving behaviour and congestion related to passenger cars," *Atmospheric Environment*, vol. 34, pp. 4649 – 4655, 2000.

[64] B. Holmen and D. Niemeier, "Characterizing the effects of driver variability on real-world vehicle emissions," *Transportation Research Part D: Transport and Environment*, vol. 3, pp. 117 – 128, 1998.

[65] I. D. Vlieger, "On board emission and fuel consumption measurement campaign on petrol-driven passenger cars," *Atmospheric Environment*, vol. 31, pp. 3753 – 3761, 1997.

[66] R. Ghorbani, E. Bibeau, and S. Filizadeh, "On conversion of hybrid electric vehicles to plug-in," *IEEE Transactions on Vehicular Technology*, vol. 59, no. 4, pp. 2016 –2020, may 2010.

[67] R. Limpert, *Brake Design and Safety, Sceond edition*. Socity of Automotive Engineers, 1999.

[68] G. Rizzoni, L. Guzzella, and B. Baumann, "Unified modeling of hybrid electric vehicle drivetrains," *IEEE/ASME Transactions on Mechatronics*, vol. 4, pp. 246 –257, September 1999.

[69] J. Zhang, S. Li, G. Lu, and Q. Zhou, "A novel regenerative braking method of bldcm for wheeled mobile robot," in *IEEE International Conference on Information and Automation*, 2010, pp. 676–681.

[70] E. Karden, S. Ploumen, B. Fricke, T. Miller, and K. Snyder, "Energy storage devices for future hybrid electric vehicles," *Journal of Power Sources*, vol. 168, pp. 2 – 11, 2007.

[71] J. Miller, "Power electronics in hybrid electric vehicle applications," in *Eighteenth Annual IEEE Applied Power Electronics Conference and Exposition, 2003.*, vol. 1, Feburary 2003, pp. 23 – 29 vol.1.

[72] S. Lukic and A. Emadi, "Effects of drivetrain hybridization on fuel economy and dynamic performance of parallel hybrid electric vehicles," *IEEE Transactions on Vehicular Technology*, vol. 53, pp. 385 – 389, March 2004.

[73] I. Husain, *Electric and Hybrid Vehicles Design Fundamentals*. CRC Press, 2003.

[74] P. Ribeiro, B. Johnson, M. Crow, A. Arsoy, and Y. Liu, "Energy storage systems for advanced power applications," *Proceedings of the IEEE*, vol. 89, pp. 1744 –1756, December 2001.

[75] Z. Amjadi and S. Williamson, "Power electronics based solutions for plug in hybrid electric vehicle energy storage and management systems," *IEEE Transactions on Industrial Electronics*, vol. 57, pp. 608–616, 2010.

[76] R. Erickson and D. Maksimovic., *Fundementals of Power Electronics, Second edition*. Kluwer academic publishers, 2000.

[77] W. Page, *EPCOS Web Link*, EPCOS, *http* : *//www.epcos.com*, 2010.

Chapter 8

Appendix

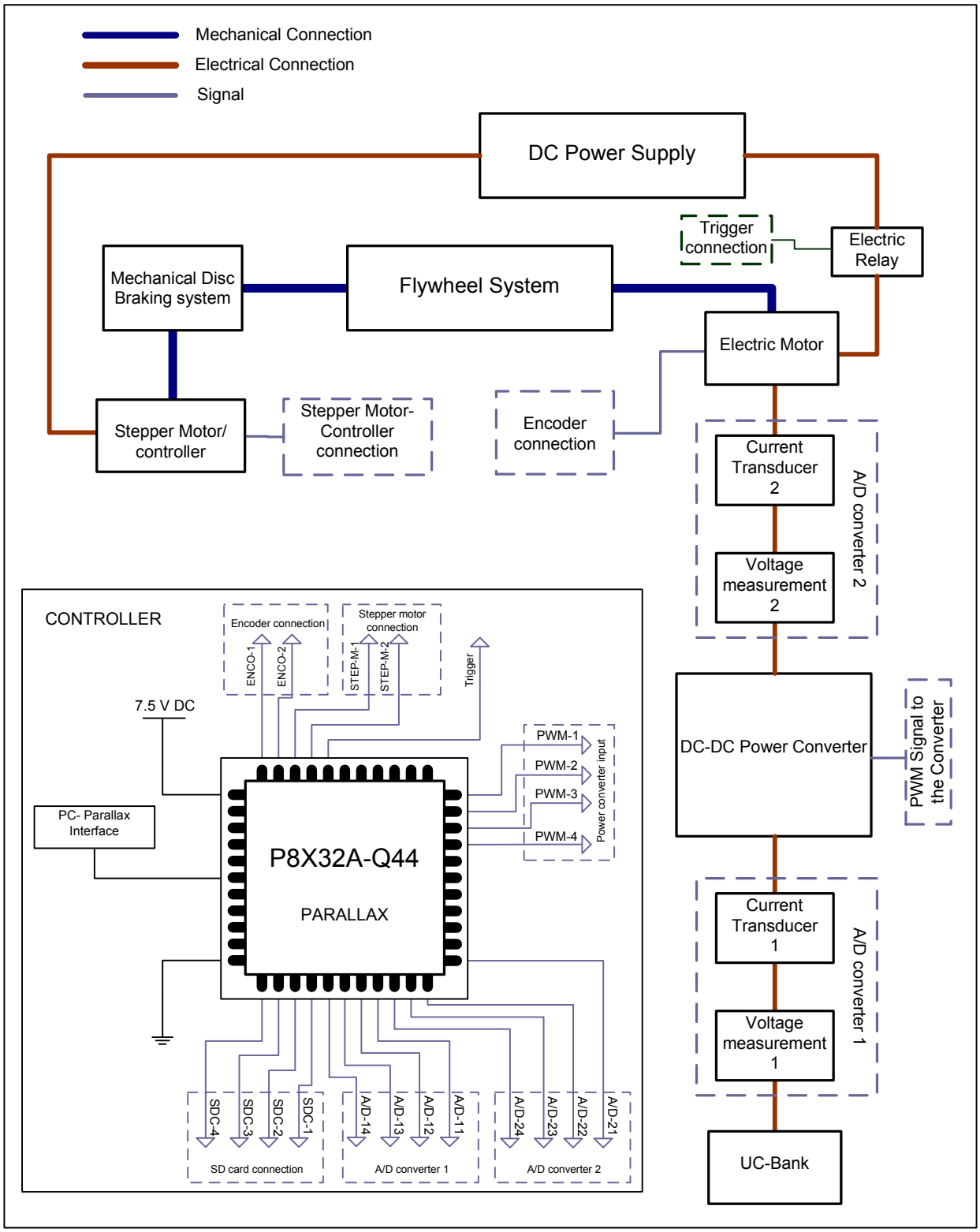

Figure 8.1: Layout of the Developed Regenerative Braking System

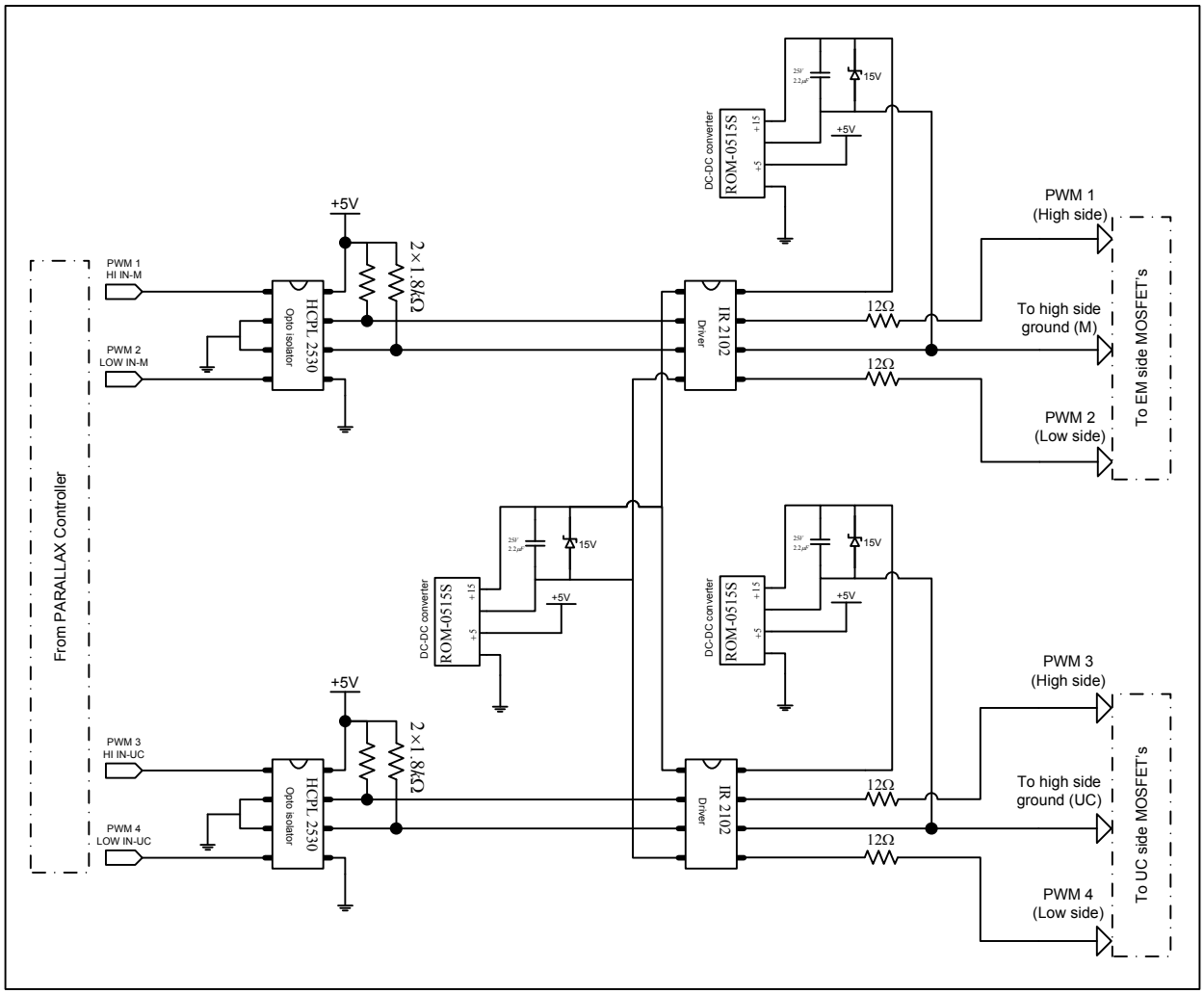

Figure 8.2: Detailed Circuit diagram for the Power Electronic Semiconductor Switches

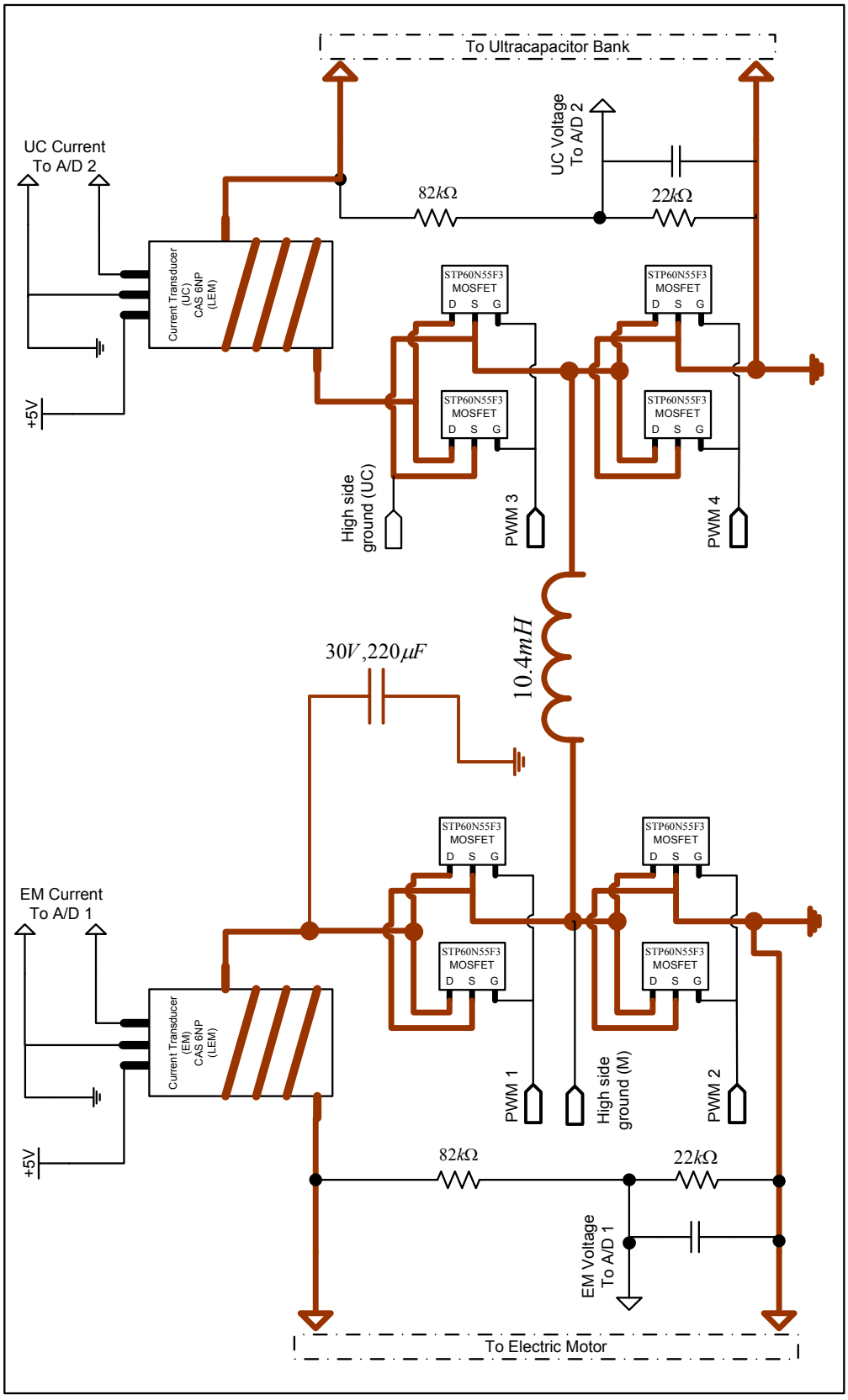

Figure 8.3: Detailed Circuit diagram of the DC-DC Bi directional Buck/ Boost Power Converter

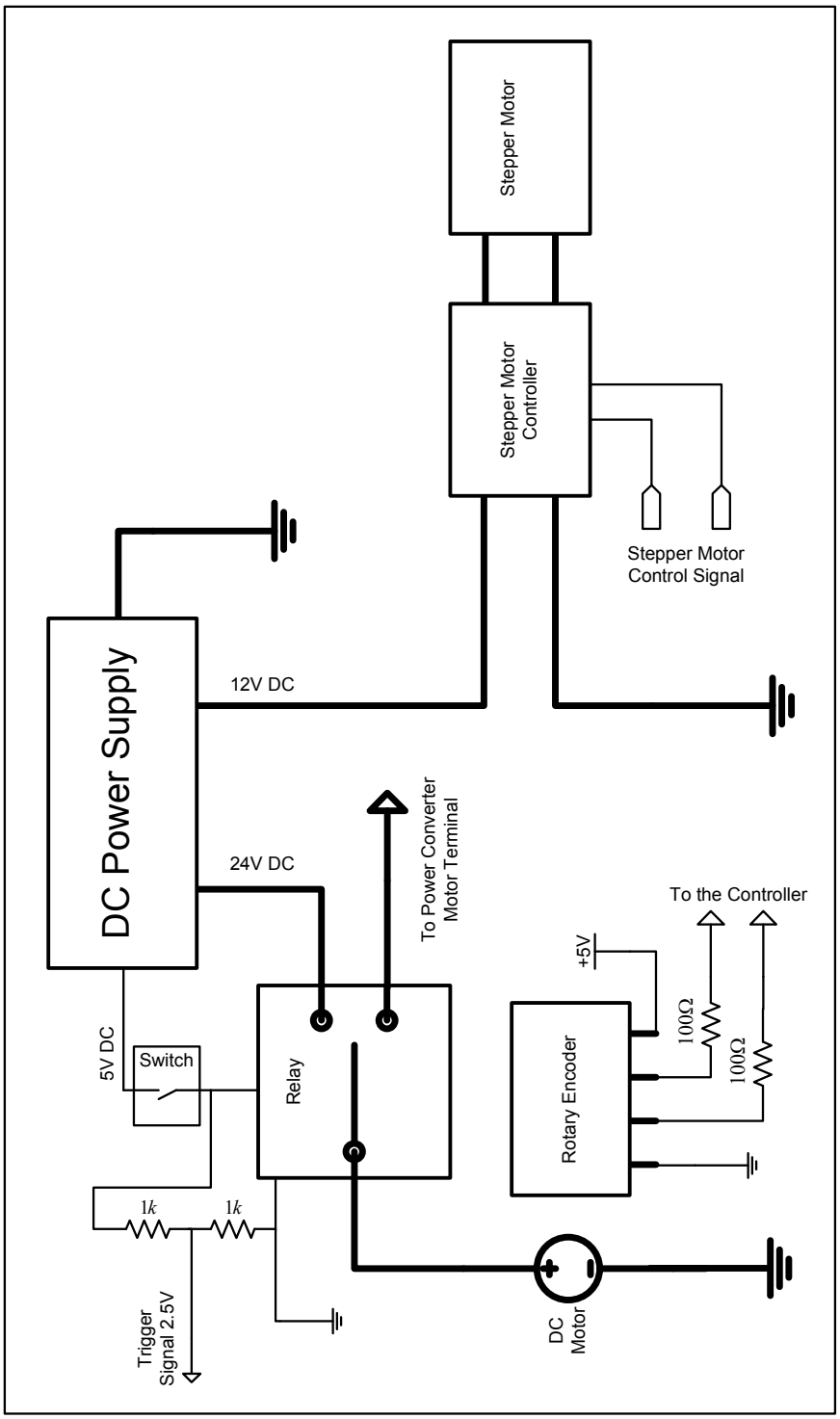

Figure 8.4: Connect Diagram of the Power Supply

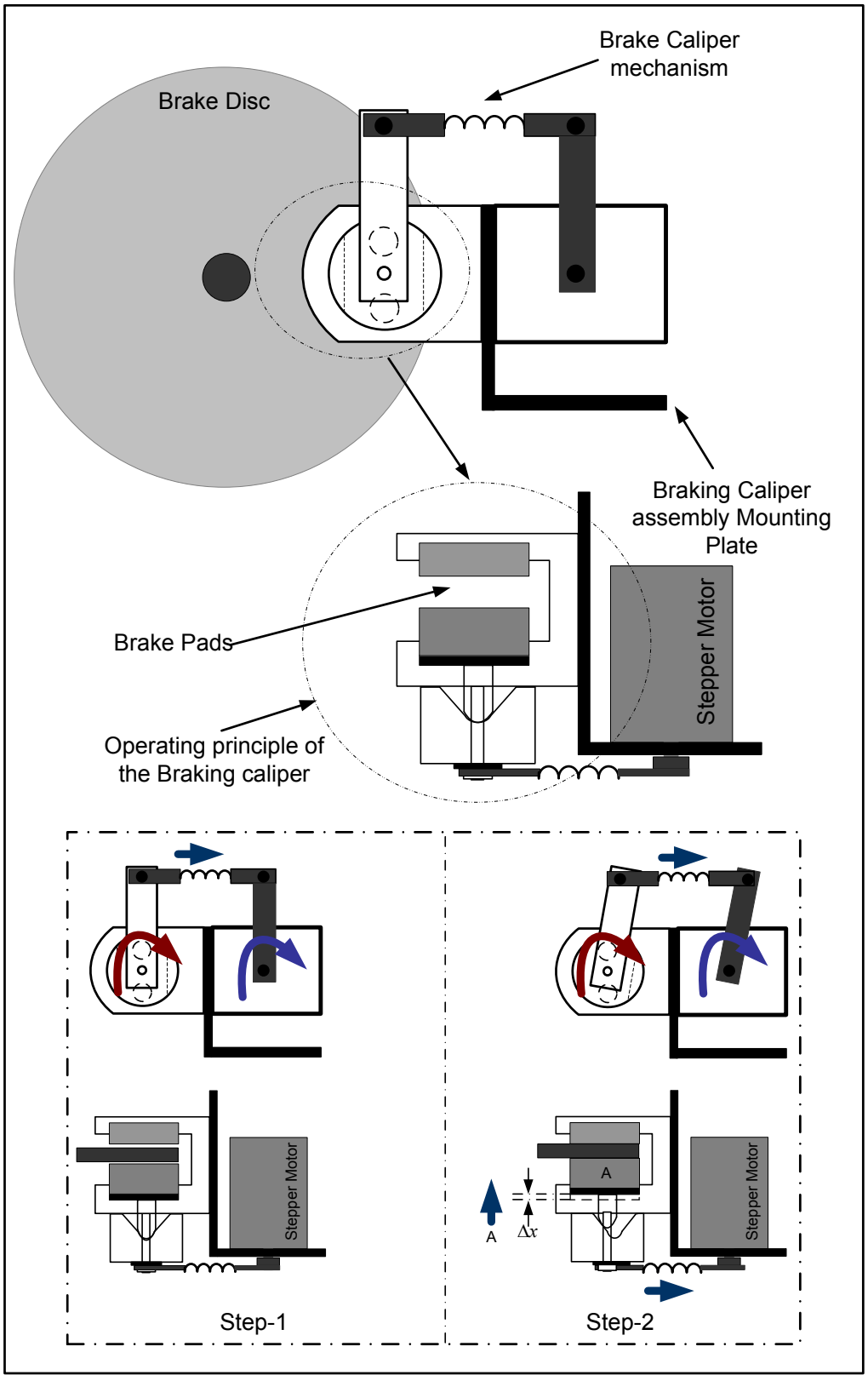

Figure 8.5: Mechanical braking system

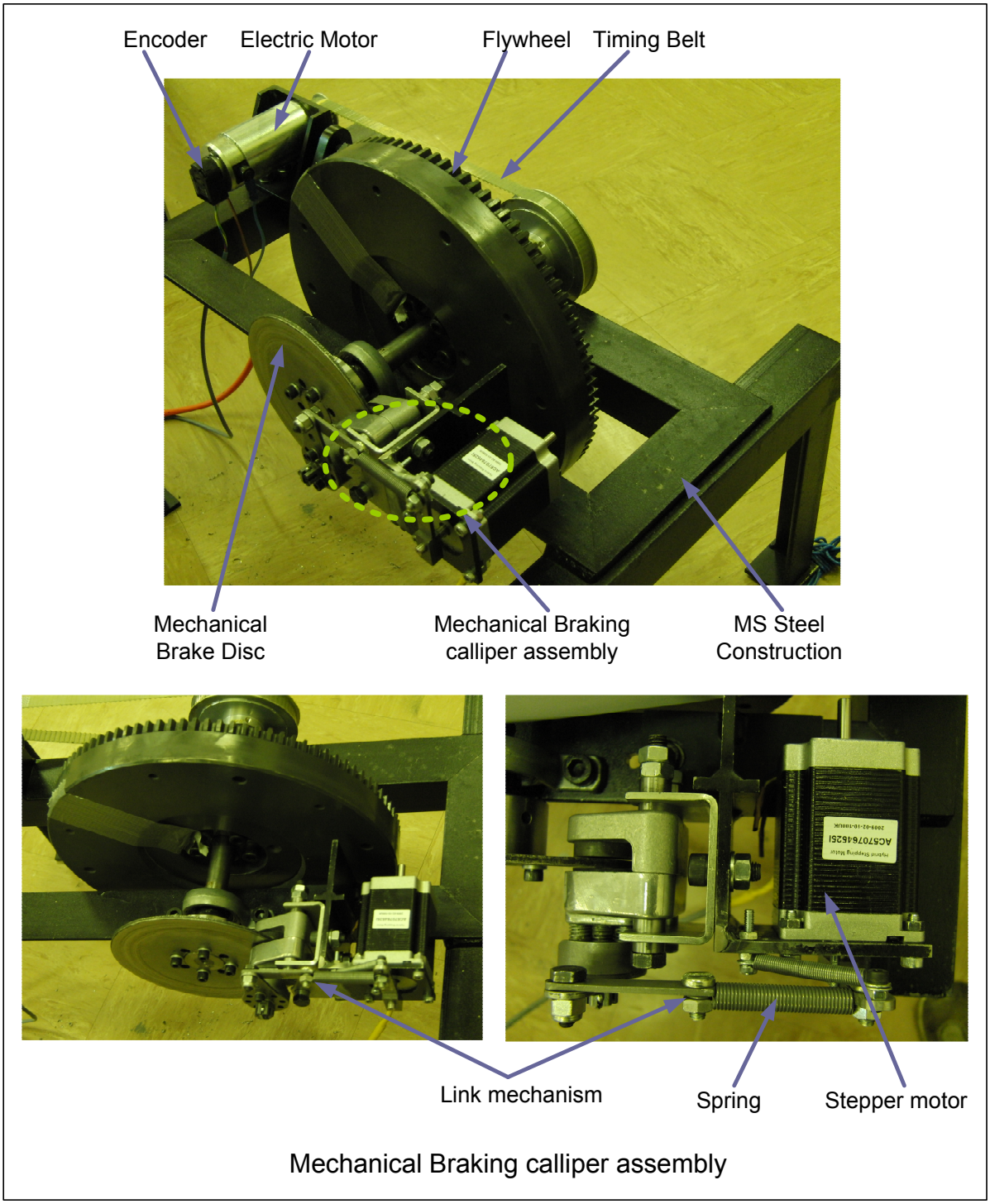

Figure 8.6: Photograph of the Flywheel Rig and Calliper assembly

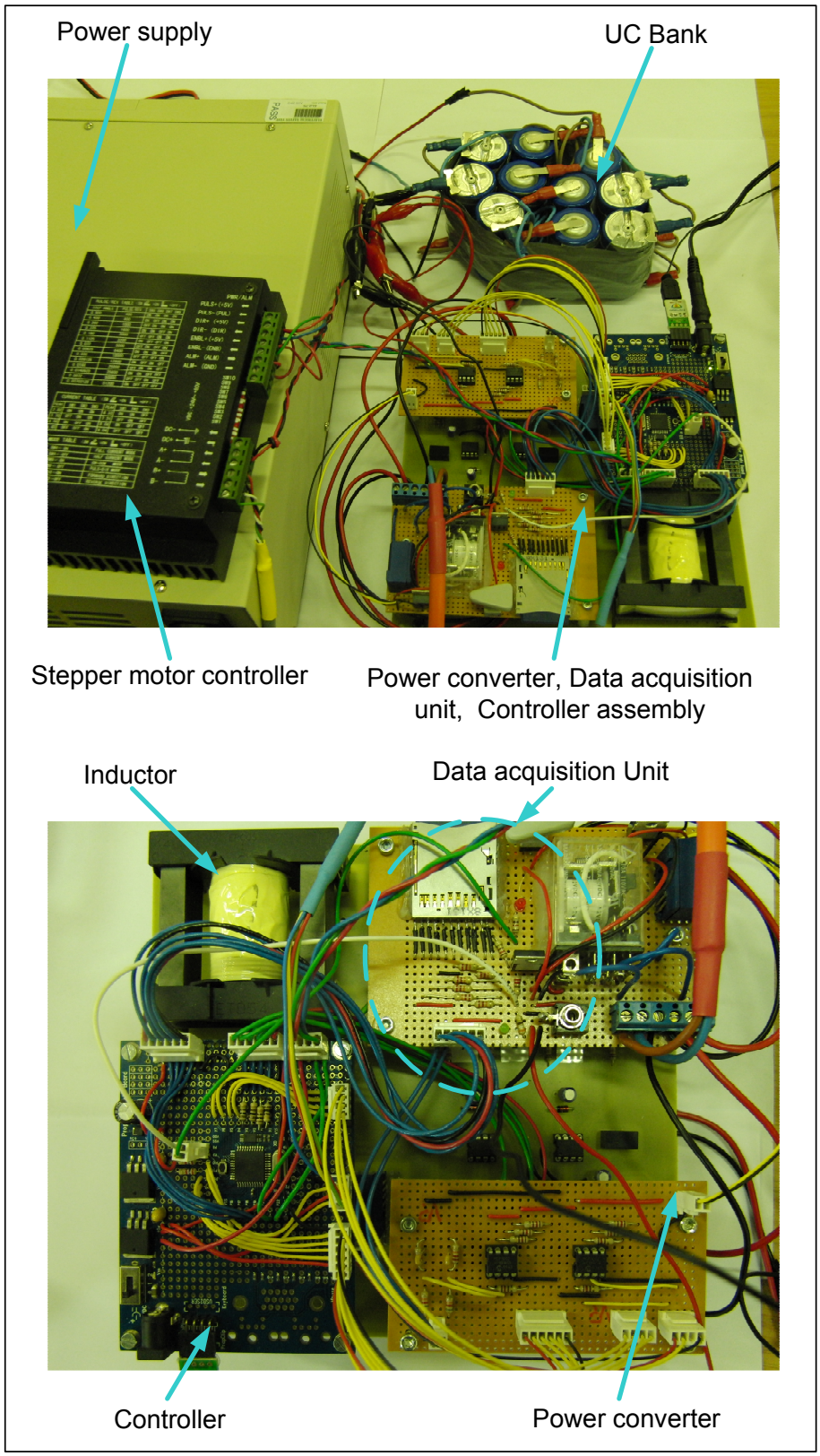

Figure 8.7: Photograph of the electric power system